IOWA STATE UNIVERSITY
Digital Repository

1979

Oxygen reduction on a graphite paste and a catalyst loaded graphite paste electrode

Dennis Michael DiMarco
Iowa State University

Follow this and additional works at: https://lib.dr.iastate.edu/rtd

Part of the Analytical Chemistry Commons

8010226

DiMarco, Dennis Michael

OXYGEN REDUCTION ON A GRAPHITE PASTE AND A CATALYST LOADED GRAPHITE PASTE ELECTRODE

Iowa State University   Ph.D.   1979

University
Microfilms
International 300 N. Zeeb Road, Ann Arbor, MI 48106   18 Bedford Row, London WC1R 4EJ, England

Oxygen reduction on a graphite paste and a

catalyst loaded graphite paste electrode

by

Dennis Michael DiMarco

A Dissertation Submitted to the

Graduate Faculty in Partial Fulfillment of the

Requirements for the Degree of

DOCTOR OF PHILOSOPHY

Department: Chemistry
Major: Analytical Chemistry

Approved:

In Charge of Major Work

For the Major Department

For the Graduate College

Iowa State University
Ames, Iowa

1979

TABLE OF CONTENTS

iii

I. INTRODUCTION

When Sir William Grove first experimented with the
hydrogen/oxygen fuel cell, he had little knowledge of the
importance of his discovery (1). Not until the 1900s
when the consequences of Carnot's work with heat engines
were realized, was serious consideration given to direct
electrochemical oxidation of fuels. Haber (2) and then
Nernst (3) and Bauer (4) tried to construct high temperature,
solid electrolyte fuel cells which would use coal as fuel
and air as the oxidant. Their problems proved too difficult
to surmount and fuel cells were relegated to a curiosity
until the mid-1900s. Then Davtyan (5) and Bacon (6-8)
began rather extensive tests aimed at constructing a useful
fuel cell. Bacon's development -- the bilayer electrode --
later became the basis of the NASA Apollo fuel cell (8),
and with this foothold fuel cell research increased. Work
was done on low temperature cells using hydrogen, hydrazine,
methanol and various other lower hydrocarbons as fuels. In
the intermediate temperature range, 300 to 650°C, molten
carbonate salts were used as electrolyte with hydrocarbon
gases used as fuels. At even higher temperatures -- up to
1100°C -- solid electrolytes were used which are capable of
transporting $O^=$ ion within the electrolyte matrix. Coal has
been used in these cells which convert it directly into CO_2.
For the two higher temperature systems, catalysis is a

secondary problem, since rates are vastly enhanced at these temperatures. The main problem under these conditions is stability of electrode, electrolyte, and container materials. From these fields, interest has branched out to metal/air batteries and biological fuel cells. The former are hybrid cells that have recently received attention for vehicle propulsion purposes. Lithium, zinc, and ferrous alloys have been used as the oxidizable "fuel" for these cells with air, as usual, as the oxidant. Biological fuel cells have been envisioned that could be subcutaneously implanted and could provide power for a pacemaker. The device would use simple sugars as fuel and oxygen as oxidant directly from the blood stream. Figure I-1 shows the similarity between a fuel cell and a battery. Both have an anode and a cathode and will supply direct current when connected across a load. Considering this device as an energy producer, oxidation occurs at the negative pole and reduction occurs at the positive electrode. At the cathode, a fuel -- most simply H_2 -- is oxidized, giving up electrons to the circuit and making that electrode negative.

$$H_2 \rightleftharpoons 2H^+ + 2e^- \qquad E_o^1 = -0.25 \qquad (I-1)$$

---
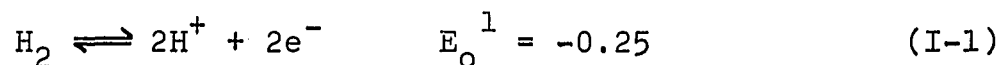
[1] All potentials listed herein will be standard reduction potentials referenced to the standard calomel electrode (SCE). The SCE will be taken as +0.25 volts versus the standard hydrogen electrode.
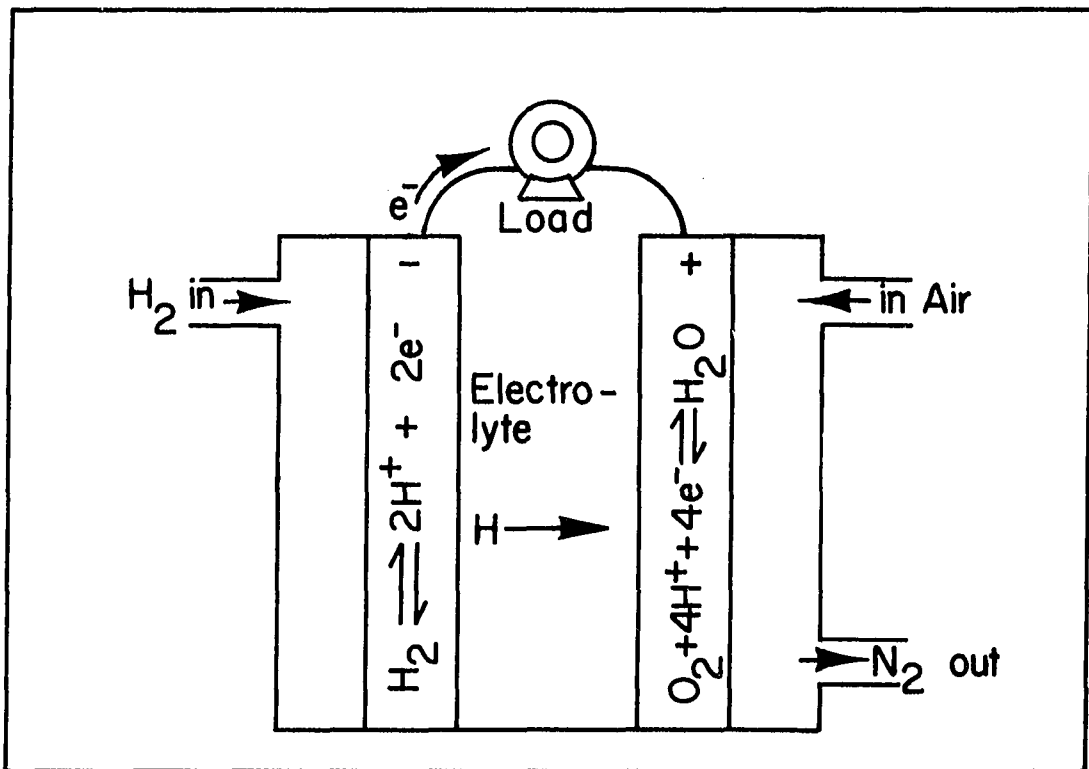
Figure I-1. Fuel cell

As with a battery, energy is produced when a
substance at the cathode gives electrons up to
the substance at the anode. Ion flow through
the electrolyte retains electroneutrality

O_2 is reduced at the anode, taking electrons from the circuit, making this electrode positive.

$$O_2 + 4H^+ + 4e^- \rightleftharpoons 2H_2O \qquad E_o = +0.98 \qquad (I-2)$$
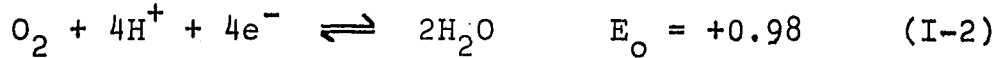
This picture can be generalized for any material that will combust in O_2. Possible fuels other than H_2 include gaseous hydrocarbons, liquid hydrocarbons, coal, oxidizable metals, and other inorganic materials. The cell potential is theoretically determined by the standard reduction potentials of the two electrode reactions.

There are several important advantages to this type of energy converter. The first is that the theoretical efficiency of a battery is $\Delta G/\Delta H$ for the total reaction. For example, the total reaction for the cell in figure 1 is given by equation I-3.

$$O_2 + 2H_2 \longrightarrow 2H_2O \qquad \begin{array}{l} -\Delta H^\circ = 68.3 \text{ kcal/mole} \\[6pt] -\Delta G^\circ = 56.7 \text{ kcal/mole} \end{array} \qquad (I-3)$$
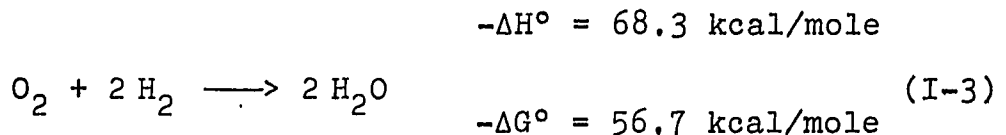
This efficiency is generally much greater than that attainable in an expansion combustion process, which is limited by Carnot's equation

$$E_{eff} = (T_{in} - T_{out})/T_{in} \qquad (I-4)$$

where temperature is in degrees Kelvin. Another advantage of fuel cells is the multiplicity of available fuels. Finally, this battery can be mechanically recharged or

fueled just like an internal combustion powered device.
Although no electrical recharging is necessary, the H_2/O_2
cell can be used to store energy by using the cell in the
reverse mode, that is, as a producer whereby the H_2 and O_2
produced can be saved until needed. This type of fuel cell
would thus be useful in power storage and load leveling
applications.

With all these advantages, one might think that we have
been fools for ignoring fuel cells all these years; however,
there are yet obstacles in the road to development of
practical fuel cells. The theoretical potential of a
H_2/O_2 fuel cell is 1.23 volts, but even under laboratory
conditions the zero load potential difference is about
1.00 volts. Under normal load conditions, the potential
drops to around 0.75 volts, or about 60% of the theoretical
value. This results in a similar 60% decrease in
efficiency. Even this performance is achieved using the
best electrodes and catalysts available today. The
difference between the actual potential and the theoretical
equilibrium potential is the overpotential (η) and is an
indicator of the reversibility of a reaction. The closer η
is to zero, the more nearly reversible is the reaction.
Since a battery requires two electrode reactions -- one at
each electrode -- the η of both reactions contribute to cell
irreversibility, but one may be dominant. The basic

knowledge that the H^+/H_2 electrode is used as a reference potential indicates that a hydrogen electrode can be prepared which is nearly reversible. Thus the large η for operating fuel cells must be caused by irreversibility in the oxygen electrode reaction, making it the object of fuel cell research. As is common in attempts to catalyze a reaction, the first step is gaining an understanding of the principles and chemistry involved. Armed with these basics one can then attack the problem of enhancing the catalysis and improving efficiency.

A. Oxygen Reduction

The more recent reviews of oxygen reduction give both a good introduction and an indication of the volume of work done on this topic (9-14). The realization of a reversible oxygen electrode is advantageous for both practical and theoretical reasons. In theory, an electrode should act as a source or a sink of electrons. Any participation by the electrode in the reaction will impugn the thermodynamic measurements.

1. Equilibria

Initially, the potential measured at an oxygen electrode was found to be non-Nernstian. This meant that either something blocked the reduction of oxygen or that another reaction was potential controlling. Peroxide had sometimes

been detected as a product of oxygen reduction suggesting
that the two-electron reduction of oxygen may be important
in the electrode process.

$$O_2 + 2 H^+ + 2e^- \rightleftharpoons H_2O_2 \qquad E_o = 0.43 \qquad \text{(I-5)}$$
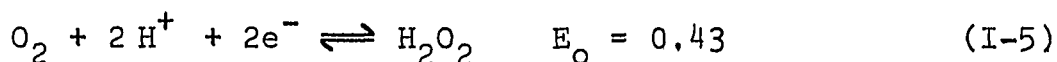
Oxide formation was also suspected of interfering with
oxygen reduction. For example, on platinum the following
reaction occurs:

$$Pt(OH)_2 + 2 H^+ + 2e^- \rightleftharpoons Pt + 2 H_2O \qquad E_o = 0.73 \quad \text{(I-6)}$$
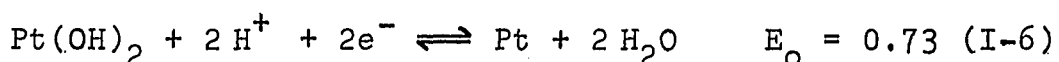
Early investigators felt that at low current levels the
reduction of oxygen could be shunted by the oxidation of
platinum at the electrode surface. Other research indicated
that oxygen slowly diffused into the bulk of a platinum
electrode. Finally, the question seemed resolved with the
work of Damjanovic et al. (15) who found that in acid
solution, oxygen reduction current decreased with time. In
stringently purified solutions, this decay in current was
very slow, and the reversible potential for oxygen reduction
was achieved. These results indicated that impurities in
solution had prevented the attainment of the reversible
potential in previous studies. A more recent study confirmed
this finding by determining that the deactivation was not
only time dependent but also dependent on the flux to the
electrode surface (16).

Despite these advances, the fact remained that the currents measured near the reversible potential were extremely low. The exchange current density (i_o) for oxygen reduction on platinum is 10^{-10} amps/cm^2. Comparison of this value to the i_o of the H^+/H_2 couple on platinum -- 10^{-3} amps/cm^2 -- indicates the irreversibility of oxygen reduction. Whatever the cause of the irreversibility, investigators continued to have trouble relating the thermodynamic data to a four e^- process. More investigators were finding that peroxide was present either as an intermediate or an end product. A series of papers came out in the 1960s and early 1970s describing the use of a rotating disk electrode with concentric ring for studies of oxygen reduction (17-26). Using this technique, the experimenters were able to determine when peroxide was formed as an intermediate in oxygen reduction. This point had been in controversy since the absence of peroxide may also have resulted from either the further reduction of peroxide or its decomposition at the electrode surface. As noted earlier, the reversible potentials of the two and four electron oxygen reduction reactions are +0.43 and +0.98 in acid solution. The loss in cell potential of an electrode capable of only the two electron reduction is 0.55 volts. This loss can be reduced by decomposing or further reducing the peroxide formed. Using the Nernst equation, one can write the

following for equation I-5:

$$E_{eq} = E_o + \frac{0.059}{2} \log \frac{P_{O_2}[H^+]^2}{[H_2O_2]} \qquad (I-7)$$

To obtain an E_{eq} of +0.98 volts using $P_{O_2} = 1 = [H^+]$, the necessary concentration of peroxide is 10^{-18} moles/liter. This concentration would require a most ambitious catalyst and recent studies indicate that these levels are not attainable using present catalysts (27). As work progressed, the importance of the first electron transfer was recognized, especially when data were taken in higher current ranges (14). The first electron transfer to oxygen results in the formation of superoxide ion (O_2^-).

$$O_2 + e^- \rightleftharpoons O_2^- \qquad E_o = -0.58 \qquad (I-8)$$
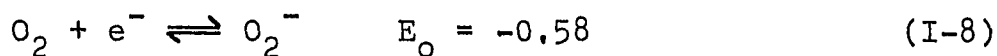
Formation of superoxide ion as an intermediate would restrict the potential of oxygen reduction even more severely than peroxide formation. The existence of superoxide ion was first shown in aprotic media where it is a stable product of oxygen reduction (28-30). The reduction wave conforms to a one electron process and is reversible. Furthermore, the reduction potential (-0.80 volts) is independent of electrode material. The effect of protons on this reduction wave is striking. With increasing concentration of water the wave shifts in a positive direction and becomes irreversible. At about 30% water in organic solvent,

superoxide ion can no longer be found and peroxide is the
product (31). In this process the ultimate result is known
but the pathway is yet in doubt. As with peroxide, the
superoxide ion formed could be either reduced to peroxide,

$$O_2^- + H_2O + e^- \rightleftharpoons HO_2^- + OH^- \qquad E_o = -0.08 \qquad (I-9)$$
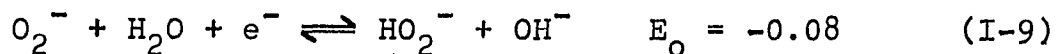
or dismutation to peroxide ion and oxygen can occur.

$$2\,O_2^- + H_2O \longrightarrow O_2 + HO_2^- + OH^- \qquad (I-10)$$
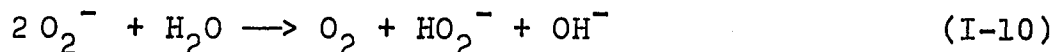
The further reduction of superoxide ion is very slow in
aprotic media (29,32) while disproportionation is inhibited
by electrical repulsion of the superoxide ions. These
results explain the stabilization of superoxide ion in non-
aqueous media. Certain metals are known to catalyze the
dismutation of superoxide ion and since the oxygen formed
can be recycled at the electrode the result is a two-
electron reduction. Dubrovina and Nekrasov (33) and
others (34) found evidence that oxygen reduction in basic
solutions could be halted at the one, two, or four electron
stage. The addition of the surfactant -- triphenyl-
phosphine oxide -- scavenged superoxide ions, preventing
their decomposition and shifting the two-electron reduction
in a negative direction. Thus depending on potential, they
were able to separate the three oxygen reduction processes.
It is also instructive that in basic solution oxygen
reduction begins at about -0.2 volts independent of electrode

material (35-37)[1]. Furthermore, peroxide ion is the major product on mercury, carbon, and gold and is found to some extent on the rest of the noble metals.

In acid solutions other processes may occur which account for the increased potential of oxygen reduction on some noble metals. The oxide mechanism operates by dissociatively adsorbing oxygen on the metal electrode with subsequent reduction of the oxide to form water. A representative example would be the following sequence.

$$2 M + O_2 \longrightarrow 2 MO \tag{I-11}$$

$$MO + H_2O \rightleftharpoons M(OH)_2 \tag{I-12}$$

$$M(OH)_2 + 2 H^+ + 2 e^- \rightleftharpoons M + 2 H_2O \tag{I-13}$$
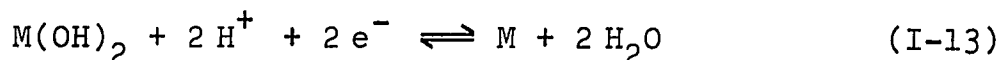
In this situation no peroxide is formed and the reduction potential would be dependent on the electrode material, as is generally found. In acid solution the fate of any superoxide formed would also be changed due to the following protonation (41).

$$HO_2 \rightleftharpoons O_2^- + H^+ \qquad pK_a = 4.88 \tag{I-14}$$

---
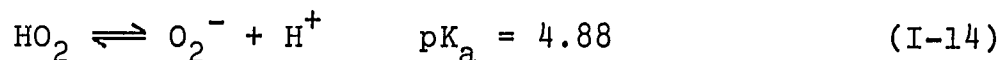
[1]The reduction potential on most carbons is shifted slightly negative; a major exception to this seems to be the basal plane of highly oriented graphite as noted in (38-40) and also found in the present study on a graphite paste electrode.

HO_2 is a strong oxidizing agent

$$HO_2 + H^+ + e^- \rightleftharpoons H_2O_2 \qquad E_o = +1.17 \qquad (I-15)$$
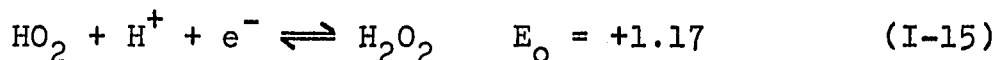
and will also undergo dismutation according to reactions 16 and 17 (41).

$$2\,HO_2 \longrightarrow H_2O_2 + O_2 \qquad k = 7.6 \times 10^5 \qquad (I-16)$$

$$O_2^- + HO_2 + H_2O \longrightarrow H_2O_2 + O_2 + OH^- \qquad (I-17)$$

$$k = 8.5 \times 10^7$$
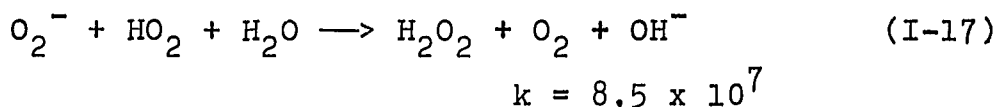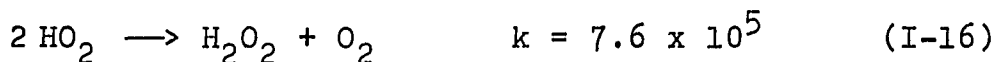
The oxygen formed in these steps could be recycled as before via reaction I-8. The dismutation of peroxide can also occur resulting in a net four-electron reduction when the oxygen formed is recycled at the electrode.

$$2\,H_2O_2 \longrightarrow O_2 + 2\,H_2O \qquad (I-18)$$

This reaction is catalyzed on some metals, notably platinum and silver, while not on others, for example gold and mercury. This may account for the difficulty in finding peroxide on platinum and silver reported in some studies while others were able to detect it. Under proper conditions, peroxide is the major product at gold, mercury, and carbon electrodes, highlighting their inability to decompose peroxide.

Thus, the rotating disk electrode with a ring seems particularly suited to studies of oxygen reduction. It can be used not only to detect peroxide but also to determine if the peroxide is further reacted on the electrode of interest.

2. Mechanism

Oxygen reduction at an electrode involves a sequence of steps, each of which is affected by some property of the electrode. For example, adsorption energy of intermediates, geometrical arrangement of surface atoms, concentration of surface defects, and electronic characteristics have at one time or another been invoked to implicate a particular step as rate controlling. Depending on the reaction conditions any one of the possible steps may be rate determining. It is thus essential to know the reaction path and the effect of the electrode and electrolyte properties on the basic steps. The ultimate ideal is to selectively vary one parameter of the reaction to evaluate its effect on the rate. In this way conclusions can be drawn about the mechanism if the rate determining step has not changed. Thus, it is conceptually possible to systematically find and catalyze the rate limiting step.

Few studies of oxygen reduction have had sufficient scope to achieve the above objectives. The reasons for this deficiency are: 1) A small number of electrodes are stable under the conditions of oxygen reduction, 2) there are a large number of possible intermediates, 3) electrode surfaces are, in general, poorly defined, and 4) impurities often obscure proper evaluations. As a solution to the first problem, many different types of materials have been

investigated other than metals. Since oxides are commonly formed under conditions of oxygen reduction, these types of materials seemed likely candidates for investigation (42-58). A problem of electrode conductivity arises here since most oxides are poor conductors. Doping is a common solution to this which leads to an increase in conductivity as well as complexity of the electrode. Metal organic complexes were also investigated due to their relationship with biological oxygen reduction (59-70). For these electrodes, stability is a problem as their performance decays with time. The other problems can be solved only by advances in techniques and procedures. For new as well as older catalysts, correlations were sought between oxygen reduction activity and physical properties. Some of the properties studied were metal-to-oxygen bond strength,[1] d orbital occupancy,[1] and other electronic characteristics of the catalysts (54, 55,64,71). Since platinum was the best oxygen reduction catalyst, the change in activity was explained as the difference between platinum characteristics and the other catalysts characteristics. For example, the platinum-oxygen bond strength was considered optimum for intermediate stabilization and those metals with weaker oxide bonds did not afford adequate stabilization while those metals with

---

[1]See reference 12, pp. 454-455.

stronger bonds suffered from slow desorption of the intermediate. In a similar manner d-orbital occupancy was optimized at an intermediate value. According to this theory (71), oxygen will form one sigma bond with the surface and exhibit some degree of pi bonding. Accordingly, the adsorption site should have an empty or half empty dz^2 orbital with filled xy or yz orbitals. The dz^2 orbital forms the sigma bond while the others back bond into the pi antibonding orbitals of the oxygen molecule. These ideas agree with the results of oxygen binding to homogeneous metal macrocyclic complexes.

One view of the mechanism that has gained recent acceptance is that of a catalytic redox mechanism. This requires a catalyst that can both react swiftly at the electrode and swiftly with oxygen in solution. This method can be viewed as shown in Figure I-2. The redox couple must have a reversible potential less than that of oxygen so oxygen can extract electrons from the reduced species, but the potential should be as close to that of oxygen as possible to achieve maximum efficiency. This idea has already been attempted in a fuel cell where the nitrite/ nitrate couple was used to mediate oxygen reduction (72). This concept is directly applicable to the catalysis afforded by macrocyclic metal complexes and biological materials (66, 68).
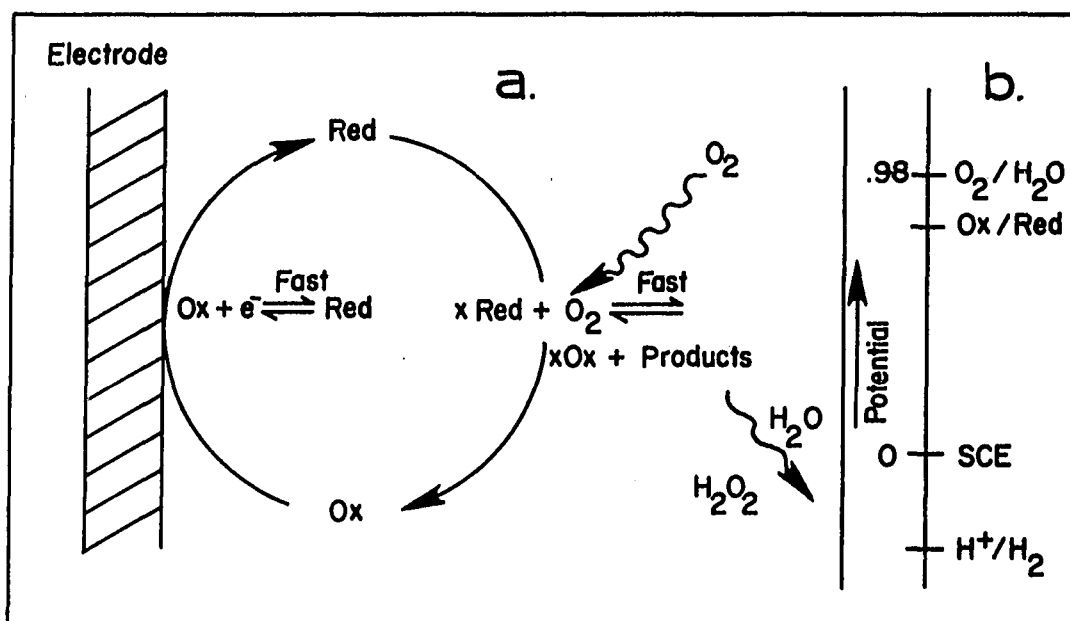
Figure I-2.   Catalytic oxygen reduction:
(a) catalytic redox mechanism for oxygen
reduction, (b) potential diagram for involved
species

With the recent advent of surface modification procedures, the concept of a surface redox catalyst has evolved. Now metal macrocycles have been attached to the surface which should greatly enhance electron transfer from this species to the surface. Surface groups can be attached by either adsorption or covalent bonding. In this way cheap carbon electrodes can be made into effective oxygen reduction catalysts. Many different catalysts have been surface attached from phthalocyanine structures to biological materials. The reaction scheme is the same for almost all. The metal macrocycles are able to bind oxygen and, with electrons from the surface, reduce it. The product is most often peroxide except with some more complex biological materials where direct four electron reduction to water results (63,70,73). These materials have not yet been subject to studies using a rotating disk electrode with a ring, however, to determine if peroxide is formed in the reaction and thereafter decomposed. The combination of a carbon electrode in the rotating disk configuration would seem ideal for studies on these materials (68). The idea of a surface redox couple has been suggested to extend to materials other than metal macrocycles. Its method for operation thus deserves close scrutiny.

Recently, the advantages of underpotential deposited metals as catalysts for oxygen reduction have been realized

(74,75). Lead ion deposited on gold in acid solution can
increase the potential for oxygen reduction by +0.5 volts.
It was noted by the author that the catalysis began at the
point of underpotential deposition. Figure I-3 shows an
example of this type of catalysis using lead on gold in acid
solution. It seems likely that oxygen could oxidize the
deposited lead which will again undergo underpotential
deposition and start the cycle again. The lead essentially
acts as a surface redox couple described earlier.
Unfortunately, gold is such a poor oxygen reduction catalyst
in acid solution that even this 0.5 volt shift in potential
is not enought to create a useful catalyst. In basic
solution, gold is a much better oxygen electrode and the
addition of lead ion to solution changes the product of
oxygen reduction from peroxide to water. Thus, although no
great breakthroughs have occurred, another method of
improvement has evolved. The redox mechanism is also a
possibility on traditionally nonmodified electrodes. Oxygen
reduction on some noble metals (most notably platinum)
occurs near the potential of oxide formation. It is possible
that the oxide can be formed by the reaction of oxygen with
bare metal surface with reduction of the oxide completing
the cycle as shown in the following equations

$$2\ Pt\ +\ O_2\ +\ 2\ H_2O\ \longrightarrow\ 2\ Pt(OH)_2 \qquad\qquad (I\text{-}19)$$

$$Pt(OH)_2\ +\ 2\ H^+\ +\ 2e^-\ \rightleftharpoons\ Pt\ +\ 2\ H_2O \qquad E_o\ =\ +0.73 (I\text{-}20)$$
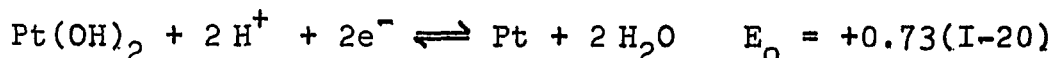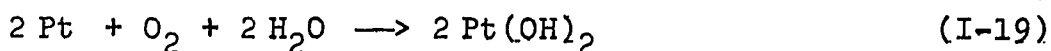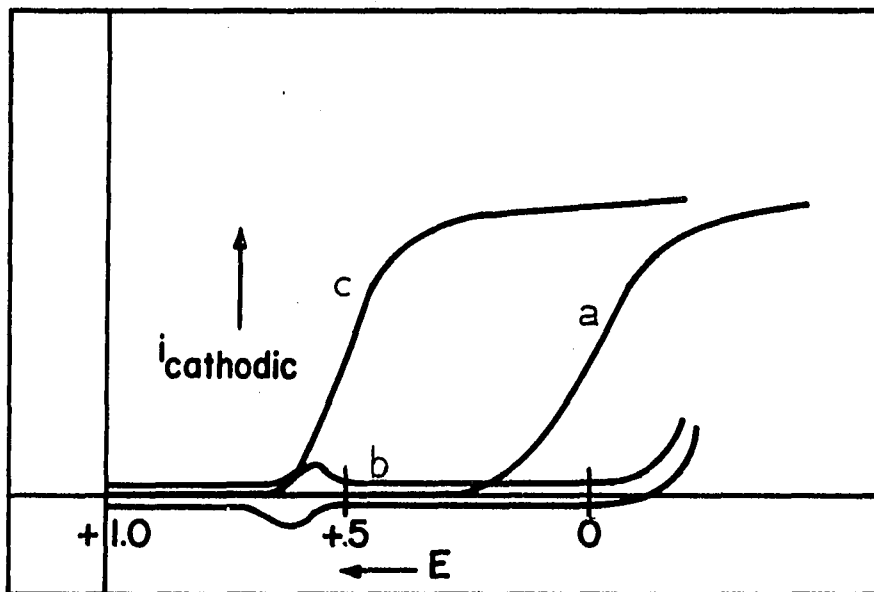
Figure I-3. Catalysis by underpotential deposit:current/
voltage scans on gold in acid solution
a) with only oxygen in solution, b) with only
Pb^{++} (10^{-4} M) in solution, and c) with both
Pb^{++} and oxygen in solution

It is therefore possible to discuss most cases of oxygen reduction catalysis in terms of a surface redox mechanism.

As can be imagined, there is more than one way to view the catalysis of oxygen reduction. Evans (42) first introduced the advantage of two site -- or side on -- oxygen adsorption. Platinum, which is by no means inert to oxygen, is thought to adsorb oxygen in this manner. In the gas phase, platinum adsorbs oxygen dissociatively above 150°K (76). This indicates that two adjacent platinum sites are needed to adsorb oxygen. This two-site adsorption then results in scission of the O-O bond. In this mechanism, superoxide ion and peroxide are both avoided as well as their concomitant potential limitations. Evidence for this pathway on platinum has been obtained only in strenuously purified solutions (15). This side on mechanism as visualized by Evans, and later Goldstein and Tseung (44), took place primarily in basic solution as shown in Figure I-4. According to Evans' views in basic solution, hydroxyl ions were good candidates for surface species. He also considered it likely that surface exchange of these ions was very fast. Since the transfer of protons is normally considered to be very fast, the whole reaction is concerted and limited only by adsorption of oxygen at a location where two sites are adjacent and available for bonding. The resulting four electron reaction is shown in equation I-21.
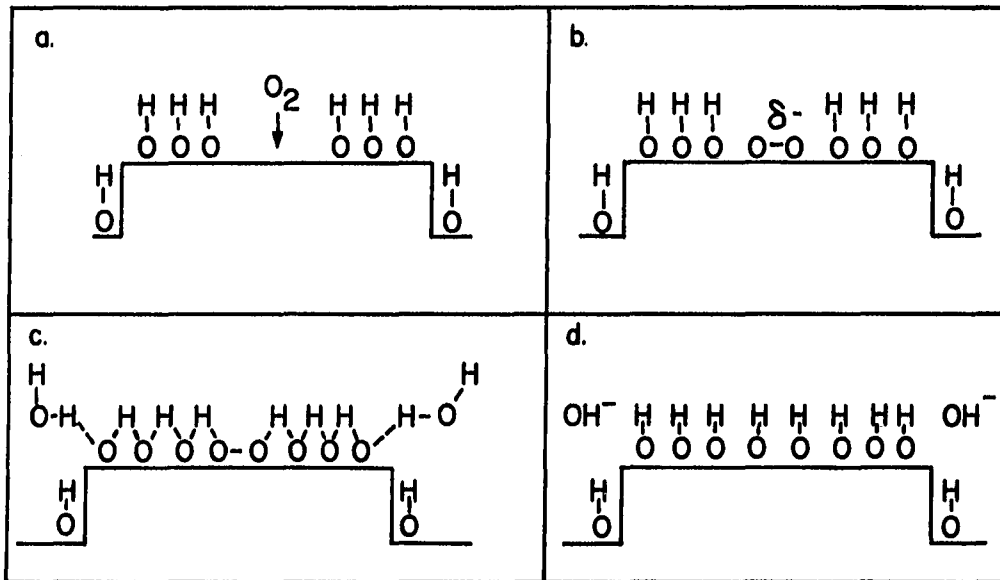
Figure I-4. Two-site oxygen adsorption:

a) shows the site necessary for adsorption and the approaching oxygen

b) adsorption occurs with possible charge transfer

c) proton switching occurs

d) bond is broken and surface hydroxides are formed

$$O_2 + 2 H_2O + 4 e^- \rightleftharpoons 4 OH^- \qquad E_o = +0.15 \qquad \text{(I-21)}$$

This view is supported by electrochemical and fuel cell studies which indicate a rate of oxygen reduction proportional to the square root of oxygen pressure. Note that in this case adsorption of oxygen cannot be the slow step, this step must happen after the O-O bond is broken. A series of papers by Tseung et al. related this mechanism to magnetic properties of transition metal oxide electrodes. These authors found that in concentrated base and at high temperatures ($\sim$ 220 C) electrodes catalyzed with nickel oxide operated reversibly with respect to oxygen (45). An interesting feature found in this work was the increase of the reversible potential with increasing temperature, contrary to thermodynamic predictions. Note was made here of the change of NiO from antiferromagnetic to paramagnetic at about 230 C. The idea of paramagnetic materials having an effect on catalysis was not unknown (77) and since oxygen is paramagnetic, they decided to investigate this phenomena further. The continuing series of experiments tested electrode catalysts known to be paramagnetic at room temperature. Eventually, a catalyst was found whose open circuit potential equalled the oxygen reversible potential at room temperature (47). Although this material showed low currents at room temperature, at 170 C its performance surpassed that of a platinum black electrode (52). Other

work on these materials gave different results (53) and the nonreproducible nature of the electrode precluded proper kinetic analysis. Thus, at this point it is impossible to say if this catalysis is due to magnetic properties or to other changes in the bonding of oxygen at the surface. These and other studies attempted to relate characteristics of the oxides to catalytic activity but offered only generalizations with respect to pathway determination. Oxygen reduction was also evaluated as a function of magnetic properties of certain metal macrocyclic compounds (60).

One characteristic of these catalysts was the need to deposit them on a conductive substrate of wire mesh or carbon. The effect of the substrate was considered negligible but this is not necessarily the case (59). This problem is especially significant for carbon electrodes where the catalyst does not completely cover the substrate as is the case with a wire mesh support.

These two concepts converged in recent work involving catalysts with more than one metal macrocylic entity, similar to biological materials. Electron transfer in biological systems is very fast. Even so, oxygen reduction is irreversible (probably as much to regulate metabolism as for other reasons). Recent work done with cytochrome C oxidase determined that the active site for oxygen reduction was a bimetallic site (73). The process was described by

the following equations:

$$A_3^+ - Cu^{+2} + e \rightleftharpoons A_3^+ - Cu^+ \qquad (I-22)$$

$$A_3^+ - Cu^+ + e \rightleftharpoons A_3 - Cu^+ \qquad (I-23)$$

$$A_3 - Cu^+ + O_2 \rightleftharpoons A_3^+ - O_2^= - Cu^{+2} \qquad (I-24)$$

$$A_3^+ - O_2^= - Cu^{+2} + H^+ \rightleftharpoons A_3^+ - HO_2^- - Cu^{+2} \qquad (I-25)$$

$$A_3^+ - HO_2^- - Cu^{+2} + 3H^+ + 2e^- \xrightarrow{\text{fast}} \text{products} \qquad (I-26)$$
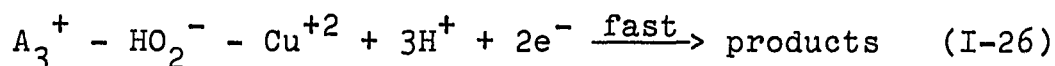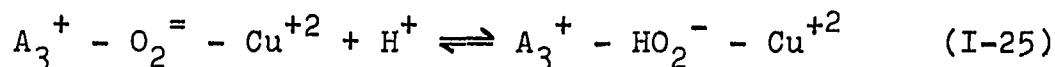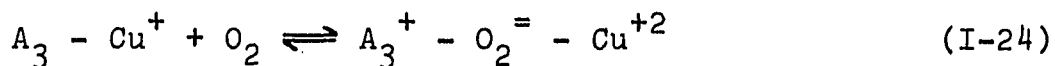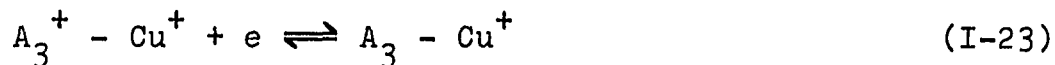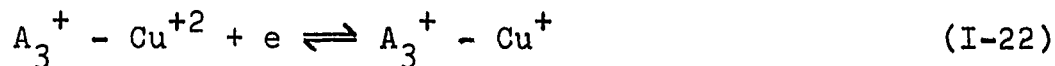
where $A_3^+ - Cu^{+2}$ describes the functional unit of cytochrome A_3. The main points in this mechanism are that 1) although electrons transfer one at a time to the complex, their transfer to oxygen in adsorption is almost simultaneous, 2) two metal centers are necessary for complete reduction to water, and 3) a bridged structure seems necessary to promote the metal-to-oxygen interaction required to cleave the oxygen double bond. Similarly, studies of oxygen reduction in homogeneous solution obtain the following reaction scheme (78):

$$O_2 + Fe(II)P \cdot L_2 \longrightarrow Fe(II)P \cdot LO_2 + L \qquad (I-27)$$

$$Fe(II)P \cdot L \cdot O_2 + Fe(II)P \cdot L_2 \longrightarrow (Fe(III)P \cdot L)_2$$
$$\cdot O_2^= + L \qquad (I-28)$$

$$(Fe(III)P \cdot L)_2 \cdot O_2^= + H^+ \longrightarrow (Fe(III)P \cdot L)_2 \cdot HO_2^- \qquad (I-29)$$

$$(Fe(III)P \cdot L)_2 \cdot HO_2^- + 3H^+ + 2e^- \xrightarrow{\text{fast}} \text{products} \qquad (I-30)$$
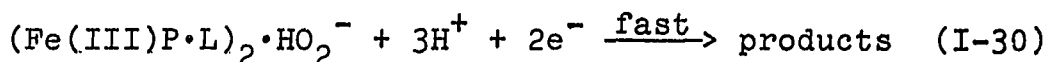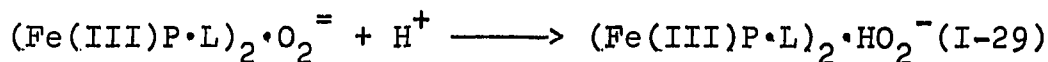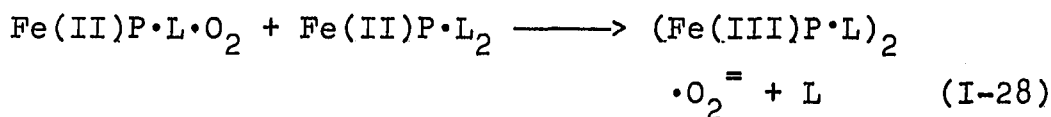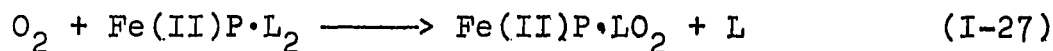
where P stands for a porphyrin complex. Accordingly, complete reduction of oxygen happens only from the

$(Fe(III)P \cdot L)_2 \cdot O_2^=$ (μ-oxo) structure. If the product of the first step is prohibited from addition of another porphyrin, oxygen will not be reduced to water. This restriction can be accomplished three ways: 1) by sterically blocking the second site; 2) by rigidly supporting the complexes -- preventing interaction; and 3) by reducing the temperature. These oxygen reduction studies gave an order of two with respect to the metal centers; thus, it seemed worthwhile to test synthetic catalysts with two bridged metal macrocycles. Collman et al. (70) synthesized several face-to-face porphyrin complexes for this exact purpose. The resulting oxygen reduction was dependent not only on the metal used but also on the distance between the two centers. Cobalt provided effective catalysis while palladium did not, and a four atom doubly bridged complex was a much more effective catalyst than a seven atom doubly bridged complex. Further studies indicated that two separate redox waves occurred in the current/voltage scan of the catalyst alone. The peak in oxygen reduction overlapped the foot of the second reduction wave of the cobalt, indicating that the complex had to be in the doubly reduced state before oxygen adsorption and subsequent reduction could take place. This corresponds to the earlier work with biological materials and the mechanism

given was very close to that shown in equations I-22→I-26. The result was four-electron reduction of oxygen with very little peroxide detected. It thus appears that for oxygen to undergo direct four-electron reduction, a dual-site catalyst must be available that can simultaneously adsorb oxygen and transfer two electrons. The catalyst must then stabilize the two species formed by cleavage of the O-O bond.

Though there have been many attempts to describe oxygen reduction in terms of properties of electrocatalysts, few have endeavored to first scrutinize the characteristics of the oxygen molecule. This deficiency was alleviated by Goddard in a very lucid description of simple oxygen interactions (79). Figure I-5 shows a simple picture of two oxygen atoms joining to form an oxygen molecule. The characteristic double bond has been replaced by a sigma bond and two pi bonds containing three electrons each. This makes each oxygen a diradical with the radicals held 90 degrees to each other. On adsorption the radical centers will interact with the surface. A simple example of this is given in Figure I-6 in which oxygen reacts with an olefin. The first step is simple with interaction of two radical centers; however, the second step involves a strain energy required to rotate the second radical center by 90 degrees. If the oxygen cannot overcome the strain energy or is
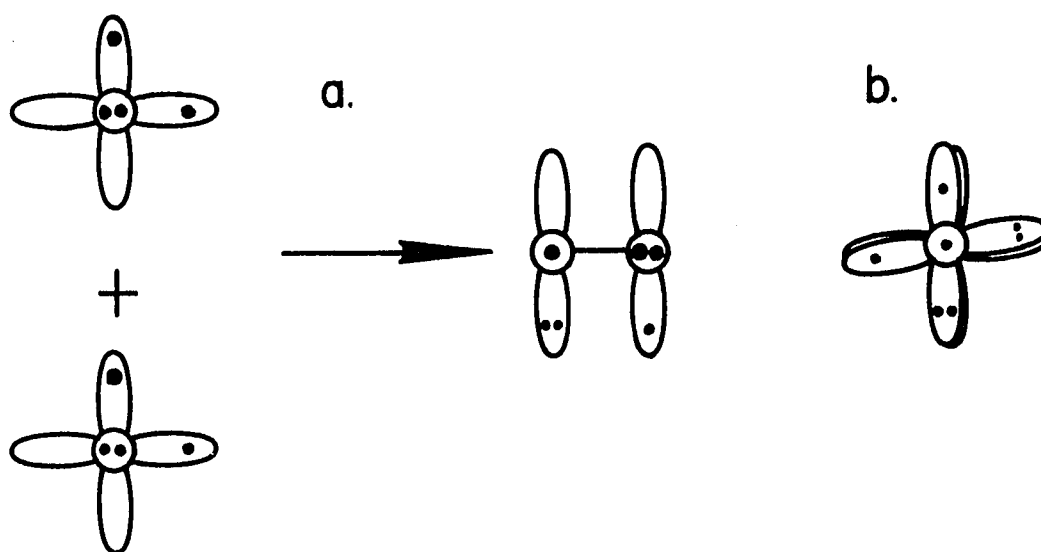
Figure I-5. Oxygen atom interaction: (a) to form an
oxygen molecule, (b) Newman projection
viewed along the O-O bond
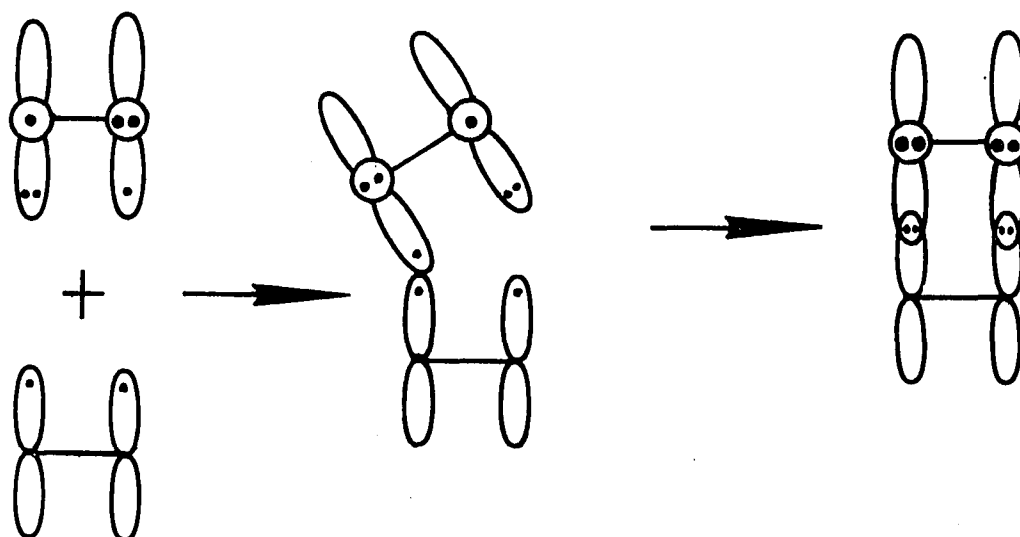
Figure I-6. Oxygen-olefin interaction

otherwise denied interaction with the second site, the O-O

bond remains intact, forming superoxide and peroxide species.

However, as shown in figure I-5, if the second interaction

takes place, the O-O bond loses all double bond character

as is necessary to enhance bond breakage. This interaction

is general and can be applied to other types of oxygen-

substrate interactions. Applying this to oxygen reduction,

one would predict that catalysts that operate by the dual-

site adsorption would not form any dioxygen species as

products. Similarly, those which use the single-site pathway

will form superoxide and peroxide and must rely on speedy

decomposition of these to obtain water as the final product.

This explanation also agrees with the finding that oxygen

will best bind metals with empty or half empty dz^2 orbitals

while other interactions necessarily involve the pi anti-

bonding orbitals of oxygen.

B. Rotating Ring Disk Electrode

The rotating ring disk electrode (RRDE) has been used

to study intermediates, determine end products, and elucidate

the kinetics of electrode reactions. Figure I-7 shows a

typical ring-disk electrode while Figure I-8 shows the

fluid flow to the disk surface. The electrolyte is entrained

from the bulk up to the electrode surface where centrifugal

force spins it out across the face, parallel to the surface,
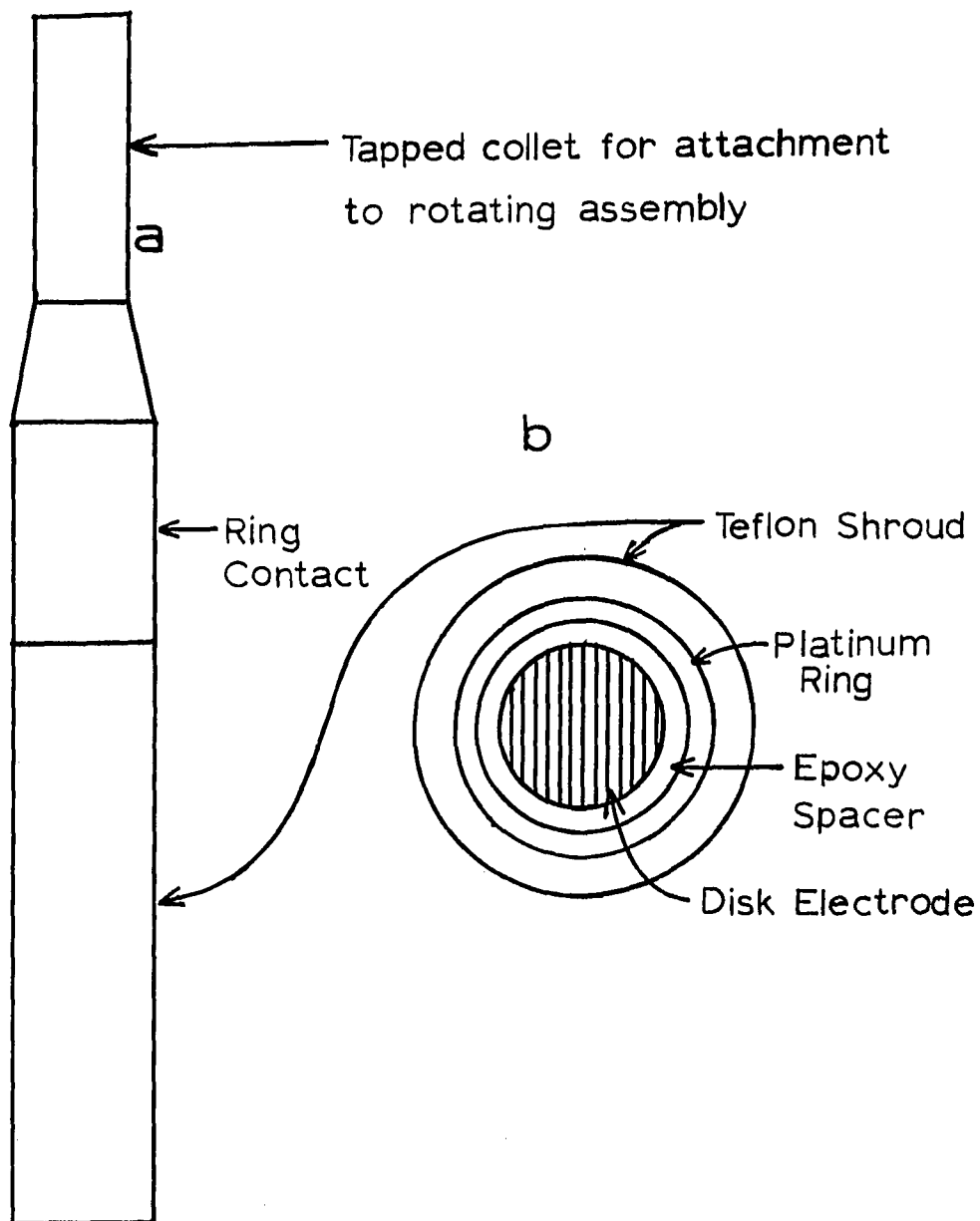
Figure I-7. Rotating ring disk electrode: a) side view,
b) electrode face
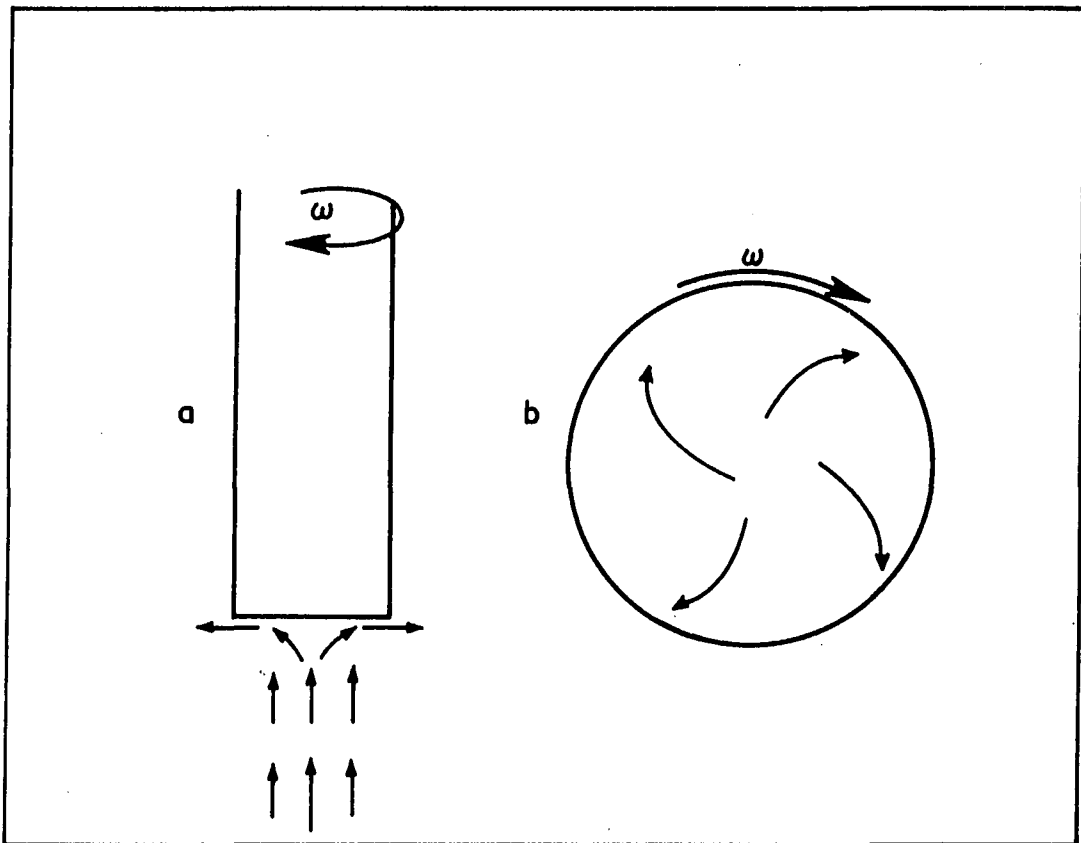
Figure I-8. Flow patterns at a rotating disk.
a) Axial and radial flow of fluid past a
rotating disk surface, b) angular flow with
rotation as shown viewing the disk face from
a stationary position

and then back into the solution bulk. According to this
pattern, the electroactive species are first allowed to react
at the disk and are then swept across the concentric ring,
where further electrochemistry can happen. If the ring is
set at a potential to reverse the electrochemical process
occurring at the disk, a certain fraction of the disk
product will react at the ring. This fraction -- called the
ring/disk efficiency -- designated N, is a function of the
geometry of the RRDE. The characteristics and utility of
these electrodes have been reviewed in two recent
publications (80,81). The primary advantage of a RRDE is
the quantitative description of mass transport to the
electrode surface. At a constant rotation speed (ω), the
flow of fluid past the disk surface is constant. With a
constant flow, the flux of electroactive species to the
electrode surface can be represented by two regimes; a
convection region, and a diffusion region.[1] The diffusion
region is a thin layer immediately adjacent to the electrode
surface where viscous forces control the flow processes.
Outside this region, all flow is convective. Material flux
through the diffusion layer is much slower than convective
flux up to this layer; thus, concentration gradients develop

---

[1]This assumes that the concentration of supporting
electrolyte is large enough to preclude electromigration.

only inside the diffusion layer. Material flux being slower within the diffusion layer, the limiting process is considered to be diffusion. The Levich equation (82) describes the current at a rotating disk electrode.

$$i = \frac{n\,F\,A\,D\,(C^b - C^s)}{\delta} \tag{I-31}$$

n = number of electrons transferred

F = Faraday constant

A = electrode area

D = diffusion coefficient of the electroactive species

δ = diffusion layer thickness

C^b = bulk concentration

C^s = concentration at the electrode surface

δ is given by

$$\delta = 1.61\ D^{1/3}\ \nu^{1/6}\ \omega^{-1/2} \tag{I-32}$$

where ν = kinematic viscosity, and ω = rotation speed in radians/sec. This points out another feature of the electrode, the constant diffusion layer thickness across the electrode surface. Due to this feature, and to the fact that there are no concentration gradients outside the diffusion layer, the surface is said to be equally accessible. Thus, the current flow is constant across the whole disk electrode and under normal conditions varies only with bulk concentrations and ω. At a constant ω, the current is said to be at a limit when $C^s \to 0$. This current is the mass

transport limited current (i_ℓ)

$$i_\ell = \frac{n\,F\,A\,D\,C^b}{\delta} \qquad\qquad (I\text{-}33)$$

Since this current is related to obtainable values, it can
be calculated. The fact that it is related to C^b makes i_ℓ
useful for analytical purposes. i_ℓ is also a function of
$\omega^{1/2}$ and a plot of i_ℓ versus $\omega^{1/2}$ is often considered a
check for proper operation of the electrode. As an example
of the use of an RRDE, Figure I-9 shows current/voltage
scans of a $Fe(III)(CN)_6^{-3}/Fe(II)(CN)_6^{-4}$ solution. In this
example, the voltage is scanned as a triangular wave while
the resulting current at the disk is recorded.
Simultaneously, the potential of the ring is held at a
value that will oxidize $Fe(II)(CN)_6^{-4}$. The resulting scans
show the type of data recorded with a RRDE. The reaction
is,

$$Fe(CN)_6^{-3} + e^- \rightleftharpoons Fe(CN)_6^{-4} \qquad\qquad (I\text{-}34)$$
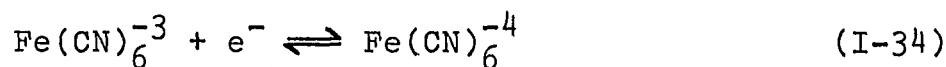
At the point where $E = E_{eq}$, i disk should be zero and the
ring current is that measured with no disk current. When
the disk potential is more negative, the reduced species is
being formed and its concentration in the flow stream going
to the ring is increased. This results in an increased
ring current and the increase is directly proportional to
the disk current. When the disk potential is higher than
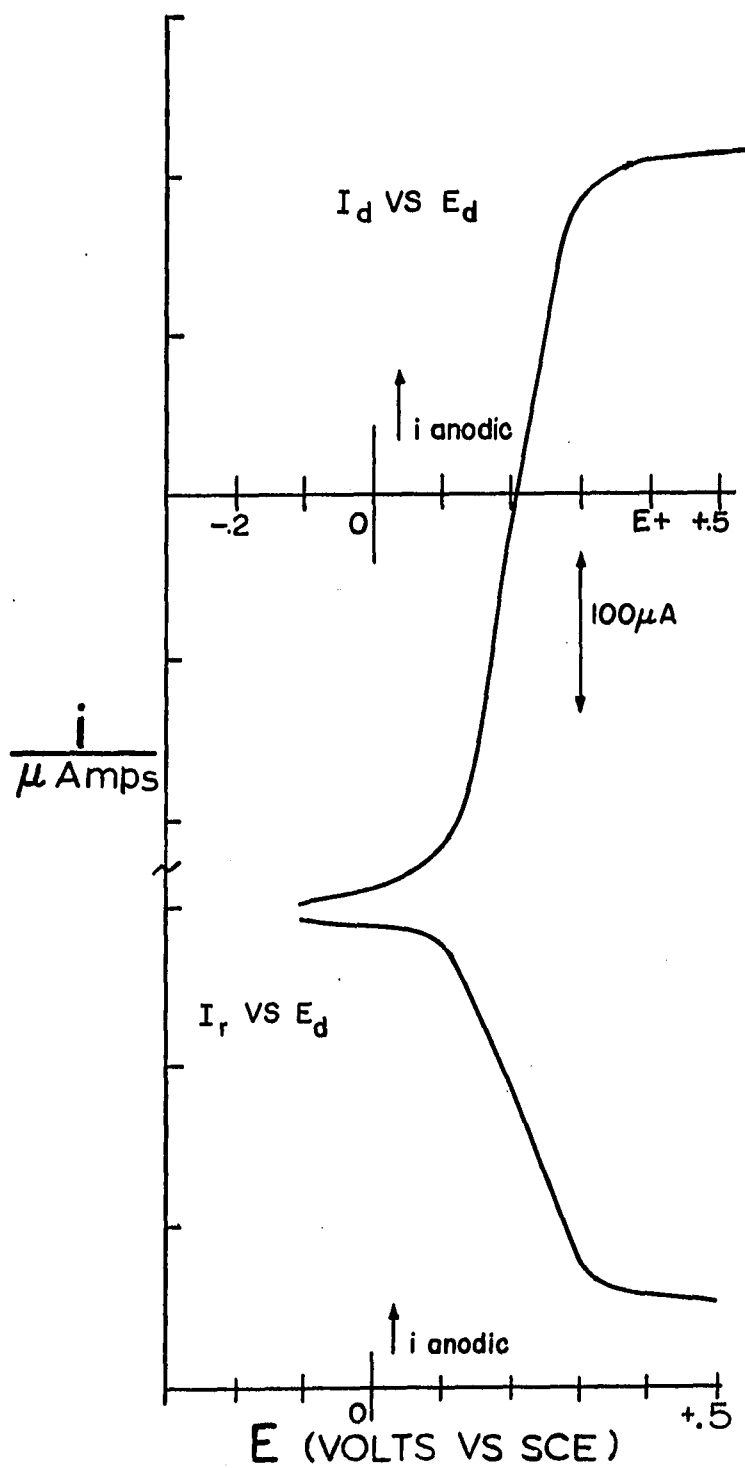
Figure I-9. Ring and disk currents in ferri/ferrocyanide solution

E_{eq}, less of the reduced species gets to the ring and the ring current decreases. The ratio between the ring and disk currents -N- can then be calculated and compared to the theoretical value calculated according to ref. (83). More on the use of the ring disk electrode will be included in the section on theoretical development.

C. Carbon Paste Electrode

The carbon paste electrode, initially pioneered by Adams (84-87) has several advantages for electrochemical studies. The electrode is made by mixing graphite with Nujol (spectral quality mineral oil) until a thick paste results. The paste is mounted into an electrode holder and can be used like a solid electrode. Almost no pretreatment is needed unless the reaction products form a surface film. The surface is then easily renewed by scraping out the old paste and depositing a new electrode. The scan range is wider than for any other electrode except mercury in alkaline solution, and similar to mercury, the background is very low. A study of the relative merits of differential pulse measurements with respect to scanning voltammetry indicated that both methods had similar detection limits (88). This is indicative of the low level of background currents on a carbon paste electrode. Its residual current in a scanning mode is lower than on either pyrolytic carbon

or glassy carbon (89). Carbon paste electrodes have been
adapted to nonaqueous solutions (90). Carbon paste
electrodes were quickly introduced to rotating disk
electrodes (86) and have since then been used for several
studies of oxygen reduction (91-94). Initial studies of
oxygen reduction consisted of comparing the change in over-
potential at a constant current when catalysts were added
to the paste (91,92). Only recently was an attempt made
to obtain some kinetic parameters for oxygen reduction on a
carbon paste electrode (94). This work studied activated
carbons which are known to have different properties than
graphite. Thus, no definitive work has yet been done to
describe oxygen reduction at a graphite paste electrode.
Oxygen reduction on most carbon electrodes exhibits certain
general characteristics. A two wave reduction process is
generally observed beginning at a potential of about -0.4
volts in basic solution with the second wave beginning at
about -1.0 volts. Their performance is even poorer in acid
and neutral solutions. This change in performance is
depicted in Figure I-10 which is a Pourbaix-type diagram.
The potential plotted is the reversible potential for
reactions while for electrodes it is the half wave potential.
This figure sums up a large portion of the work so far
reported and shows the improved performance of gold and
mercury as well as carbon in more basic solutions. For this
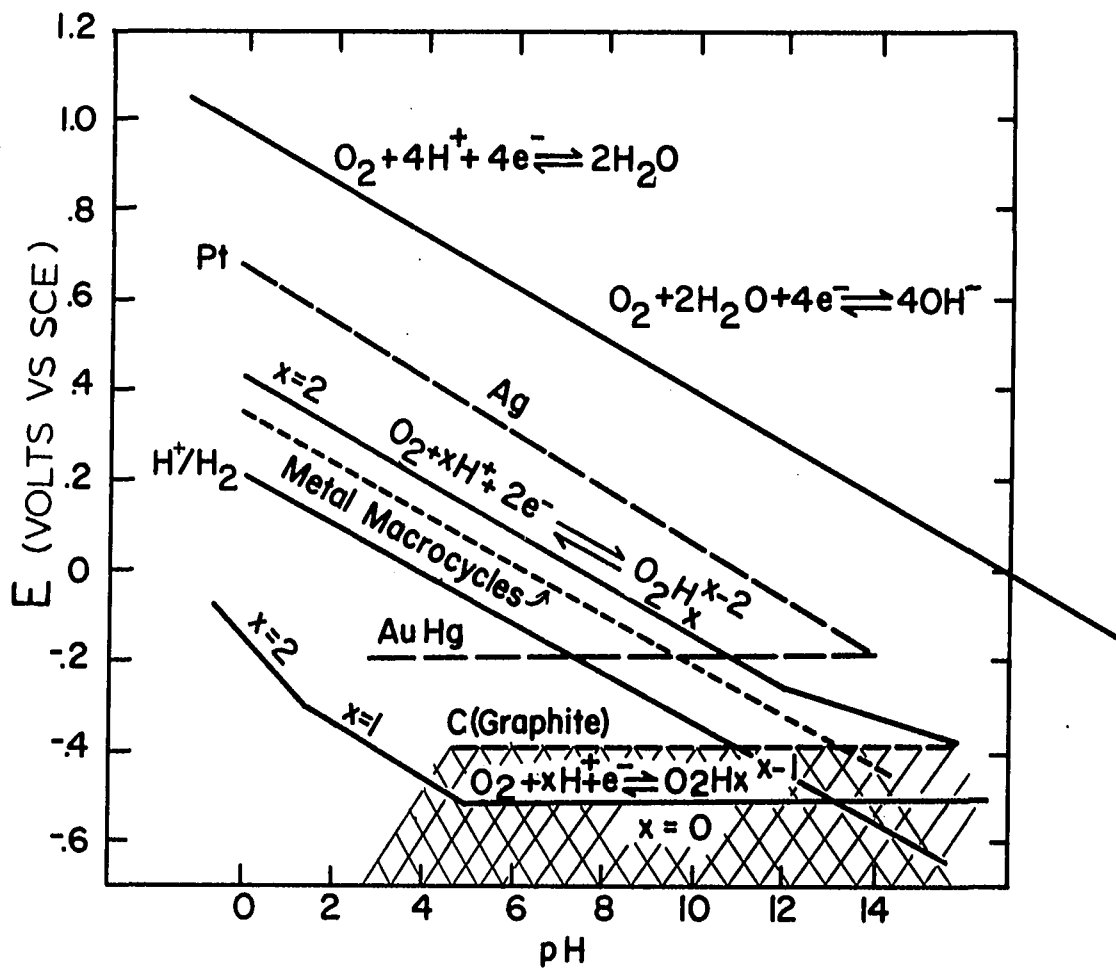
Figure I-10. Pourbaix diagram of oxygen electrochemistry.
Solid lines represent reversible potentials,
dashed lines indicate approximate half-wave
potentials (66,95), x indicates the number
of protons transferred per unit reaction.
The cross-hatched region is the experimental
range for various kinds of carbon electrodes

reason, and because more materials can withstand oxygen reduction in basic solution, most recent studies have been done in this media. Thus, much has been recently accomplished on the problem of oxygen reduction. There still, however, remains many loose ends to be tied together and many more catalysts to be tested in the milder conditions of basic solutions.

D. Statement of the Problem and Objectives

With the advent of fuel cells and oxygen electrolysis cells, the problem of oxygen reduction has been attacked with renewed vigor. Research in this area has frequently used solid metal electrodes (that is, platinum, gold, palladium, etc.) and has been done under strict conditions of purity. The electrodes are frequently preconditioned to establish a particular surface. In such studies significant strides have been made with respect to mechanism determination. Equally significant is the work done on catalysts deposited on electrode substrates, especially carbon. Due to the cost of noble metals, no industrial or commercial process could use solid platinum or palladium or other noble metals for oxygen reduction electrodes. For this reason, most large scale uses of these catalysts involve their dispersion on a conductive substrate. Graphite and other forms of carbon are often used because of their conductivity, low cost, and stability. The

frequent use of graphite as an electrode and as an electrode substrate necessitates a thorough study of its characteristics under the reaction conditions. This has been done for oxygen reduction on several forms of solid carbon electrodes. However, carbon and graphite paste electrodes have been less thoroughly studied. The study of oxygen reduction catalysis on graphite pastes (96) has been limited to observations of potential and current changes as catalysts were added. One recent study using an active carbon paste in an RRDE setup has shown the utility of the ring electrode in detecting the amount of peroxide formed as the final product (94). The ability of an RRDE had previously been shown using solid electrodes (15-26) as discussed earlier. Thus, the use of a graphite paste electrode in an RRDE configuration should give additional information on oxygen reduction at this electrode. Studies of oxygen reduction at catalyzed carbon electrodes have been published (60-71, 97,98), but none have obtained the information available to an RRDE. In work done by Morcos (97) a thin film of silver electrodeposited on graphite was found to give greater currents than a solid silver electrode of the same area. These data were explained on the basis of a more active form of silver in the deposited catalyst as opposed to the solid silver electrode. Thus, it appears that the catalysis of a metal catalyst electrodeposited on carbon may be greater

than that of the solid metal. This phenomenon deserves further study on a wider basis. Other electrodeposited metals should be studied for a similar effect.

The primary purpose of this research is to increase the understanding of the catalysis of oxygen reduction. Since electrode substrates are frequently carbonaceous materials, a graphite paste electrode will be used for this study. The advantages of the RRDE are significant and will be used to hold the graphite paste. Most useful electrodes require catalysts to enhance the rate of oxygen reduction. Thus, after a thorough study of oxygen reduction on the graphite paste, the characteristics of several known catalysts will be studied. These catalysts will be in some way deposited on the graphite paste. Their performance for oxygen reduction will be compared to their respective bulk characteristics when possible. And finally, mechanisms will be discussed when warranted by the data.

II. THEORETICAL DEVELOPMENT

By making models, one acquires a more complete under-
standing of any phenomena. If one can envision the process
that occurs, then the theory to describe it can be developed.
With the theory, one can obtain values for rate constants
and other diagnostic parameters. Comparison of these
results with experimental data could be used to test the
theory. Finally, knowledge of the proper theory allows one
to manipulate the reaction in desired manners.

In this section the theories used in this study, along
with pertinent modifications, will be described. The theory
of electron transfer (insofar as it is related to this work)
will be described in the section on heterogeneous kinetics.
Then mass transfer restrictions will be introduced detailing
the use of the Levich equation. This theory will then be
applied to oxygen electrochemistry, and deviations and
corrections to the basic equations will be described either
in this section or in the appropriate appendix.

A. Heterogeneous Kinetics

Considering a first order single electron transfer
reaction such as

$$Ox + e^- \underset{k_{anod}}{\overset{k_{cath}}{\rightleftharpoons}} Red \qquad\qquad (II-1)$$

the current can be described by equation II-2

$$i = n \, F \, A \, (\text{Net Rate}) \tag{II-2}$$

n = number of electrons transferred

F = Faraday constant (96500 coul/equiv)

A = electrode surface area

The net rate is given by,

$$\text{Rate} = k_{cath} \cdot C^S_{ox} - k_{anod} \cdot C^S_{Red} \tag{II-3}$$

where k's are cathodic and anodic rate constants and C's
are concentrations of oxidizing and reducing species.
The superscript on the concentration terms indicate that
surface concentrations are being used. The rate constants
can be described by a potential dependent and a potential
independent term, as shown in Appendix A. Combining
equations II-2 and II-3 results in the following,

$$i = F \, A \, (k_{cath} \, C^S_{ox} - k_{anod} \, C^S_{Red}) \tag{II-4}$$

where, by convention, cathodic current is considered
positive while anodic current is negative. Substituting
for k_{cath} and k_{anod} from Appendix A, the following is
obtained,

$$i = F \, A \, k_o \left[\exp\left\{ \frac{-\beta F (E-E_o)}{RT} \right\} C^S_{ox} - \exp\left\{ \frac{(1-\beta)F(E-E_o)}{RT} \right\} C^S_{Red} \right] \tag{II-5}$$

This equation describes the current as a function of the difference between the actual electrode potential and the standard electrode potential. However, it is often more convenient to relate potentials to the equilibrium potential. At equilibrium the current is equal to zero and surface concentrations are equal to bulk concentrations. In this situation, the rates of the anodic and cathodic currents are equal; their value is designated the exchange current (i_o).

$$F A k_o \exp\left\{\frac{-\beta F(E_{eq}-E_o)}{RT}\right\} c_{ox}^b =$$

$$F A k_o \exp\left\{\frac{(1-\beta)F(E_{eq}-E_o)}{RT}\right\} c_{Red}^b = i_o \qquad (II-6)$$

Solving these equations for the concentration terms, the following two equations are obtained:

$$c_{ox}^b = \frac{i_o}{F A k_o} \exp\left\{\frac{-\beta F(E_o-E_{eq})}{RT}\right\} \qquad (II-7)$$

and

$$c_{Red}^b = \frac{i_o}{F A k_o} \exp\left\{\frac{(1-\beta)F(E_o-E_{eq})}{RT}\right\} \qquad (II-8)$$

By multiplying the first section of equation II-5 by c_{ox}^b/c_{ox}^b and the second section by c_{Red}^b/c_{Red}^b equation II-9 is obtained.

$$i = F A k_o \left[\exp -\left\{\frac{\beta F(E-E_o)}{RT}\right\} \frac{c_{ox}^s}{c_{ox}^b} \cdot c_{ox}^b - \exp\left\{\frac{(1-\beta)F(E-E_o)}{RT}\right\} \frac{c_{Red}^s}{c_{Red}^b} \cdot c_{Red}^b\right] \qquad (II-9)$$

Using equations II-7 and II-8 in equation II-9, gives i

in terms of i_o and $E-E_{eq}$.

$$i = i_o \left[\frac{C^s_{ox}}{C^b_{ox}} \exp\left\{ \frac{-\beta F(E-E_{eq})}{RT} \right\} \right. $$
$$\left. - \frac{C^s_{Red}}{C^b_{Red}} \exp\left\{ \frac{(1-\beta)F(E-E_{eq})}{RT} \right\} \right] \qquad (II-10)$$

Equation II-10 is the general relation between current and

electrode potential for a one electron transfer reaction.

B. Mass Transport Limitations

The concentration of an electroactive species at a

surface is a function not only of its rate of use but also

of its replenishment rate. Therefore, a relationship

between surface concentration and bulk concentration must

be developed. For this general situation, the flux of

electroactive species to a surface is dependent on

convection and diffusion fluxes. Appendix B shows the

method of obtaining a solution to the flux equation for a

rotating disk electrode (RDE). Accordingly, cathodic

current at an RDE is given by

$$i_c = \frac{n F A D (C^b_{ox} - C^s_{ox})}{\delta} \qquad (II-11)$$

where D is the diffusion coefficient of the electroactive

species, δ is the diffusion layer thickness given by

$$\delta = 1.61 \; \nu^{1/6} \; D^{1/3} \; \omega^{-1/2} \tag{II-12}$$

where ω is the rotation rate in radians/sec and ν is the kinematic viscosity. All other terms have their usual significance. A limiting current is established when $C^S = 0$.

$$i_{\ell,c} = \frac{n \, F \, A \, D \, C^b_{ox}}{\delta} \tag{II-13}$$

Equation II-11 can be rearranged as follows:

$$i_c = \frac{n \, F \, A \, D \, C^b_{ox}}{\delta} \left(1 - \frac{C^S_{ox}}{C^b_{ox}} \right) \tag{II-14}$$

and combining II-13 and II-14 one obtains

$$\frac{i_{\ell,c} - i_c}{i_{\ell,c}} = \frac{C^S_{ox}}{C^b_{ox}} \tag{II-15}$$

This equation describes cathodic current to a RDE, similarly anodic current could be described by

$$\frac{i_a - i_{\ell,a}}{i_{\ell,a}} = \frac{C^S_{Red}}{C^b_{Red}} \tag{II-16}$$

The final form of the one electron transfer relationship can now be obtained by substituting equations II-15 and II-16 into equation II-10

$$i = i_0 \left[\left(\frac{i_{\ell,c} - i_c}{i_{\ell,c}} \right) \exp - \left\{ \frac{\beta F(E-E_{eq})}{RT} \right\} - \right.$$

$$\left. \left(\frac{i_a - i_{\ell,a}}{i_{\ell,a}} \right) \exp \left\{ \frac{(1-\beta)F(E-E_{eq})}{RT} \right\} \right] \tag{II-17}$$

This equation is called the wave equation and is used to describe the current versus potential behavior of a single electron transfer reaction at a rotating disk electrode. The current is thus a function of the following: 1) the kinetic rate as described in i_0, 2) the rate of mass transport as given by the terms $(i_{\ell,c} - i_\ell)/i_{\ell,c}$ and $(i_a - i_{\ell,a})/i_{\ell,a}$, and 3) the electrode potential, $(E-E_{eq})$. The kinetic parameters of interest in this situation are i_0, and β. To obtain these parameters let us consider a case where only cathodic current is important, that is, anodic current is much less than cathodic current. Then we can rearrange equation (II-17) as follows:

$$i = i_c = i_0 \left(\frac{i_{\ell,c} - i_c}{i_{\ell,c}} \right) \exp \left\{ - \frac{\beta F(E-E_{eq})}{RT} \right\} \tag{II-18}$$

$$\frac{i_c \cdot i_{\ell,c}}{i_{\ell,c} - i_c} = i_0 \exp \left\{ - \frac{\beta F(E-E_{eq})}{RT} \right\} \tag{II-19}$$

$$\ell n \left(\frac{i_c \cdot i_{\ell,c}}{i_{\ell,c} - i_c} \right) = \ell n \, i_0 - \frac{\beta F}{RT} (E-E_{eq}) \tag{II-20}$$

$$E = E_{eq} + \frac{RT}{\beta F} \ln i_o - \frac{RT}{\beta F} \ln f(i) \qquad \text{(II-21)}$$

$$\text{where } f(i) = \left(\frac{i_c \cdot i_{\ell,c}}{i_{\ell,c} - i_c}\right) \qquad \text{(II-22)}$$

A plot of E $\underline{vs}$. $\ln$ f(i) is called a Tafel plot and has a slope that gives β and an intercept from which i_o can be determined. For a one electron transfer, β is often found to be near 1/2 while i_o varies widely depending on the heterogeneous rate constant (eqn. II-6).

C. Multi-electron Processes

Application of this analysis to a process with more than one step involves more rate constants, and intermediate species. As shown in Appendix C, β is replaced by α_c and (1-β) by α_a, which are given by:

$$\alpha_c = \frac{\vec{\gamma}}{V} + r\beta \qquad \text{(II-23)}$$

and

$$\alpha_a = \frac{n - \vec{\gamma}}{V} - r\beta \qquad \text{(II-24)}$$

α's are called transfer coefficients; $\vec{\gamma}$ is the number of electrons transferred prior to the rate determining step in the cathodic direction; V is the number of times the rate determining step occurs per unit reaction; and r is

the number of electrons transferred in the rate determining step.

An example of the use of these relationships can be seen by examining previous results concerning oxygen evolution on a platinum electrode. In basic solution, data show Tafel slopes of $-2 RT/F$ and $-RT/F$ (-120 and -60 mV per decade f(i), respectively). A Tafel slope of $-RT/F$ corresponds to an α_a of 1.0 and with $\beta = 1/2$ could correspond to either of the following situations: 1) an initial electron transfer step is followed by a rate limiting chemical step;

$$OH^- + S \rightleftharpoons SOH + e^- \qquad \text{(II-25)}$$

$$SOH + OH^- \rightleftharpoons SO^- + H_2O \qquad \text{slow} \qquad \text{(II-26)}$$

$$2SO^- \rightleftharpoons O_2 + 2e^- \qquad \text{(II-27)}$$

The proper values for equation II-24 are: $n = 4$, $\vec{\gamma} = 2$ ($\vec{\gamma}$ referring to the reduction process), $V = 2$, and $r = 0$;

$$\alpha_a = \frac{n - \vec{\gamma}}{V} - r\beta = \frac{2}{2} = 1$$

2) an initial step which transfers two electrons can be rate controlling.

$$S + H_2O \longrightarrow SO + 2H^+ + 2e^- \qquad \text{(II-28)}$$

$$2SO \longrightarrow 2S + O_2 \qquad \text{(II-29)}$$
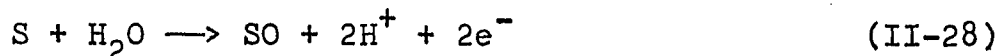
With $\vec{\gamma} = 0$, $n = 4$, $V = 2$, and $r = 2$, α_a is given as follows:

$$\alpha_a = \frac{4 - 0}{2} - 2(1/2) = 1$$

Although these two mechanisms are not the only possibilities, they are representative of the possible pathways for the case of $\alpha_a = 1$. When the Tafel slope is $-2RT/F$, $\alpha_a = 1/2$. The primary example for this case is the sequence of equations II-25 → II-27 with the first electron transfer now rate controlling. For this case, the parameters in equation II-24 are as follows: $n = 4$, $\vec{\gamma} = 2$, $V = 2$, $r = 1$ and $\beta = 1/2$.

$$\alpha_a = \frac{4 - 2}{2} - 1/2 = 1/2$$

From these examples, the use of the Tafel slope to differentiate between suspected mechanisms can be seen. For the above situations, however, the assumption was made that surface coverage by adsorbed species had no effect on the reaction. Under more common conditions, one frequently must account for the adsorption of reaction intermediates on the electrode. For these cases, one normally considers the adsorption of a species in the form of an isotherm where the concentration of adsorbed species ($\emptyset$) depends on its bulk concentration. Thus, in equation II-25, the forward

rate would be dependent not only on $C_{OH}-$ but also on the concentration of uncovered electrode sites $(1-\emptyset)$. Suppose adsorption follows a Langmuir adsorption isotherm, and that the hydroxyl radical is the primary adsorbed species (designated SOH in adsorbed form). Since adsorption and desorption of hydroxyl radical is not likely to be an important reaction (due to its instability in solution), equations II-25 and II-26 will be used to describe SOH coverage. Making the initial assumption that all SO⁻ species are rapidly used up according to II-27, the rate can be described by:

$$\overrightarrow{R}_{26} = \overrightarrow{k}_{26}\emptyset[OH^-] \qquad (II-30)$$

where $\emptyset$ is the fractional coverage of SOH. Employing the steady state approximation for SOH coverage, one can write:

$$\frac{d\emptyset}{dt} = \overrightarrow{k}_{25}(1-\emptyset)[OH^-] - \emptyset(\overleftarrow{k}_{25} + \overrightarrow{k}_{26}[OH^-]) = 0 \quad (II-31)$$

and

$$\frac{\emptyset}{1-\emptyset} = \frac{\overrightarrow{k}_{25}[OH^-]}{\overleftarrow{k}_{25} + \overrightarrow{k}_{26}[OH^-]} \qquad (II-32)$$

where $\overrightarrow{k}_{25}$ and $\overleftarrow{k}_{25}$ are electrochemical rate constants (cf. Appendix A) and the reverse of reaction II-26 is considered negligible. To illustrate this method, two limiting conditions will be examined. It will be assumed, in the first case, that reaction II-25 is in equilibrium.

That is, $\overleftarrow{k}_{25} \gg k_{26}[OH^-]$. One can then solve equation II-32

for $\emptyset$, obtaining:

$$\emptyset = \frac{K_{25}[OH^-]}{1 + K_{25}[OH^-]} \tag{II-33}$$

where $K_{25} = \overrightarrow{k}_{25}/\overleftarrow{k}_{25}$. Substituting for $\emptyset$ in equation II-30

results in the expression:

$$\overrightarrow{R}_{26} = \frac{\overrightarrow{k}_{26}[OH^-]^2 \, K_{25}}{1 + K_{25}[OH^-]} \tag{II-34}$$

Two limiting cases of equation II-34 will likewise be

considered. For very low surface coverage ($K_{25}[OH^-] \ll 1$)

equation II-34 can be rewritten:

$$\overrightarrow{R}_{26} = \overrightarrow{k}_{26} \, K_{25} \, [OH^-]^2 \tag{II-35}$$

where K_{25} can be replaced by:

$$K_{25} = K'_{25} \exp\left\{\frac{-F(E-E_{eq})}{RT}\right\} \tag{II-36}$$

remembering that $K_{25} = \overrightarrow{k}_{25}/\overleftarrow{k}_{25}$ which are electrochemical

rate constants. Assuming equation II-35 describes the net

rate, we can write (cf. equation II-2):

$$i = n F A \overrightarrow{k}_{26} K'_{25} \exp\left\{\frac{-F(E-E_{eq})}{RT}\right\} [OH^-]^2 \tag{II-37}$$

A plot of E versus ℓn i would give a slope (Tafel slope)

of $-RT/F$ and the order with respect to hydroxide ion would

be two. For the case when surface coverage is very high

($K_{25}[OH^-] \gg 1$) equation II-34 becomes:

$$\vec{R}_{26} = \vec{k}_{26}[OH^-] \tag{II-38}$$

and since $\vec{k}_{26}$ is not potential dependent[1] the Tafel slope would approach infinity. The second example using equation II-32 is that reaction II-25 is the slow step ($\overleftarrow{k}_{25} << \vec{k}_{26}[OH^-]$). Equation II-32 can be rewritten as:

$$\frac{\emptyset}{1-\emptyset} = \vec{k}_{25}/\vec{k}_{26} \tag{II-39}$$

$$\emptyset = \frac{\vec{k}_{25}/\vec{k}_{26}}{1 + \vec{k}_{25}/\vec{k}_{26}} \tag{II-40}$$

Again invoking our assumption that step II-25 is slow, we can write:

$$\emptyset = \vec{k}_{25}/\vec{k}_{26} \tag{II-41}$$

Substituting this relationship into equation II-30, one obtains:

$$\vec{R}_{26} = \vec{k}_{25}[OH^-] \tag{II-42}$$

$$i = nFA\, k'_{25}[OH^-]\, \exp\left\{\frac{-\beta F(E-E_{eq})}{RT}\right\} \tag{II-43}$$

The Tafel slope for this equation is $-RT/\beta F$ and the hydroxide ion order is one.

---

[1]Actually though this reaction involves no electron transfer, it does transport a charged species (OH^-) across the double layer. Thus, some potential dependence might be expected.

These cases used the limiting conditions of zero and complete surface coverage. The intermediate situation can be rigorously determined under Langmuir conditions by solving for $\emptyset$ in equation II-32 and substituting this $\emptyset$ into equation II-30. The solution to this problem has also been given under conditions of the Temkin isotherm (17). These situations are more complex but examples and tabulations of Tafel parameters have been compiled for the oxygen reactions (10).

D. Slow Kinetic Step

The examples considered thus far have been fairly ideal in assuming mass transport limited currents and well-defined electrode surfaces. In the following portions of this section, perturbations on this ideal system will be introduced. The effect of a slow kinetic process on mass transport equations will be shown. Then, the effect of having only a partially active electrode surface will be discussed. Finally, recycling at the electrode surface will be discussed as well as new methods to determine its occurrence, qualitatively and quantitatively.

For a kinetically controlled electron transfer reaction, one can write,

$$i = n\,F\,A\,k(C^S)^\mu \qquad\qquad\text{(II-44)}$$

where μ is the reaction order with respect to the initial (reactant) species. The current can be characterized as kinetically limited when $c^s = c^b$, that is, when further increase in the rate of mass transport does not increase the current. This limit is given by,

$$i_k = n F A k (c^b)^\mu \qquad \qquad \text{(II-45)}$$

Dividing II-44 by II-45, one obtains

$$\frac{i}{i_k} = \left(\frac{c^s}{c^b}\right)^\mu \qquad \qquad \text{(II-46)}$$

Combining this equation with equation II-15, the following equation results

$$\frac{i}{i_k} = \left(\frac{i_\ell - i}{i_\ell}\right)^\mu \qquad \qquad \text{(II-47)}$$

where the current considered is cathodic. The corresponding equation for anodic current can be acquired by combining equations II-46 and II-16. Taking logs, equation II-47 can be rearranged to

$$\log i = \log i_k + \mu \log \left(\frac{i_\ell - i}{i_\ell}\right) \qquad \qquad \text{(II-48)}$$

where a plot of $\log i$ versus $\log ((i_\ell - i)/i_\ell)$ yields an intercept of $\log i_k$ and a slope of μ. A simplification arises when $\mu = 1$. Now equation II-47 can be solved for i as shown below:

$$\frac{1}{i_k} = (1 - i/i_\ell),$$

$$i\left(\frac{1}{i_k} + \frac{1}{i_\ell}\right) = 1,$$

and

$$1/i = \frac{1}{i_k} + \frac{1}{i_\ell} \qquad\qquad\qquad (II\text{-}49)$$

Since i_ℓ is proportional to $\omega^{1/2}$, a plot of $1/i$ versus $1/\omega^{1/2}$ should be linear with an intercept of $1/i_k$ and a slope of $\omega^{1/2}/i_\ell$. Orders other than one do not give this dependence. This relationship is sometimes more useful than the Levich equation since when i_k is less than i_ℓ the Levich plot (i vs $\omega^{1/2}$) is nonlinear whereas the above relationship will still yield values of i_ℓ and i_k.

E. Partially Inactive Surface

Equal accessibility of the electrode surface is of paramount importance to the theory of a rotating disk electrode. A problem is posed when one has an electrode only part of which is active. This problem is particularly appropriate for a carbon paste electrode. A microscopic view of such a surface shows islands of carbon particles surrounded by nonconductive nujol. Figure II-1 shows the surface as described by Landsberg and Thiele (99) who developed a theory to deal with this situation. When the diffusion layer thickness is much greater than the inactive
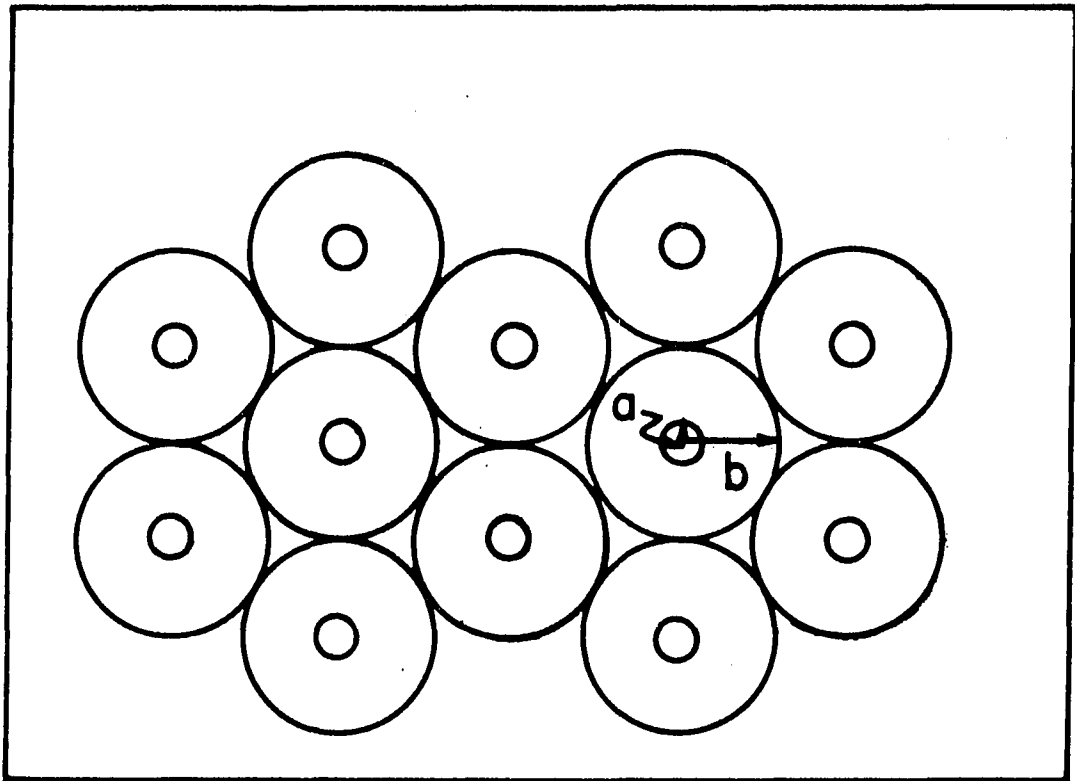
Figure II-1. Model for partially active electrode. Active
sites shown with radius a are surrounded by
inactive areas of radius b

region, the lateral diffusion length of electroactive species is much less than the axial diffusion length, and Levich behavior is found. The current per active area is much greater, however, than if the whole surface were active. With higher current densities at these active sites, kinetic limits are reached at lower absolute current levels than in the case where the whole surface is being used. As the diffusion layer thickness approaches the size of the inactive sites, nonlinear diffusion becomes appreciable and deviations from Levich behavior are found. In the limit (δ much less than the radius of the inactive regions) diffusion occurs only over the active areas and little non-linear diffusion is taking place. A solution to this problem is shown in Appendix D and the result is

$$ i = \frac{n\,F\,A\,D\,(C^b - C^s)}{\delta + |\Sigma\,A_n|} \qquad \text{(II-50)} $$

or

$$ \frac{1}{i} = \frac{\delta}{n\,F\,A\,D\,(C^b - C^s)} + \frac{\Sigma A_n}{n\,F\,A\,D\,(C^b - C^s)} \qquad \text{(II-51)} $$

where ΣA_n is a tabulated constant depending on the geometry of the active sites and δ. In the limiting current region ($C^s = 0$), a plot of $1/i$ versus $\omega^{-1/2}$ will give a straight line with a nonzero intercept. Though this theory has not been rigorously proven, it has been observed to apply for model electrodes. As mentioned earlier, this theory also

faces trouble when δ approaches b (the radius of the inactive sites) since equal accessibility of the electrode no longer holds. One can now see that a nonzero intercept on a $1/i$ versus $\omega^{-1/2}$ plot can be thought of in two ways: 1) a kinetically limited process, or 2) an electrode with a partially blocked surface.

F. Recycling

The use of the ring electrode in conjunction with the disk can be very informative with respect to end products and intermediates. It is possible to monitor the concentration of an electroactive product by setting the ring at a potential where only that species will react. However, the real power of a ring-disk electrode does not lie in the visual portrayal of the corresponding currents, but in the kinetic relationships which link these currents to a mechanism. One such treatment was developed for oxygen reduction (17,18) and has subsequently been formalized and refined (100,101). The final form takes into account catalytic recycling originally described by McIntyre (102). The reaction scheme is shown in Figure II-2. This mechanism depicts the diffusion of oxygen to the surface where it may undergo either a two or four electron reduction to peroxide or hydroxide, respectively. The peroxide can subsequently be reduced (k_3), disproportionated (k_4), or returned to the

$$O_2^b \rightleftharpoons O_2^s \xrightarrow{\substack{+2H_2O+4e^- \quad k_1}} 4OH^-$$

$$O_2^s \underset{}{\overset{+H_2O+2e^- \quad k_2}{\rightleftharpoons}} HO_2^-(ads.) + OH^-$$

$$HO_2^-(ads.) \xrightarrow{+H_2O+2e^- \quad k_3} 4OH^-$$

$$HO_2^-(ads.) \xrightarrow{k_4} O_2^s \quad (\frac{1}{2}O_2 + OH^-)$$

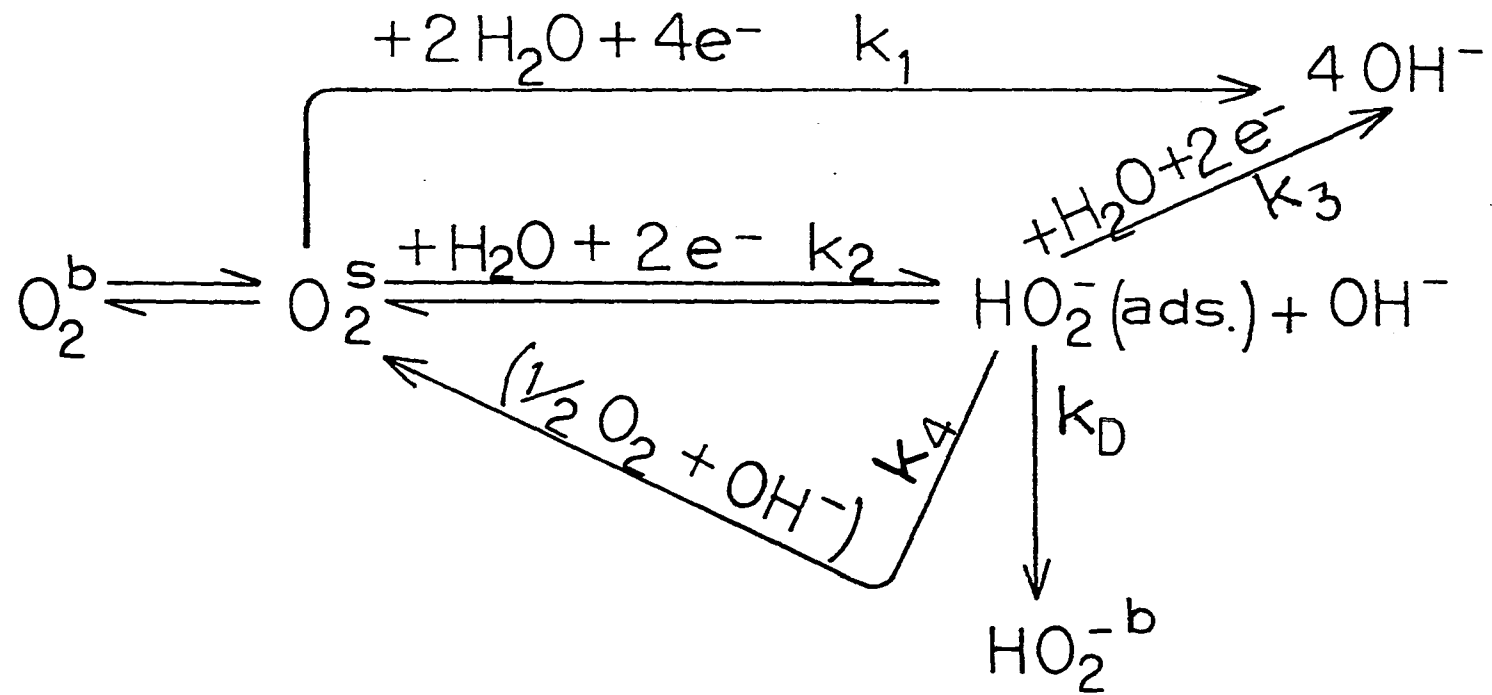$$HO_2^-(ads.) \xrightarrow{k_D} HO_2^{-b}$$

Figure II-2.   Oxygen recycling scheme

solution (k_D). The conditions assumed in this derivation are a diffusion limited regime and a bulk peroxide concentration equal to zero. Catalytic recycling is a direct result of the disproportionation of peroxide to hydroxide and oxygen. The oxygen formed by this process can react again at the electrode. Unless the desorption of HO_2^- is very slow, it will have no effect on the outcome of this analysis. Desorption is therefore considered to be in equilibrium. With concentration of peroxide equal to zero in the bulk, all desorbed peroxide will diffuse into the bulk. Thus, no second site peroxide reactions will be considered. Under these conditions, the disk current is given by

$$i_d = 2F[O_2^S] \ (2 \ k_1 + \tau \ \vec{k}_2) \qquad (II\text{-}52)$$

where τ is determined by the fraction of peroxide recycled[1] and the order with respect to oxygen is one. Assuming peroxide disproportionation to be first order and making the steady state approximation one can write

$$\vec{k}_2[O_2] = (k_3 + k_4 + k_D) \ [O_2H^-] \qquad (II\text{-}53)$$

---

[1] τ is between one and two for zero and full conversion, respectively.

The reverse of process two is neglected since at the potentials of interest, back reaction is negligible. Diffusion controlled current at the ring, where peroxide is being oxidized, is given by

$$i_r = 2 \; F \; N \; k_D \; [O_2H^-]^S \qquad \text{(II-54)}$$

where N is the ring/disk electrode efficiency.[1] k_D is given by

$$k_D = 0.62 \; A \; D^{2/3} \; \nu^{-1/6} \; \omega^{1/2} \; . \qquad \text{(II-55)}$$

Substituting for $[O_2H^-]^S$ in equation II-54 using the steady state relation, one obtains

$$i_r = 2 \; F \; N \; k_D \; k_2 [O_2]^S / (k_3 + k_4 + k_D)$$

and it follows that

$$N \; \frac{i_d}{i_r} = \frac{1}{k_D} \left(\frac{2 \; k_1}{k_2} + \tau \right) \; (k_3 + k_4) + \left(\frac{2 \; k_1}{k_2} + \tau \right) \qquad \text{(II-56)}$$

Plots of $N \; i_d/i_r$ versus $1/k_D$ are useful to elucidate the progress of oxygen reduction through the series-parallel mechanism shown earlier. Applying the final equation certain limiting conditions that are representative are shown in Figure II-3. For the case where only the four-electron reduction occurs there is no ring current and no plot is possible. When only k_2 is nonzero, the plot is as
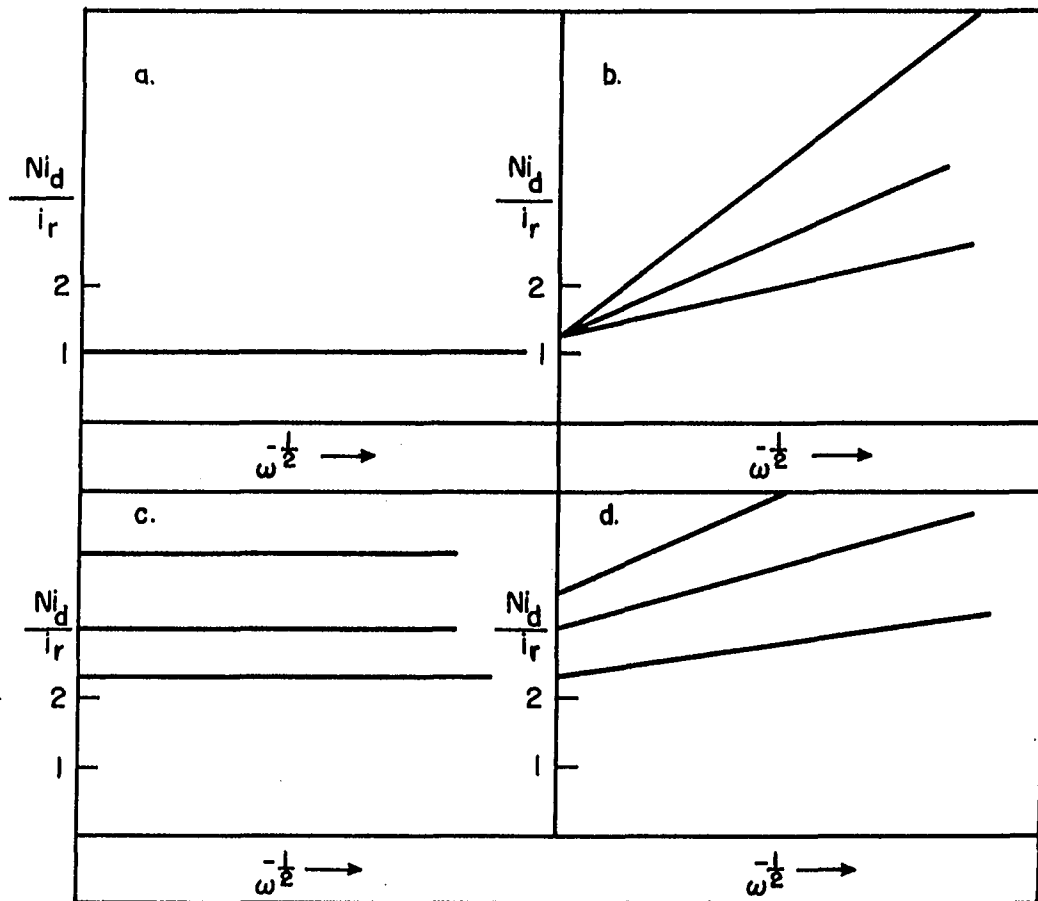
---

[1]Cf., Experimental methods section.

Figure II-3.   Theoretical N i_d/i_r curves for limiting cases:

(a) $k_1 = k_3 = k_4 = 0$, (b) $k_1 = 0$,

(c) $k_3 = k_4 = 0$, (d) all k's > 0

shown in figure II-3a. The slope is zero and the intercept equal to τ. Since no recycling occurs, τ (which will have values between one and two) is equal to one. Figure II-3b shows the plots for k_1 equal to zero. The intercept is again τ where τ can now range from one to two. The slopes are nonzero and positive and will probably be potential dependent since only k_4 and k_D will be potential independent. When k_3 and k_4 are zero, the slope is again zero but the intercept is greater than τ and dependent on the value $2k_1/k_2$, which will also likely be potential dependent. When all the reactions have nonzero rates, the slopes and intercepts will all be greater than zero and τ, respectively, and also potential dependent.

In this section the mathematics and theory used to develop the present study have been described. Since a rotating disk electrode was the primary tool, all kinetic relationships have been developed with it in mind. Adjustments of the theory, when appropriate, to account for the behavior of carbon paste electrodes have been included.

III. EXPERIMENTAL

A. Materials

All oxygen reduction experiments were done using a graphite paste electrode (GPE) as the disk of a rotating ring disk electrode (RRDE). Spectral graphite (sp-2 powder from Union Carbide) was used which had total maximum allowable impurities of 6.0 ppm. The major reported impurity was iron at .6 ppm. The oil used to make the paste was nujol (USP #21 mineral oil from Standard Oil Co.) whose major impurities were trace levels of iron and copper as determined by X-ray fluorescence. Triply distilled water was used for all solutions with the second stage boiling from a basic permanganate solution. Certified A.C.S. sodium hydroxide (Fisher Scientific Co.) was used for all 1 $\underline{M}$ NaOH solutions. Oxygen and nitrogen (from the Air Products Co.) were supplied in standard cylinders. Typical analyses of the gases showed the major contaminant in the nitrogen to be argon at 14 ppm, and in oxygen, nitrogen was the major impurity at 55 ppm. No purification was used for either gas stream. Earlier use of a heated copper-on-asbestos oxygen getter for the nitrogen stream proved unneeded. The gases were bubbled through distilled water before entering the reaction cell. This was done to prevent the evaporation of water from the reaction cell during the experiment.

Metal catalysts were deposited on the electrodes from plating solutions of the respective metals. A 10% platinic chloride solution (Reagent grade from Fisher Scientific Co.) was diluted to 0.1% in 1 $\underline{M}$ HCl, and a 0.4% auric chloride solution was made using chlorauric(III) acid trihydrate (Reagent grade from Fisher Scientific Co.). Silver nitrate, sodium cyanide (Reagent grade from the Baker Chemical Co.) and sodium carbonate (Certified A.C.S. from Fisher Scientific Co.) were used to prepare the silver plating solution of 0.04% silver. All metal catalysts were electrodeposited onto the graphite paste. In addition to this, silver and platinum were reduced in an aqueous graphite slurry to provide an additional method of catalyst deposition. The metal macro-cyclic compounds were introduced directly into the solution used. The cobalt and iron porphyrin catalysts were furnished by Ted Kuwana and Ray Chan at Ohio State University, Columbus, Ohio (66,68). The porphyrins were qualitatively identified using U.V./vis. spectrophotometry.

The electrochemical cell used is shown in Figures III-1 and III-2. Figure III-1 shows the body of the cell. The water jacket is shown in the side view while the five ancillary ports are shown in the top view. The central opening accommodates the RRDE while the side ports hold the gas dispersion tube (Figure III-2a), the counter electrode holder (Figure III-2b), and the reference electrode salt
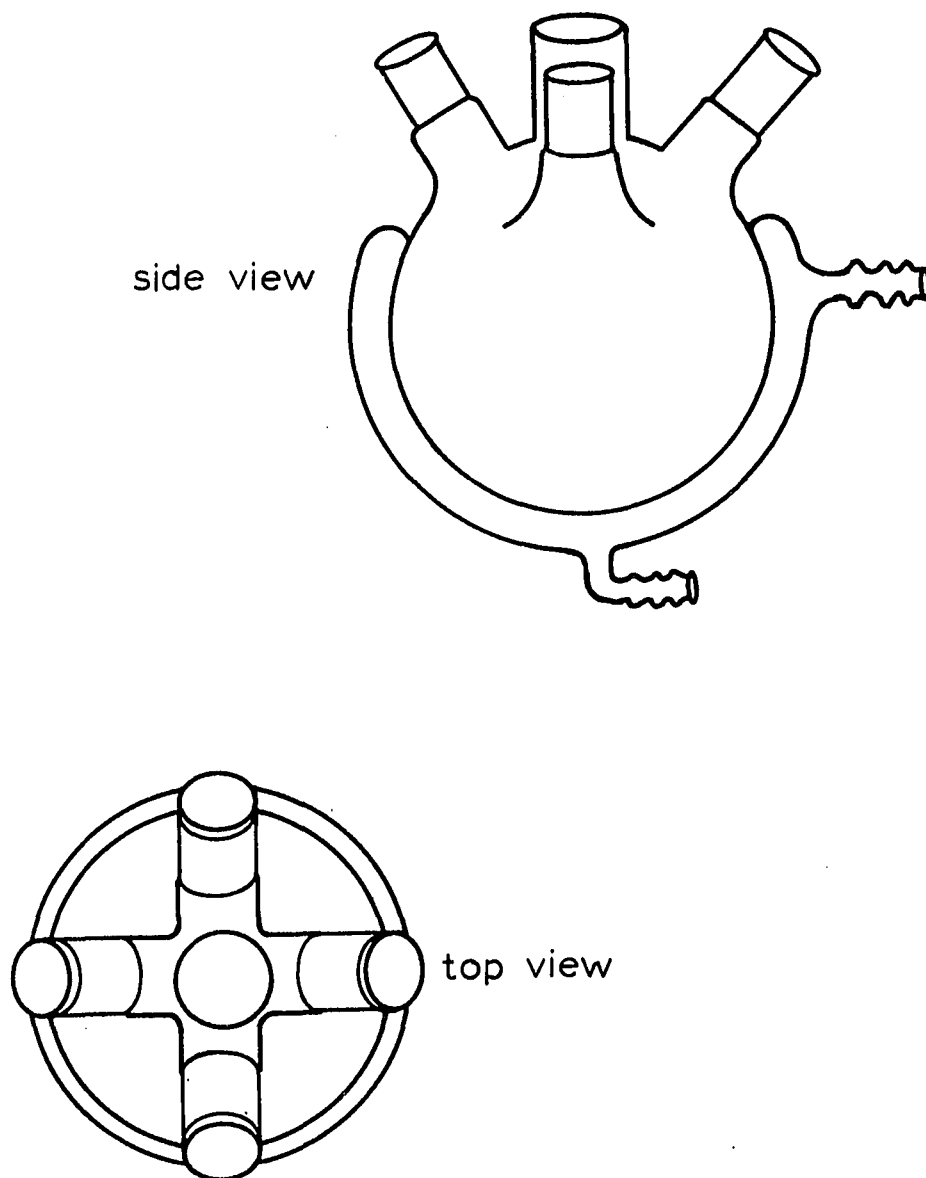
Figure III-1. Electrochemical cell. The RRDE enters the
center opening in the top view while the
other ports hold the ancillary glassware
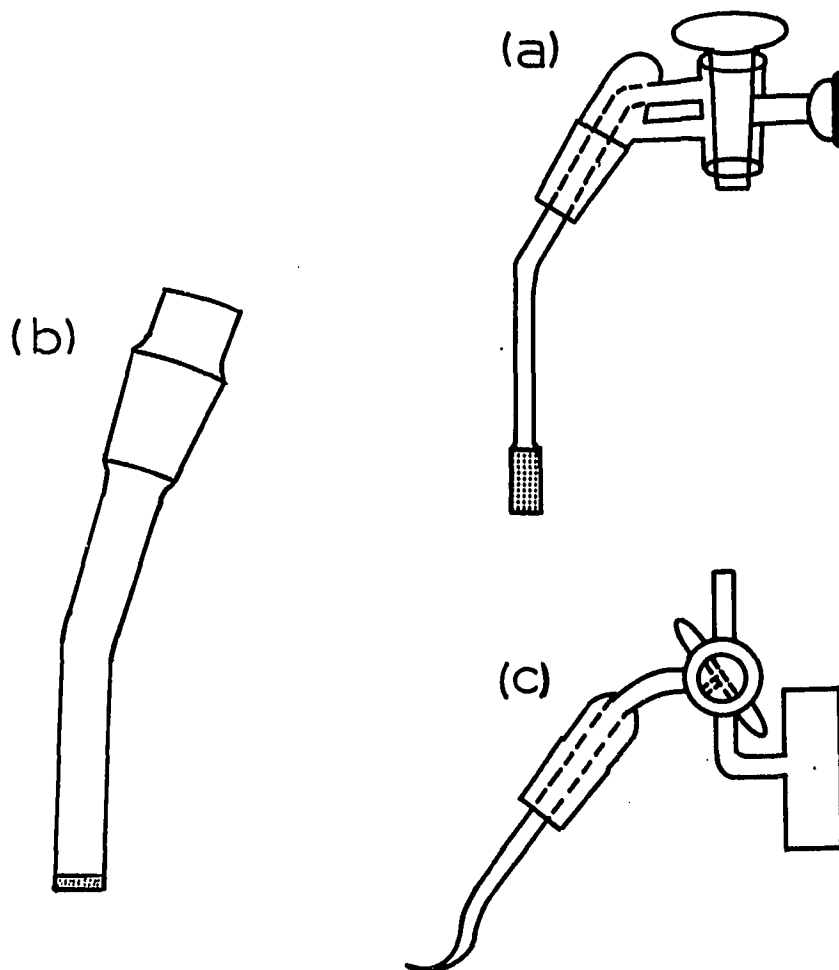shown in Figure III-2

Figure III-2. Ancillary devices used with the electro-
chemical cell: (a) counter electrode
holder, (b) gas bubbler, (c) reference
electrode bridge

bridge (Figure III-2c). The extra port was used for insertion of electroactive materials while an experiment was in progress. A flat piece of Teflon in the shape of a washer was used to cover the central opening while the RRDE was in the cell. This was done to exclude foreign substances from the cell and to prevent back flow of oxygen into a nitrogen saturated cell. Figure III-3 shows the electrode used in most of the experiments. This electrode, from Pine Instrument Company, was constructed with a disk-shaped cavity on the electrode face as shown. The dimensions of this electrode and of a similar electrode of "in-house" construction are shown in Table III-1. The efficiency (calculated) of each of these electrodes is also included.

Table III-1. Dimensions and efficiency of both electrodes used in this study: r_1 = disk radius, r_2 = inner radius of the ring, r_3 = outer ring radius, as determined by a traveling microscope. N is the percent efficiency calculated as in reference 83

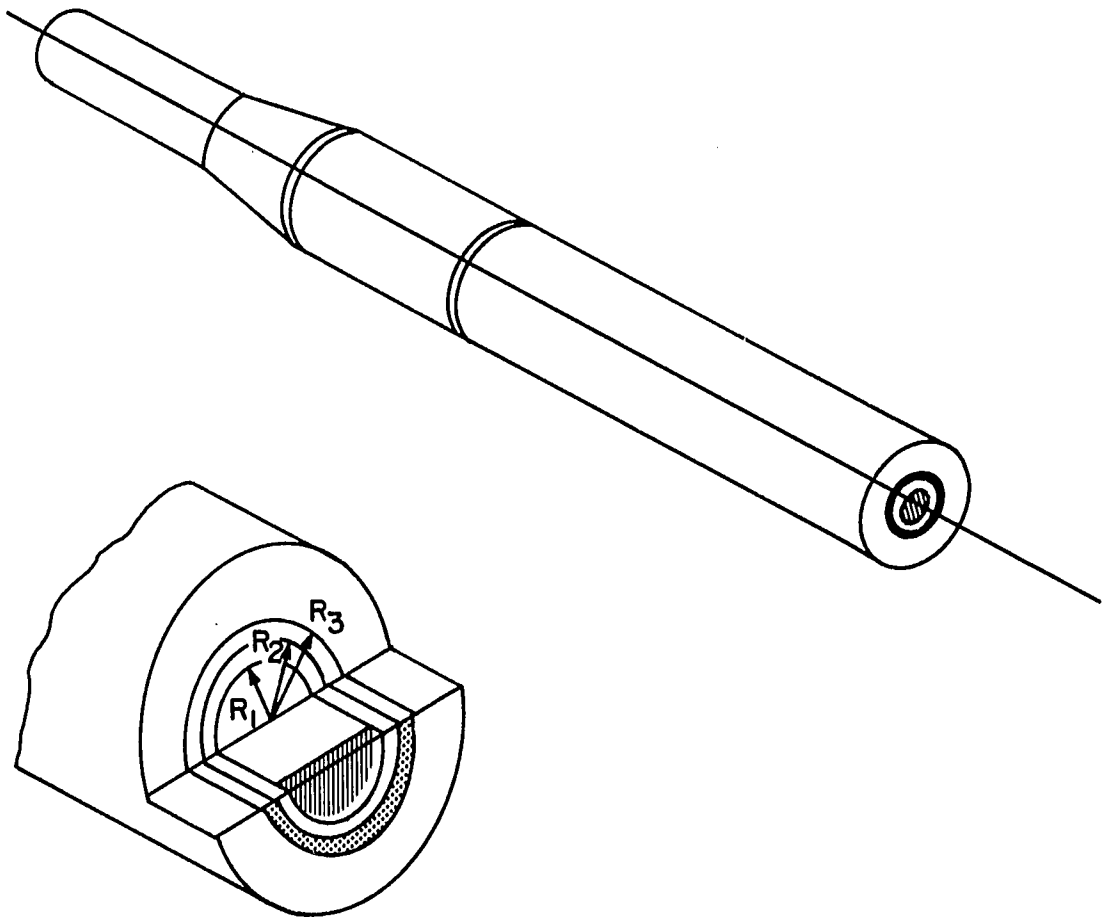| Dimension (cm)	Electrode	
	Pine Instruments	Ames Laboratory
r_1	0.319	0.476
r_2	0.395	0.548
r_3	0.410	0.584
A (disk)	0.320 cm^2	0.712 cm^2
%N	18%	16%

Figure III-3. Pine Instrument RRDE showing hollow disk
cavity for the GP electrode

The disk and ring are separated by a Teflon or epoxy spacer which extends from the electrode face to the ring wiper contact. The reference electrode was a saturated calomel electrode (SCE). A gold wire was used as the counter electrode for all experiments.

Different oxygen/nitrogen ratios were metered into the cell using two Mathison R7630 gas flowmeters to control the amount of each gas. Oxygen partial pressures of 0.01 to 1.0 atmosphere in nitrogen could be obtained by this method.

The temperature bath consisted of a thermostat-controlled heater, a stirrer/circulator pump, and cooling coils. The temperature was commonly kept to within 0.2 C of 25.0 C.

The electrode rotator was a variable speed ASR rotator from Pine Instrument Company. The speed was set using a ten turn pot accurate to 1% of the dial reading. Speeds from 0 to 10,000 RPM were available with guaranteed linearity above 200 RPM. Silver-graphite wipers were mounted on the rotator for contact to the ring and disk electrodes. These wipers were electrically connected to the RDE-2 potentiostat, also from Pine Instruments. The potentiostat controlled the potential of the ring and disk electrode utilizing a counter electrode and the SCE reference electrode. The potential of either electrode could be set at a constant value or varied using a triangular wave. The

current outputs for both electrodes were monitored using a
Moseley 7000 Autograph and an Electro Instruments 500.

B. Methods

The graphite paste was made according to Adams (84)
with 1.0 gram of graphite to 0.6 grams of nujol. The
mixture was then stirred with a spatula until it had a
consistency approaching that of peanut butter. The paste
was deposited in the disk cavity of the RRDE and carefully
smoothed using a metal spatula. The surface of the electrode
outside the disk was carefully wiped clear of any remaining
paste.

The cell components were rinsed three times in triply
distilled water prior to addition of the electrolyte.
Electrolyte was also added to the counter electrode holder
and the reference electrode apparatus. This was done by
using a suction bulb and the reference electrode stopcock
to draw solution up past the stopcock. Addition of solution
to the side arm completed the connection from the Luggin
capillary to the reference electrode holder. Care was taken
to eliminate all bubbles from the reference bridge as well
as the disk electrode surface to prevent undue noise.
Neglect of these precautions resulted not only in increased
output noise but also direct potentiostat failure. After
the electrolyte was added, the appropriate gas was bubbled

in the solution for at least fifteen minutes. The gas dispersion device could then be switched to flow gas over the electrolyte surface. At this time, all electrode apparatus, especially the Luggin capillary, were inspected for and freed of any clinging bubbles. This procedure was repeated each time gas was bubbled in the solution. Prior to recording data, the optimum ring potential was determined. To obtain this potential, current versus voltage (I/E) scans were monitored for the ring electrode alone. That is, ring voltage was scanned over a specified range using a triangular wave while current was recorded. The optimum potential was approximated as the most oxidizing potential on the limiting current plateau for the component of interest. After the ring potential was set, sufficient time was allowed for the ring to establish a steady state current. The disk electrode was commonly scanned for about ten minutes to obtain repeatable scans. No other pre-treatment was used for electrodes or materials. During an experiment, I/E scans were recorded for the disk as well as the ring, that is, ring current versus <u>disk</u> voltage. In this way a product or intermediate of the disk reaction could be monitored at the ring.

In a typical experiment, several different scans were taken to determine other characteristics of the electrode reaction. A baseline (N_2 saturated solution) scan was always

taken to make sure the electrode had no leaks, that is,
aqueous canals penetrating the disk surface to the electrode
shaft. Leaks were easily determined as anomalous currents
and the only way to alleviate this problem was to make a
new electrode. A good background scan on a GPE is shown in
Figure III-4 and over most of its range has a current less
than one μA. The background currents were subtracted from
the currents recorded with oxygen in the solution. Scans
were recorded at a one or two volts per minute scan rate.
Faster rates introduced more hysteresis into the I/E scans
while lower rates did not significantly decrease hysteresis.
The voltage range used in the scans varied somewhat but the
widest range used was -1.5 to +0.6 volts. Within these
limits, background currents on the graphite paste were
less than 5 μA with no characteristic peaks or waves. An
initial experiment was done to calibrate the flowmeters and
oxygen concentration was investigated for the purpose of
estimating limiting currents. According to the Levich
equation (82), the limiting current is given by

$$i_\ell = 0.62 \ n \ F \ A \ D^{2/3} \ \nu^{-1/6} \ \omega^{1/2} \ c_{O_2}^b \qquad \text{(III-1)}$$

using symbols previously defined. Experimental values are
required for D, ν, ω, and $c_{O_2}^b$. ν is estimated as 10^{-2}
cm^2/sec for a 1 M KOH solution (103). ω is easily determined
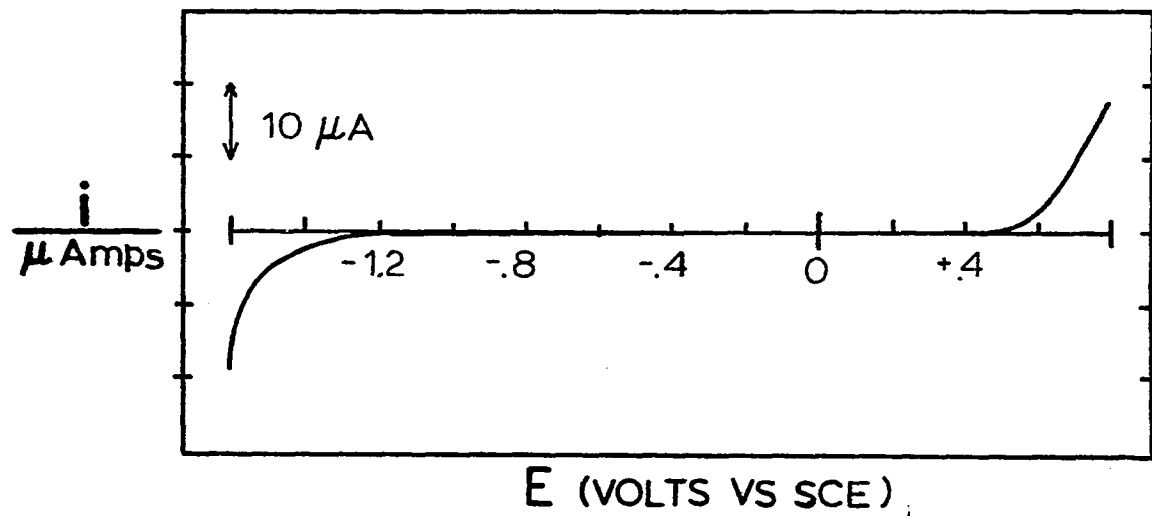from the rotation speed. D and $c_{O_2}^b$ depend on the electrolyte

Figure III-4.   I/E wave for a GP electrode in 1 M NaOH

and its concentration. The concentration of oxygen in solution has been related to electrolyte concentration for KOH (103) and this relation has been found valid for NaOH solutions also (104). This equation calculated oxygen concentration assuming P_{O_2} = 760 mm Hg. Corrections to this value for barometric pressure and the vapor pressure of water in the gas stream can be estimated. These latter two corrections decrease the P_{O_2} over an oxygen saturated solution from 760 to 715 mm Hg. Assuming Henrys' law (i.e., in dilute solutions concentrations are directly proportional to partial pressure of a solute in the gas phase) the value of the oxygen concentration is 1.19 x 10^{-3} moles/liter. The equation from reference (103) is

$$\log C_{O_2} = \log[C_{O_2}(\text{dilute})] - 0.1746 \cdot C_{NaOH} \qquad \text{(III-2)}$$

Accordingly, C_{O_2} = 8.1 x 10^{-4} moles/liter in 1 $\underline{M}$ NaOH. The diffusion coefficient for oxygen similarly decreases with increasing electrolyte concentration. A value for D of 1.75 x 10^{-5} cm^2/sec was obtained from a D versus percent KOH plot in reference (105). To check on these values, oxygen was reduced at a dropping mercury electrode (DME). A diffusion limited current is observed for oxygen reduction on a DME involving two electrons per oxygen molecule. According to the Ilkovic equation, current to a DME is given by

$$i = 706 \; n \cdot m^{2/3} \; t^{1/6} \; D^{1/2} \; c^b \qquad \text{(III-3)}$$

where m is the mercury flow rate in mg/sec, and t is the drop time in seconds. From this experiment a value of 3.89×10^{-6} was calculated for $D^{1/2} C_{O_2}^b$ in an oxygen saturated solution. Using the previously obtained values $D^{1/2} C_{O_2}^b$ is 3.41×10^{-6}. Thus, either my polarographic values are too high or the estimated values are too low. Values of D obtained by polarography are sometimes higher than those obtained by other methods (104). The calculated limiting currents have been tabulated for different ω in Table III-2. The polarographic data were also used to

Table III-2. Limiting currents for the Pine electrode calculated using equation III-1

$\dfrac{\omega}{RPM}$	$\dfrac{\omega}{Rad/sec}$	$\left(\dfrac{\omega}{(Rad/sec)}\right)^{1/2}$	$\dfrac{i_\ell}{10^{-3}\ Amps}$
100	10.5	3.24	0.292
225	23.6	4.85	0.437
400	41.9	6.47	0.583
900	94.2	9.71	0.875
1600	167.5	12.94	1.166

The following values were used in calculating i_ℓ

$n = 4$
$A = 0.320\ cm^2$
$D = 1.75 \times 10^{-5}\ cm^2/sec$
$C^b = 8.1 \times 10^{-4}\ Moles/L$
$\nu = 1.0 \times 10^{-2}\ cm^2/sec$

calibrate the flowmeters by metering in several different oxygen/nitrogen ratios and recording the limiting current for oxygen reduction. Other preliminary experiments had two primary objectives; 1) to insure that a graphite paste functioned properly as a disk, and 2) to determine what ring electrode worked best for the detection of peroxide. To test the GP RRDE, the experimental efficiency (N), calculated as the ring-to-disk current ratio in the collection mode, is compared to the theoretically calculated N (83). The theoretical efficiency of the electrode used most was 18%. Table III-3 shows experimental efficiencies for all calibration runs on this electrode. The experimental

Table III-3. Percent efficiencies (N x 100) for four different GPE electrodes as determined by calibration using the $Fe(CN)_6$ couple

$\frac{\omega}{RPM}$	100	225	400	900	1600
%N	17.1	17.2	16.2	15.2	14.2
	18.5		16.7	15.1	14.5
	18.1		16.1	15.4	13.7
	17.5	16.8	16.5	15.6	14.7
Ave.	17.8	17.0	16.4	15.3	14.3
Std. Dev.	±0.62		±0.28	±0.22	±0.44

efficiency was very near the theoretical value at low RPM; however, as ω increased, experimental efficiencies showed a negative deviation. The nonideal GPE surface was most likely the cause of the deviation. At higher rotation speeds, the fluid flow at the disk probably is nonlaminar since at 100 RPM the diffusion layer decreases to near the radius of the 200 mesh graphite particles (6.4 x 10^{-3} cm). This is a serious problem for studies when the efficiency must be accurately known. For this reason, the electrode was usually calibrated when the paste electrode was renewed. Another problem encountered in this study was the difficulty of determining limiting current plateaus. As shown in Figure III-5, the disk current at the graphite paste electrode never reached a diffusion limited plateau as in Figure I-9. There are several ways to determine the limiting slope for these data. The method used in this work is described as the most consistent of several empirical methods used in reference 106. For the plot in Figure III-5, a line would first be drawn through the continually rising portion where the limiting plateau should be. Then the current at which this line and the curve depart is used as the limiting current. Although there is no rigorous theory to back up this method, the general idea is that in the region of the limiting current
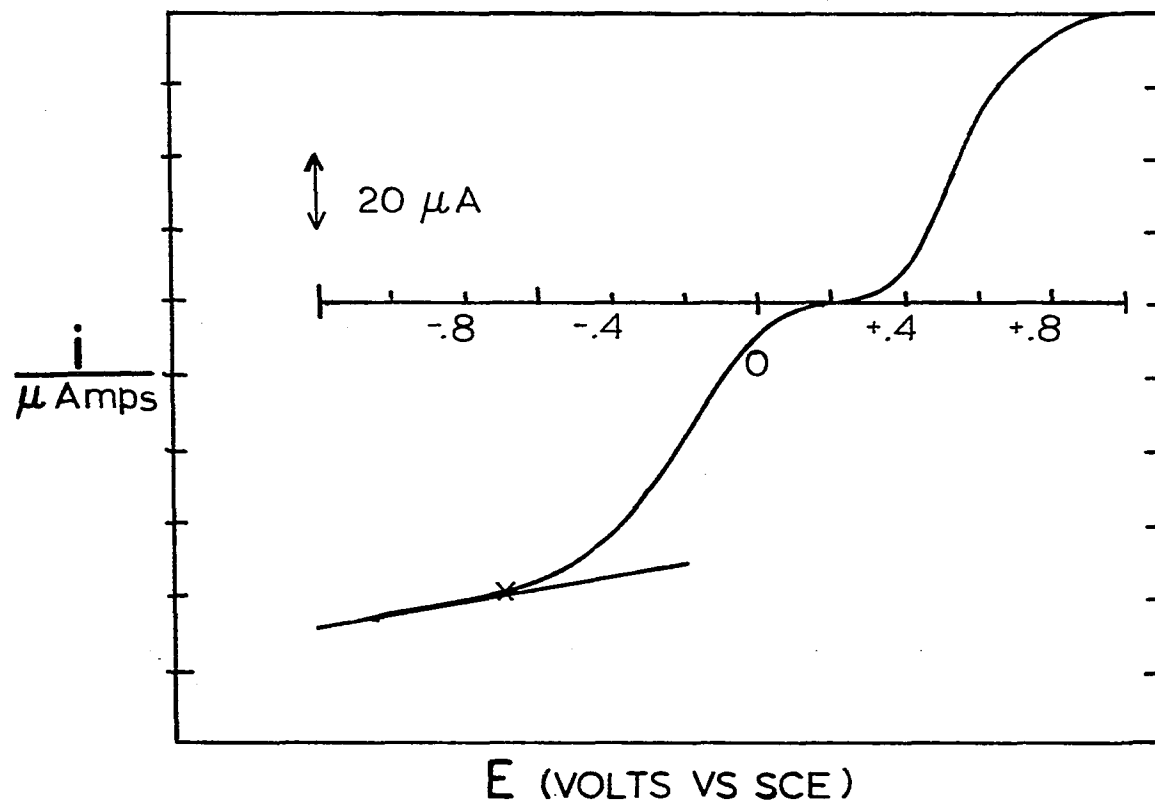
Figure III-5. I/E wave on a GP electrode in 1 $\underline{M}$ Na$_2$SO$_4$ with 10^{-3} M
ferri/ferrocyanide

another reaction takes place that should be separated from the first reaction.

In addition to being microscopically rough, the graphite paste can also be deformed. This leads to an upper limit on the rotation rate. At 3600 RPM, the graphite paste became concave and some graphite was spun out into the solution. The upper limit was determined to be about 1600 RPM and all data are taken at and below this value. Thus, a GPE appears to be useful in an RRDE configuration although certain limitations and simple corrections must be observed for accurate work.

The second objective of these preliminary experiments was to ascertain what ring material would best determine peroxide in basic solution. The Pine electrode came equipped with a platinum ring; however, gold could be plated over the platinum thus creating a gold ring. A gold ring was used originally because platinum, in acid solution, is gradually deactivated to peroxide oxidation as a function of time. This deactivation is thought to be due to adsorption of impurities from the solution. Gold does not suffer this fate in acid solution and thus is a likely candidate for the ring. However, in basic solution the tables are turned. Gold is deactivated at potentials necessary for peroxide oxidation while platinum remains active. The reason for this can be seen in Figures III-6 and III-7.
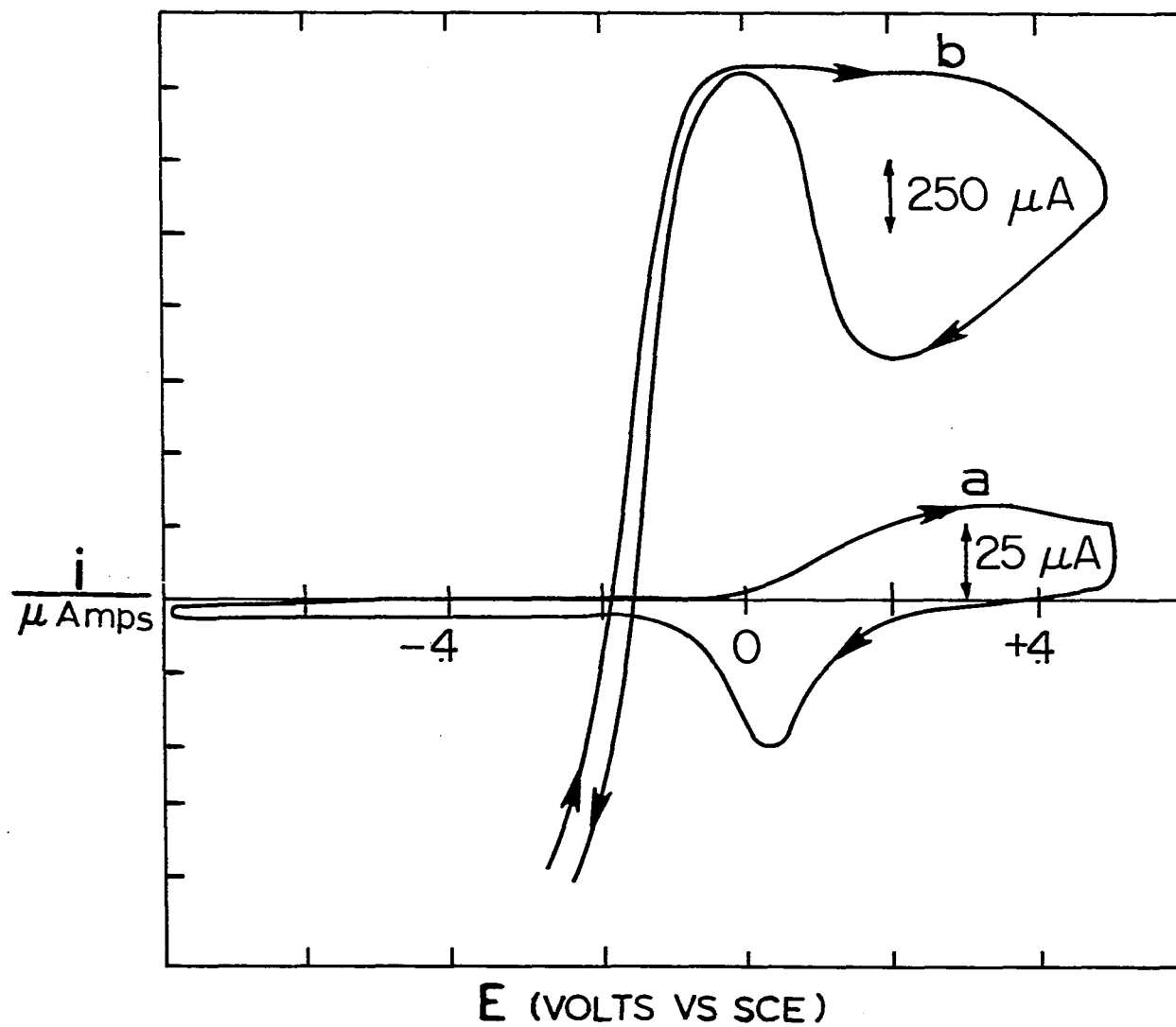
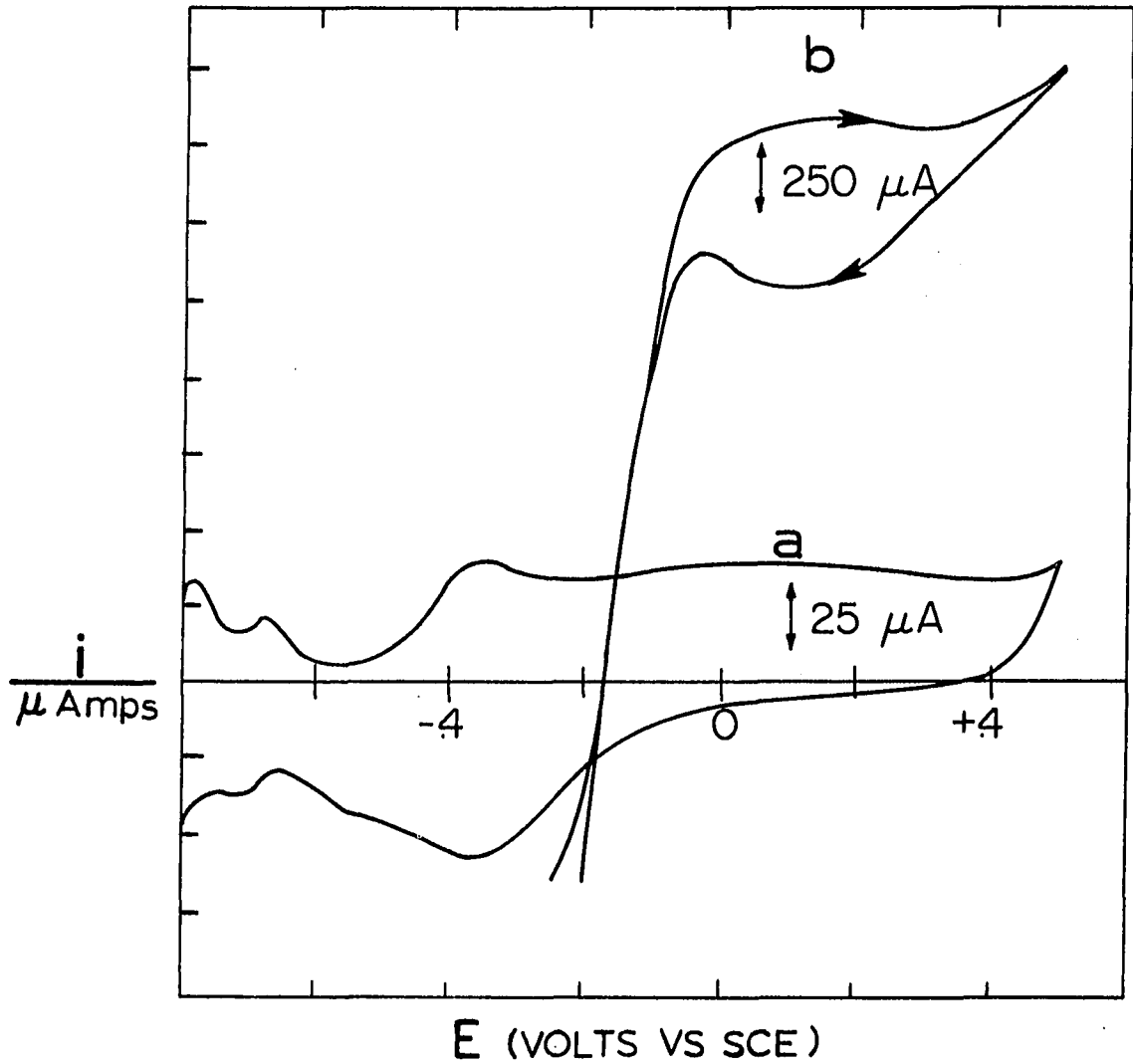Figure III-6. I/E scans on a gold electrode in 1 $\underline{M}$ NaOH; (a) no peroxide, (b) 10^{-3} $\underline{M}$ peroxide in solution

Figure III-7.   I/E scans shown on a platinum electrode in
1 $\underline{M}$ NaOH; (a) peroxide free solution,
(b) 10^{-3} $\underline{M}$ peroxide in solution

In Figure III-6, a gold electrode is scanned in 10^{-3} M

peroxide and peroxide free solutions. As the potential is

scanned positive from zero in the peroxide free solution,

anodic current corresponding to gold oxide formation appears.

As the scan is reversed, the reduction of the gold oxide

appears with a cathodic peak at about zero volts. When

peroxide is added to the solution, a large anodic wave is

seen for peroxide oxidation that diminishes as soon as the

formation of the gold oxide begins. Thus, for gold in

basic solution, the formation of a gold oxide appears to

inhibit the oxidation of peroxide. Figure III-7 shows the

same scans for a platinum electrode. In this case the

oxide is formed before peroxide oxidation begins and no

decrease in peroxide oxidation occurs on the anodic wave.

Thus, platinum appears to be the choice for a ring electrode

in basic solution. The groundwork has now been laid for the

study of oxygen reduction. Graphite paste can be a useful

electrode in an RRDE when used under the proper rotation

speed restrictions. The ring does effectively detect

changes in concentration of electroactive species caused

by the disk. N, however, should be determined for each

electrode used. And finally, the platinum ring seems to be

the best choice for detection of peroxide formed at the

disk.

IV. RESULTS AND DISCUSSION

Oxygen reduction was studied at a GPE which was used as the disk of a RRDE. The enhancements realized by adding catalysts to the GPE were also studied. The GPE was shown to reduce oxygen by a two electron pathway resulting in peroxide. The I/E data show two waves which may be due to different "active sites" on the carbon surface. The presence of gold, silver, or platinum on the GPE shifts the half wave potential 0.6 to 0.8 volts in the positive direction. The data indicate that the limiting process is the first electron transfer (or oxygen adsorption). Comparison of these electrodes with solid metal electrodes shows some similarities. Both gold electrodes and both platinum electrodes showed similar characteristics in nitrogen saturated solution. In oxygenated solution the catalyzed GPE electrodes produced more peroxide than their solid counterparts. The intermediate catalysis of metal porphyrins is also shown. Their activity is related to the oxidation/reduction wave for the porphyrin.

A. Graphite Paste

Ring and disk currents are shown in Figure IV-1 as functions of potential for oxygen reduction on a GPE in 1 $\underline{M}$ NaOH. The platinum ring was potentiostated at +0.47 volts versus the SCE where previous experiments had indicated that
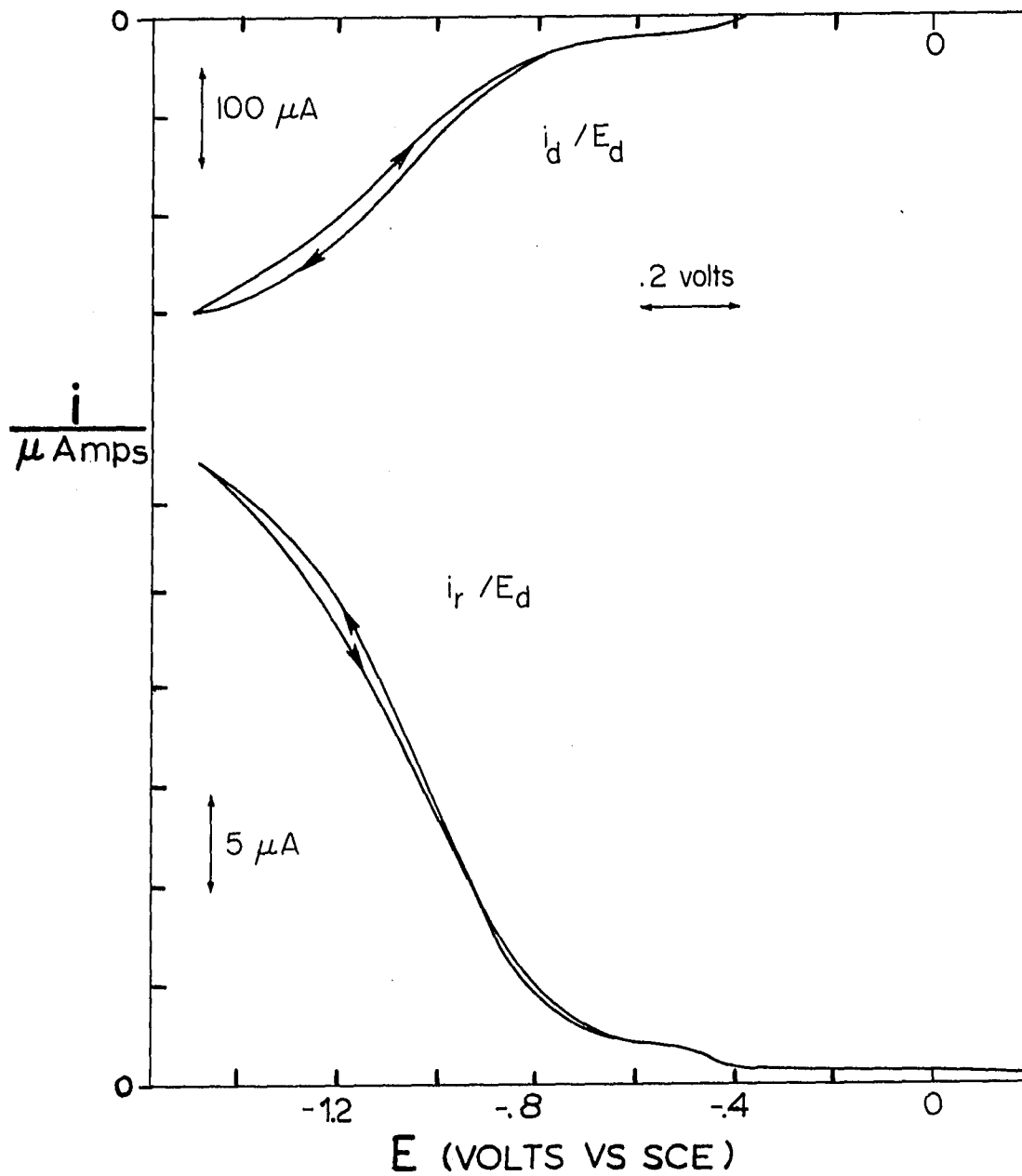
Figure IV-1. I/E scans of oxygen reduction on a GPE disk in
1 $\underline{M}$ NaOH. Ring currents are due to the
oxidation of peroxide formed at the disk

peroxide oxidation was diffusion controlled. The data show that oxygen reduction is a two wave process consisting of a small initial wave and a large second wave. While the first wave exhibits an apparent limiting current plateau, it is not dependent on the electrode rotation rate. The second wave, which only approaches a limiting plateau, equals the calculated limiting current only at the cathodic limit. This wave is dependent on rotation rate as is shown in Figure IV-2. Both waves produce peroxide as is shown by the ring current in Figure IV-1. The plots shown in Figure IV-3 indicate that the reduction process is first order in oxygen concentration (as explained in section III.D). Plots of $N \, i_d/i_r$ versus $\omega^{-1/2}$ are frequently used in studying oxygen reduction to determine the path of the reaction. These data for a GPE are shown in Figure IV-4. The zero slope of this plot indicates that the rate of decomposition and reduction of peroxide at the GPE is much less than the rate of its formation. The intercept of approximately one indicates that in addition, almost no four-electron reduction of oxygen occurs. Thus, the over-all reaction occurring at a GPE is

$$O_2 + H_2O + 2\,e^- \rightleftharpoons O_2H^- + OH^- \qquad (IV-1)$$
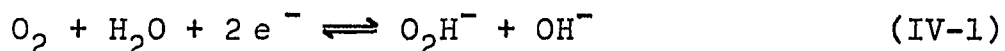
with peroxide ion the principal product in 1.0 $\underline{M}$ NaOH. Plots of E versus $\log[(i_\ell \times i)/(i_\ell - i)]$ are used to obtain the Tafel slope according to the following equation:
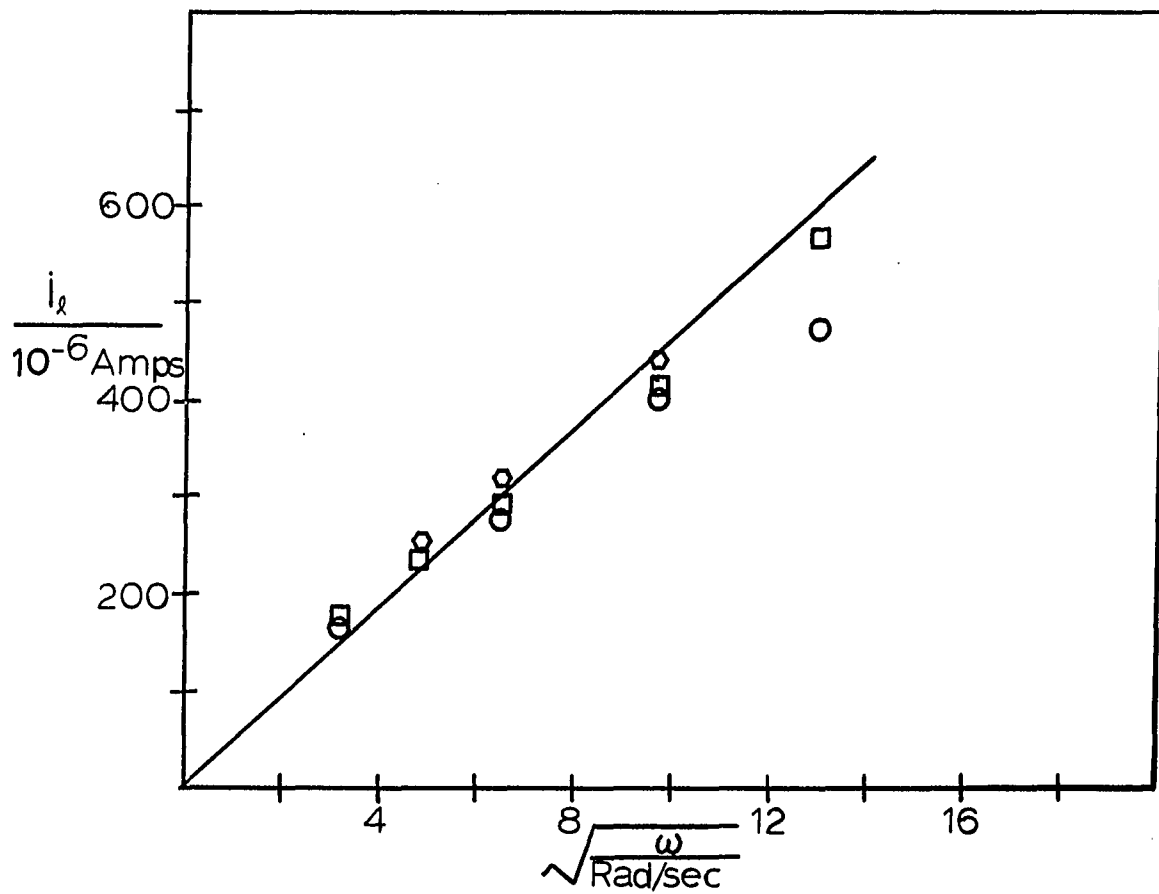
Figure IV-2. i_ℓ vs. $\omega^{1/2}$ for oxygen reduction in 1 M NaOH on several GPE's. The solid line represents theoretical data for a two electron oxygen reduction

89

Figure IV-3. $1/i_{(disk)}$ vs. $\omega^{-1/2}$ for oxygen reduction on a
GPE in 1 $\underline{M}$ NaOH. The different potentials used
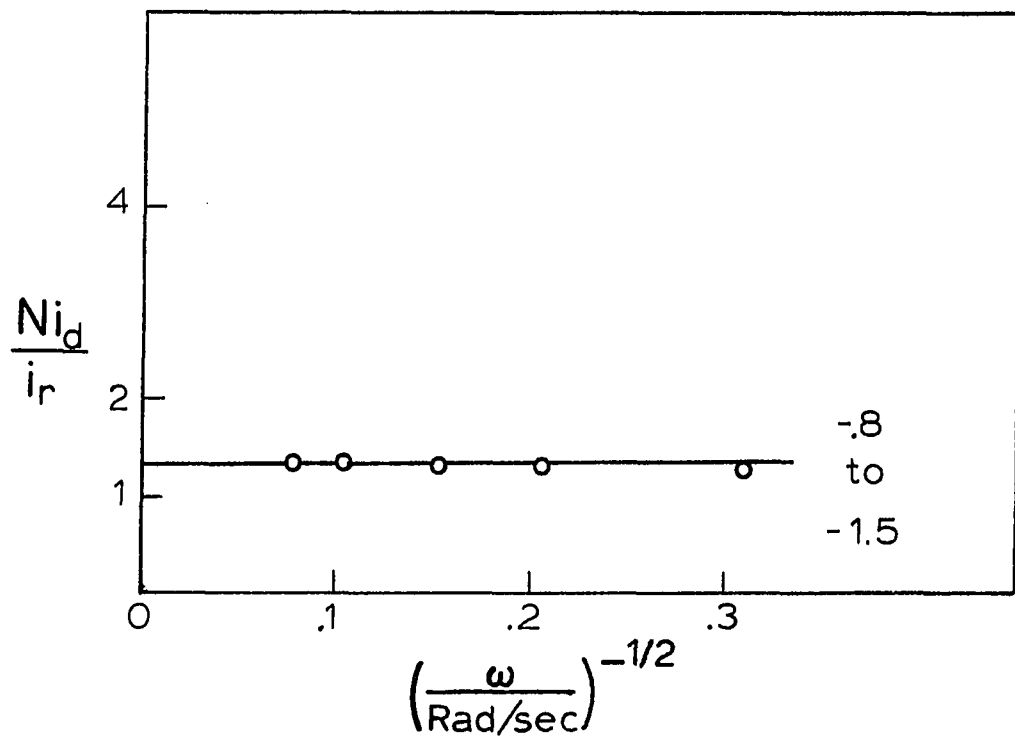are shown

Figure IV-4. N i_d/i_r versus $\omega^{-1/2}$ for oxygen reduction in
1 $\underline{M}$ NaOH on a GPE. Data showed little
variation between potentials of -0.8 to -1.5

$$E = E_{eq} + \frac{RT}{2.3\,\alpha_c F} \log i_o - \frac{RT}{2.3\,\alpha_c F} \log f(i) \qquad (IV-2)$$

where $f(i) = [i_\ell \times i/(i_\ell - i)]$. Figure IV-5 shows a plot
of this type where the limiting current was determined as
described in section III-B. The slopes vary with rotation
speed, 150 mV (per decade $f(i)$) at low rotation speeds and
about 180 mV at the highest rotation speed. A plot of
$\log i_o$ versus the log of oxygen partial pressure, shown
in Figure IV-6, can be used to determine the order of the
reaction with respect to oxygen. This plot gives a value
of 1.15 and weighing this value with the data of Figure
IV-3 the oxygen order is assumed to be one.

These data disagree on some basic points with previous
studies of oxygen reduction on graphite and carbon. In
Figure IV-7 some representative results of previous work
are compared to the present data. The primary difference
between my data and those of others is the size of the
current at the first wave. Although most comparable data
show much greater currents at the first wave, these previous
workers also find that the current on the wave is not
linearly dependent on $\omega^{1/2}$ as would be predicted by the
Levich equation, as was the case for my work. The cause of
these two waves is disputed. Some work by Brezina and
Hofmanova-Matejkova (93) was interpreted as showing that the
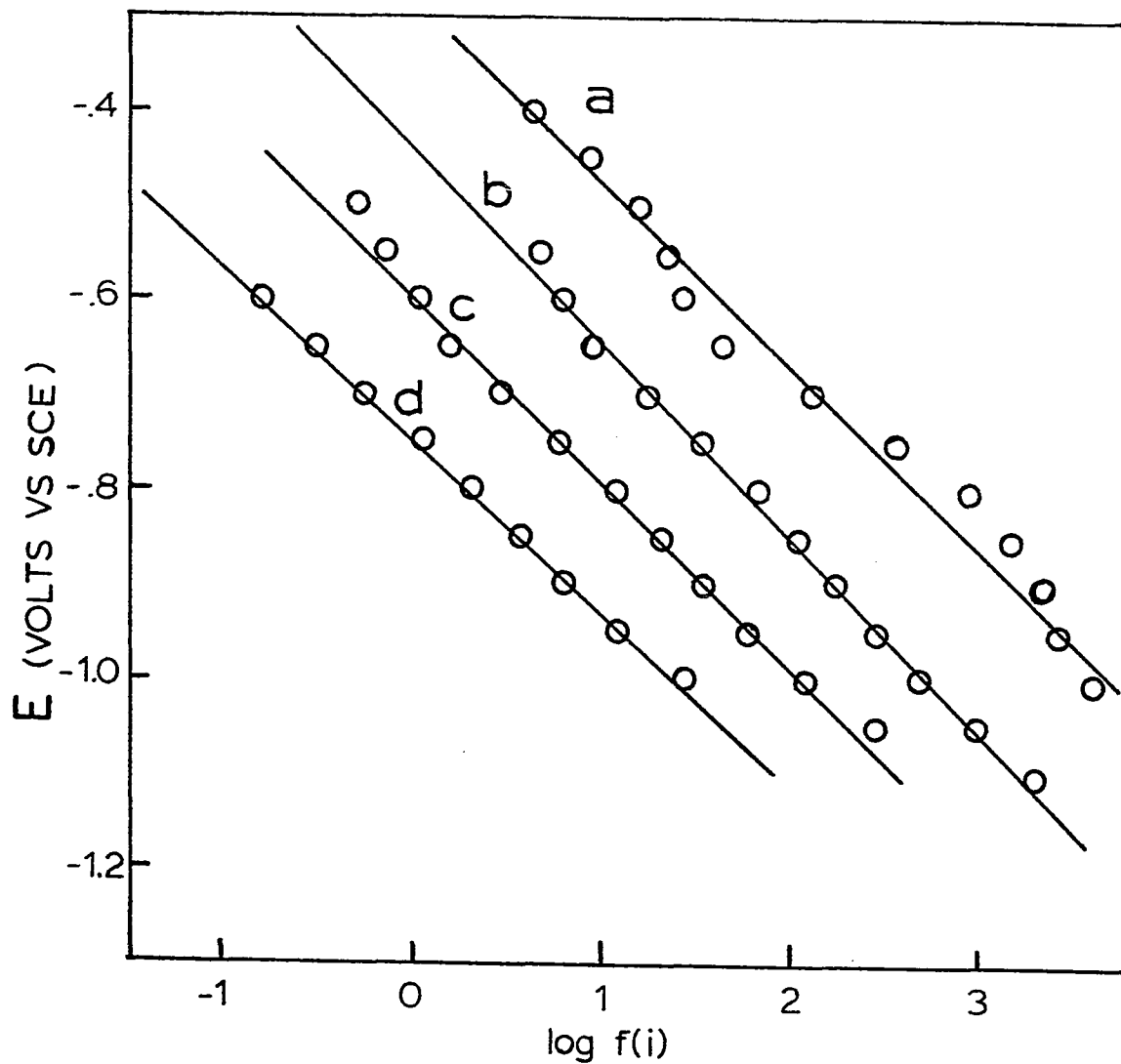first wave resulted from oxygen reduction to peroxide while

Figure IV-5.   Tafel plots for oxygen reduction on a GPE in 1 $\underline{M}$ NaOH at oxygen pressures of (a) 1.0, (b) 0.286, (c) 0.047 and (d) 0.011 atmospheres
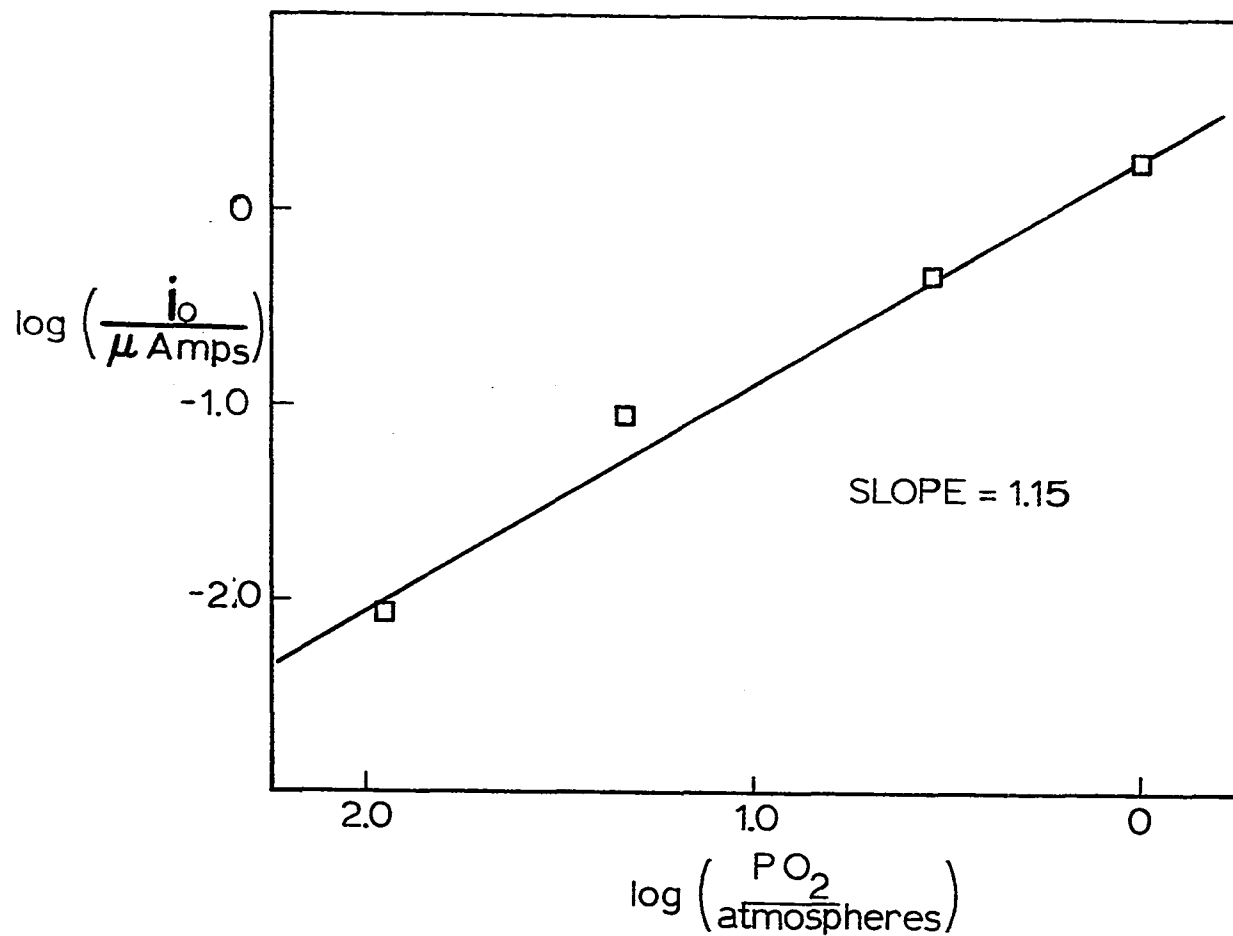
Figure IV-6. Log i_o is plotted against the log of oxygen partial pressure for oxygen reduction in 1 $\underline{M}$ NaOH on a GPE
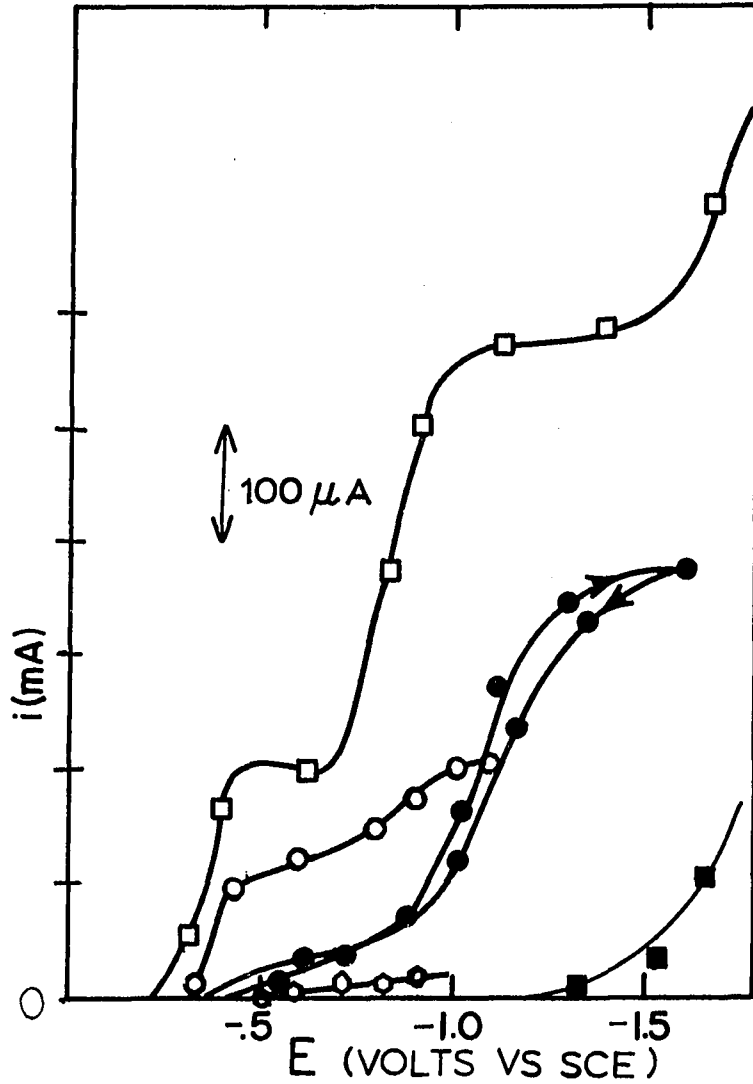
Figure IV-7. I/E wave for oxygen reduction on different
carbon electrodes: (□) Taylor and Humffray
(35), (o) Brezina and Hofmanova-Matejkova (93),
(◌) Morcos and Yeager (38), (●) present work.
(■) Results for peroxide reduction on a
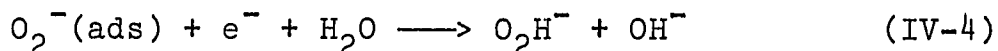graphite electrode (35)

the second wave was caused by the further reduction of peroxide. This idea disagrees with the data of the present study as little reaction of peroxide is found. Furthermore, work in this laboratory and others (35) shows that the reduction of peroxide on graphite does not begin until at least -1.2 volts and even at this potential the current is much less than for a diffusion limited process. These data are also shown in Figure IV-7. In most of these studies the second wave shows a limiting plateau at approximately the calculated current for a two-electron process. Another explanation for the first wave is the existence of certain active groups on the surface of the GPE which will catalyze oxygen reduction. This was shown in some work by Morcos and Yeager (38). In this study, oxygen reduction on the cleavage plane of highly oriented graphite substrates was compared to the same reaction on the edge planes of these materials. The first wave on the cleavage planes was found to be very small, while the edge planes showed behavior similar to the graphite electrodes in previously cited studies. The results for oxygen reduction on graphites basal plane agree with data in the present study. A suggested reason for the lack of reactivity of the basal plane is its lack of surface redox groups and defect structures. The corollary for a GPE is that the edge sites are covered by the oil or that the graphite particles have the preponderance

of their area taken up by basal graphite planes. It has been found in the present study that the amount of nujol used in the paste can shift the wave for oxygen reduction. This indicates that the oil has some effect on the active sites of the graphite particles. With increasing proportions of nujol, the second wave is shifted increasingly in the cathodic direction. For this reason, a constant composition of paste was used for all the results reported. A final possibility that the first wave could be caused by traces of catalytic metals was also considered. The only impurity in the graphite that could possibly be catalytic was iron (present at the 0.6 ppm level). Therefore, graphite doped with ferric iron at the 100 ppm level was tested as an electrode. The results of this experiment were identical to those on the undoped GPE. Thus, the possibility of catalysis by a metal impurity was discounted.

A comparison of Tafel slopes from this study and from previous results is shown in Table IV-1. The scatter in slopes is frequently attributed to the variable nature of a graphite or carbon surface. The shift of Tafel slopes from low current to high current regimes is a notable phenomenon in several studies. If the correct Tafel slope is assumed to be about 120 mV/decade $f(i)$ for the low current conditions the following sequence is a possibility:

Table IV-1. Tafel slopes for oxygen reduction on carbon electrodes

Electrode	Conditions	Tafel Slope	Reference
Paraffin filled Graphite	high i	110 mV/decade f(i)	107
Paraffin filled Carbon	high i	150 mV/decade f(i)	107
Pyrolytic Graphite	high i	130 mV/decade f(i)	107
Graphite Paste	low i to high i	90-120 mV/decade f(i)	93
Active Carbon	high i	150-180 mV/decade f(i)	108
Glassy Carbon	low i to high i	90-120 mV/decade f(i)	35
Active Carbon	low i	100 mV/decade f(i)	94
Graphite Paste	low i to high i	150-195 mV/decade f(i)	This work

$$S + O_2 + e^- \rightleftharpoons O_2^-(ads) \qquad \text{Slow} \qquad \text{(IV-3)}$$

$$O_2^-(ads) + e^- + H_2O \longrightarrow O_2H^- + OH^- \qquad \text{(IV-4)}$$

Using step IV-3 as the rate limiting reaction, the Tafel slope can be calculated (using equation II-21 where $\beta = 1/2$) as 120 mV/decade $f(i)$. There are some possible follow-ups to reaction IV-3. Sawyer and Seo (14) suggest that decomposition (disproportionation) of superoxide ion is faster on most surfaces than its further reduction. They would suggest a step like:

$$2\,O_2^- + H_2O \longrightarrow HO_2^- + O_2 + OH^- \qquad \text{(IV-5)}$$
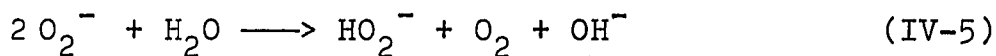
in place of step IV-4 above. The O_2 formed could be recycled resulting ultimately in a two electron process. The increase in Tafel slope with increasing current may indicate a shift of the rate determining step to a potential-independent step. An example of this might be the initial adsorption of an oxygen molecule

$$O_2 + S \rightleftharpoons O_2(ads) \qquad \text{(IV-6)}$$

where reaction IV-6 would precede step IV-3. The rate determining step might shift because a limited number of sites (S) were available for oxygen adsorption. At low currents, the limited number of sites do not significantly impede the reactions progress, thus the Tafel slope is about 120 mV. At higher currents, the sites can be swamped with arriving oxygens and step IV-6 can become the limiting step.

This step would have a much lower dependence on electrode potential because there are no obvious charged species and no charge transfer occurs. Thus, the Tafel slope would increase, eventually reaching infinity. This final situation is similar to the case for current limitation by mass transport to the electrode, that is, small changes in potential have no effect on the current.

Both waves for oxygen reduction on a GPE have been shown to result in the production of peroxide. The separation into two waves appears to be due to sites of different activity on the graphite surface. At low currents, the reduction appears to be limited by the first electron transfer. At higher currents, the availability of oxygen adsorption sites appears to limit the rate.

B. Gold

In order to study the catalysis of a material deposited on the GPE, I/E waves involved in oxygen reduction for both materials must be separable. Figure IV-8 shows the separation of the waves for oxygen reduction on a GPE and on a gold plated GPE. The increase in the oxygen reduction wave at potentials negative to -1.0 volts may be due to oxygen reduction on the GP substrate. However, this wave could also signify the onset of the reduction of peroxide at this electrode. Figure IV-9 shows the ring and
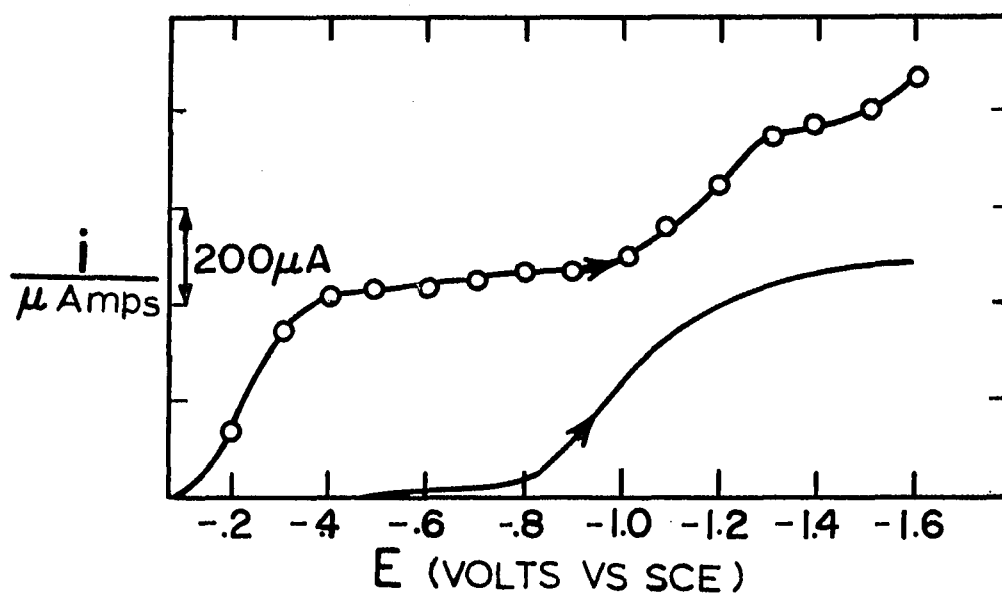
Figure IV-8.   I/E scans for oxygen reduction in 1 M NaOH,
              Solid line shows data for a GPE. Open circles
              show data for a gold plated GPE

disk scans for the gold plated GPE in oxygen and nitrogen
saturated solutions. These data are compared to corres-
ponding results using an RRDE with a platinum ring and a
gold-plated platinum disk. The nitrogen saturated scans on
gold primarily show currents due to oxide formation and
reduction. Both electrodes show similar waves for oxide
formation (anodic current) and oxide reduction (cathodic
current). The difference in magnitude of the currents
probably reflects the lack of total gold coverage of the
GPE. Likewise, oxygen reduction is similar on both
electrodes in the range shown. The ring currents are also
similar with considerable hysteresis only at very negative
disk potentials. Since the efficiencies of both electrodes
are the same, the ratio of disk-to-ring currents for each
electrode show, by inspection, that the gold plated GPE
produces a greater percentage of peroxide as product
than the solid gold electrode. This can also be observed
by noting that under the present conditions the limiting
current for a two-electron process is 300 μA (Table III-2).
This is slightly less than that recorded at the gold plated
GPE. This can be explained by an enhanced ability of the
solid gold electrode to catalyze the four-electron
reduction of oxygen. A plot of log i_o versus log P_{O_2}
shown in Figure IV-10a gives a slope of 0.94. This, along
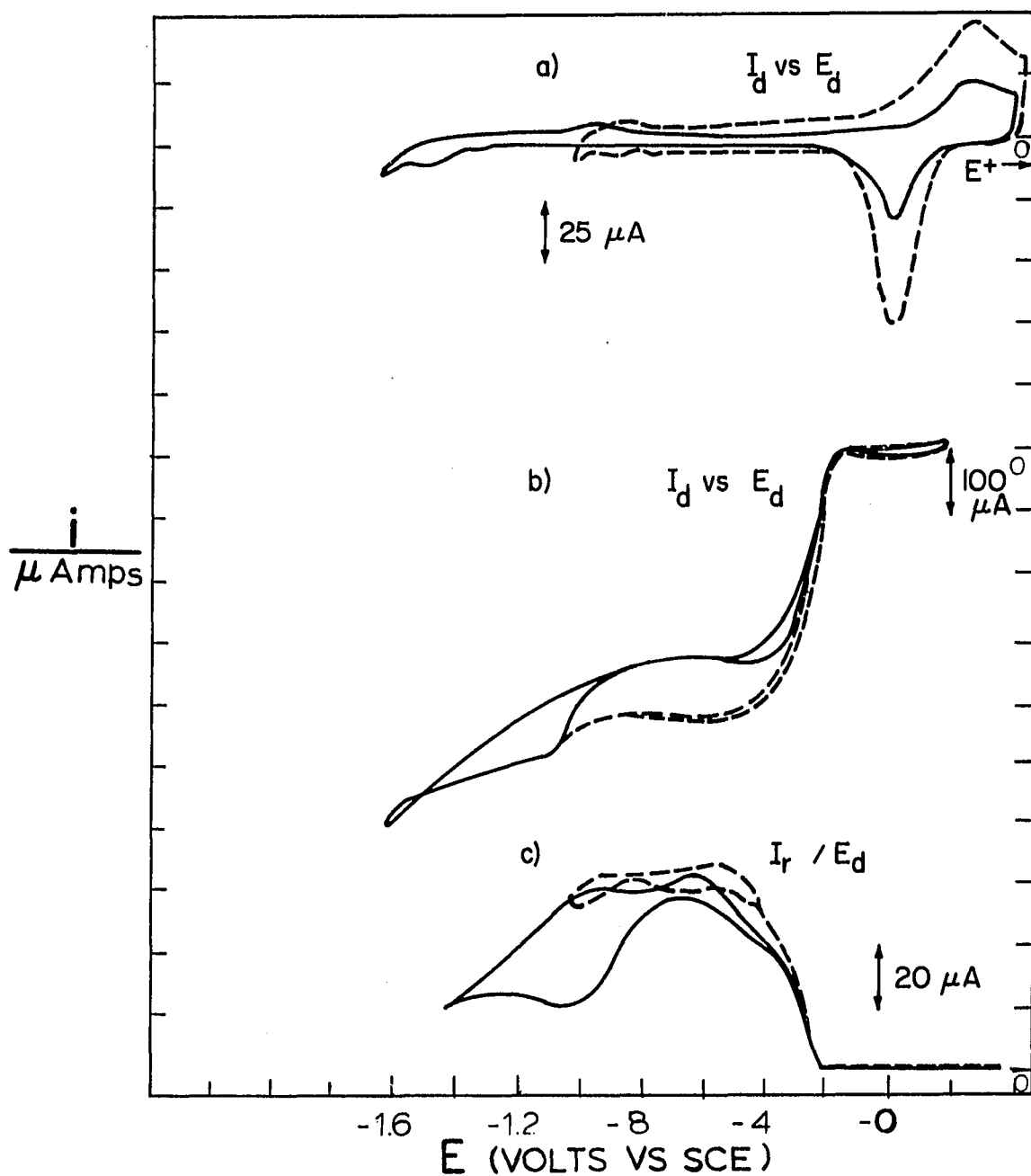with the straight lines of IV-10b, indicates that the

Figure IV-9. I/E data for oxygen reduction on gold
electrodes in 1 M̲ NaOH: (a) disk current for
a N$_2$ saturated solution, (b) disk current for
oxygen saturated solution, (c) ring current in
an oxygen saturated solution; (----) solid gold
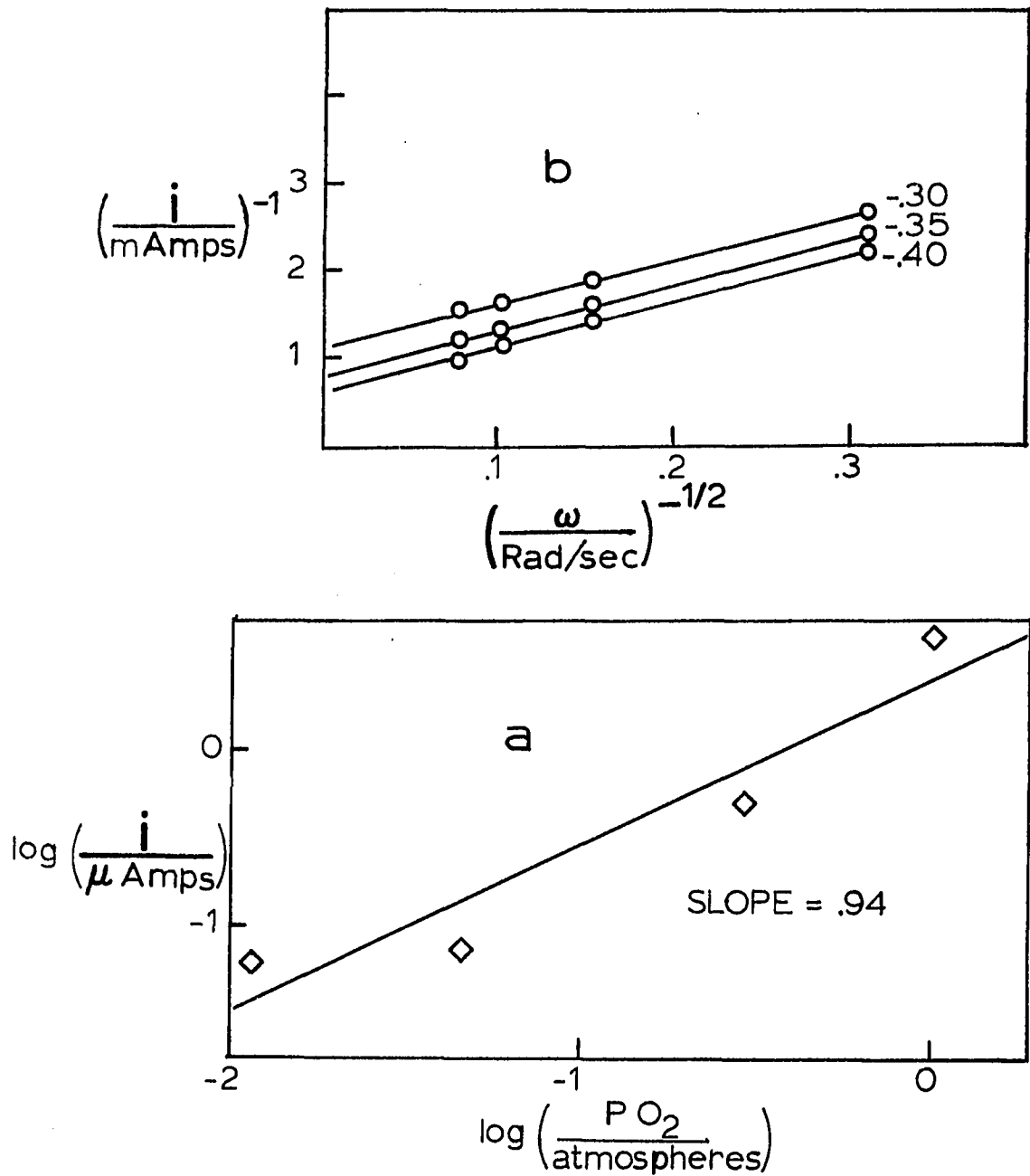RRDE, (———) gold plated GPE

Figure IV-10. Oxygen order plots for oxygen reduction on a gold plated GPE: (a) log i_o versus log PO_2 and (b) 1/i versus $\omega^{-1/2}$

reaction is first order. Plots of Ni_d/i_r obtained from experimental data are shown in Figure IV-11. These data show two trends for the reaction of peroxide at the gold plate GPE. At more positive potentials (near the front of the first wave) the further reaction of peroxide decreases at more cathodic potentials. That is, the slope of the Ni_d/i_r versus $\omega^{-1/2}$ curve $([2 \ k_1/k_2 + \tau][k_3 + k_4]/ 0.62 \ AD^{2/3}\nu^{-1/6})$ decreases while the intercept $(2 \ k_1/k_2 + \tau)$ is constant. Thus, the decrease in slope must be due to the decrease in $k_3 + k_4$, which are constants describing the rate of reaction of peroxide at the disk. With an intercept of about 1.5 and $\tau \geq 1$, the ratio of k_1/k_2 is less than 0.5 and indicates the two electron pathway is dominant under these conditions. With increasing potential (near the second wave), both the intercept and the slope of the plots in Figure IV-11 increase. However, the value of about 3.5 for the intercept shows that most of the oxygen is reduced by the two electron mechanism[1] with an enhanced rate of peroxide reaction. This increase in slope noted near the edge of the first wave was also shown in other work on solid gold electrodes (37).

---

[1]This assumes that τ is near two reflecting the increase in peroxide reaction.
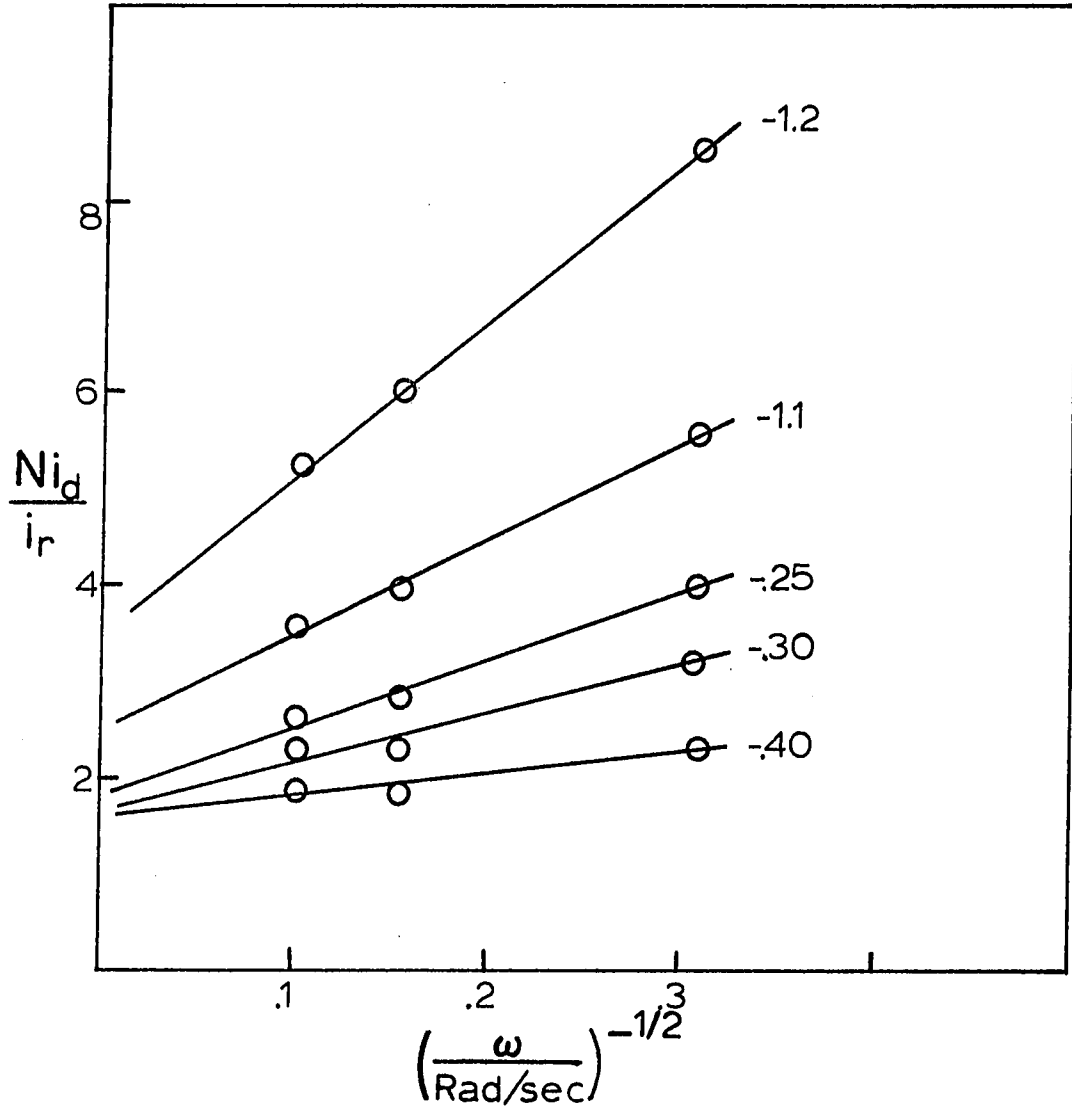
Figure IV-11. Ni_d/i_r versus $\omega^{1/2}$ plots for oxygen reduction on a gold plated GPE at different potentials

Table IV-2 compares the Tafel slope obtained from these electrodes to literature data; oxygen orders are also included. Of significance here, again, is the apparent

Table IV-2. Tafel slopes for oxygen reduction on gold in basic solution

Electrode	Tafel Slope	O_2 order	Reference
Au on GPE	120-130 mV/decade f(i)	1	This work
Au on Pt RRDE	100 mV/decade f(i)	1	This work
Au disk	36-100 mV/decade f(i)	1	109
Au disk	115 mV/decade f(i)	1	37

change of slope going from low to high current levels (109). In work where the current/voltage scan technique was used (37), only the higher slope resulted. This is due to the fact that, in general, this technique utilizes those currents greater than about 10% of i_{lim}. These authors also found a dependence of the Tafel slope on ω and attributed it to the simultaneous occurrence of two electrode processes, i.e., a two and a four electrode process. The Tafel slope (about 120 mV per decade f(i)) agrees with that of a reaction controlled by the first electron transfer step and the mechanism could be similar to oxygen reduction on graphite (37). Thus, the first step could again be represented by

equation IV-3 followed by equation IV-4, IV-5, or both. In addition to this, some of the peroxide formed is further reacted. The most likely process for this involves disproportionation of the peroxide via the following process:

$$2 \ HO_2^- \longrightarrow O_2 + 2 \ OH^- \qquad (IV-7)$$

where the oxygen formed can again be reduced at the disk.

Oxygen reduction on a gold plated GPE appears to be similar to the same reaction on a solid gold electrode. All mechanistic indicators give approximately the same values, i.e., Tafel slope and order with respect to oxygen. Finally, the direct comparison of oxygen reduction waves on both kinds of gold electrodes shows that gold plated graphite is similar to bulk gold both in nitrogen and oxygen saturated solutions.

C. Silver

Silver is a catalyst for oxygen reduction in basic solutions whose activity is similar to that of gold and platinum. A silver electrodeposit on graphite appears to form a fairly porous layer. Oxygen can chemisorb on silver in various forms differing in bond strength (21). The method of deposition of the silver on a graphite electrode may provide different environments for

approaching oxygen molecules, thus resulting in different forms of bound oxygen. These different silver active sites have been held to lead to different oxygen reduction kinetics (97). The data obtained in this study indicate that the limiting process for oxygen reduction is similar on all silver electrodes used. However, the amount of peroxide produced as product is greater on the silver loaded GPE's than on solid silver.

Figure IV-12 shows the data for oxygen reduction on silver electrodes. The background scans are featureless except for the silver plated GPE. This scan shows two anodic peaks which are probably due to oxide formation. The corresponding oxide reduction peaks are shown on the cathodic scan. The identification of these peaks is based on similar results found in reference 110. The absence of these peaks with the other two electrodes indicates the presence of active sites available only on the silver plated GPE. Morcos (97) has earlier reported that silver electrodeposition on graphite produced a silver more active for oxygen reduction. The present data for oxygen reduction on this surface indicate that the reaction is less reversible than on the other silver electrodes. More peroxide is formed as product on the graphite electrodes than on the solid silver electrode. Plots of $1/i_d$ versus $\omega^{-1/2}$ indicate (Figure IV-13) that the reduction is first order in oxygen.
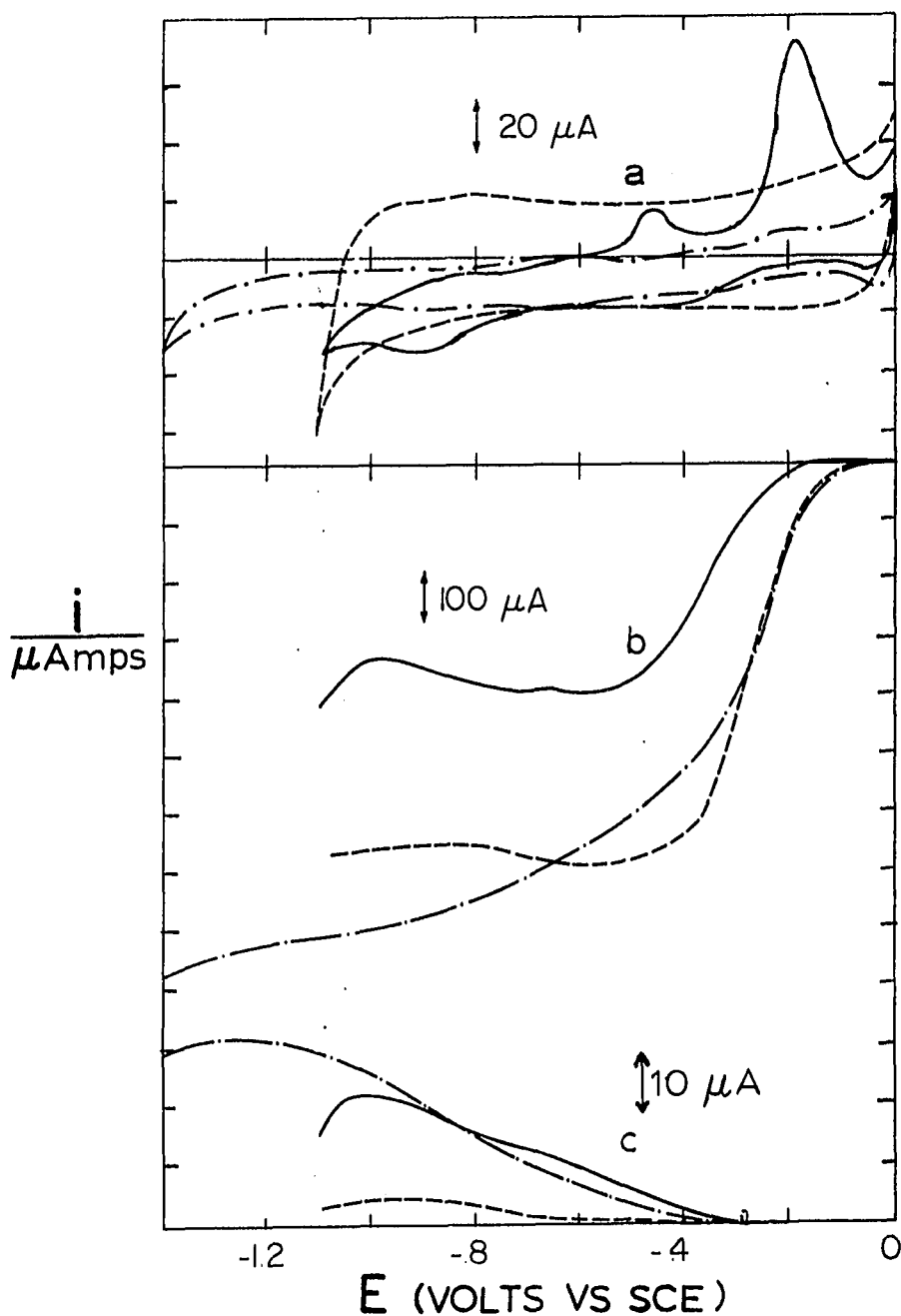
Figure IV-12. I/E scans for oxygen reduction on silver
electrodes: (a) disk current in a N_2
saturated solution, (b) disk current in an O_2
saturated solution, and (c) ring current in
an oxygen saturated solution; (---) solid
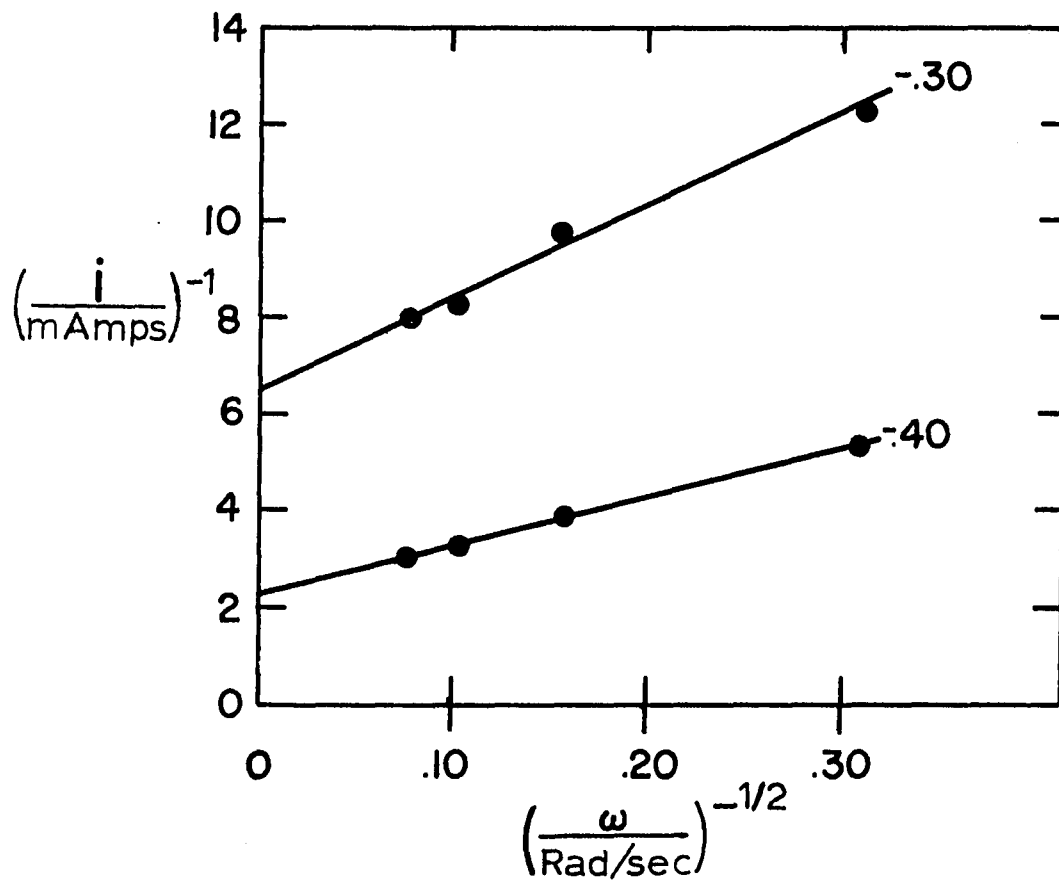silver RRDE, (——) silver plated GPE, (-•-•)
reduced silver GPE

Figure IV-13. 1/i (disk) versus $\omega^{-1/2}$ for oxygen reduction on a silver plated GPE at different potentials

Figure IV-14 shows plots of Ni_d/i_r versus $\omega^{-1/2}$ for the silver electrodes. The low intercept for plots from the silver plate GPE give the following relationship:

$$2\ k_1/k_2 + \tau \approx 2$$

(cf., eq. III-48 and subsequent discussion). By inspection one sees that the ratio of slope to intercept in these plots gives

$$\frac{slope}{intercept} = \frac{k_3 + k_4}{0.62\ AD^{2/3}\nu^{-1/6}}$$

or

$$\frac{slope}{intercept} = (k_3 + k_4)/k' \qquad\qquad (IV-8)$$

where $\quad k_D = k'\ \omega^{1/2}$ $\qquad\qquad\qquad (IV-9)$

The increase in slope with fairly constant or decreasing intercept indicates that further reaction of peroxide increases at potentials greater than about -0.9 on both electrodes. Moreover, the data for the silver plated GPE agree closely with case b of Figure II-3; i.e., $k_1 \approx 0$. This means that on this electrode most of the oxygen is reduced via the peroxide route. This is apparently not so for the reduced silver graphite paste. Data for this electrode are similar to case d of Figure II-3 in which both two and four electron reduction of oxygen occurs, as well as further reaction of peroxide. At more cathodic potentials, the four electron reduction slows while the two
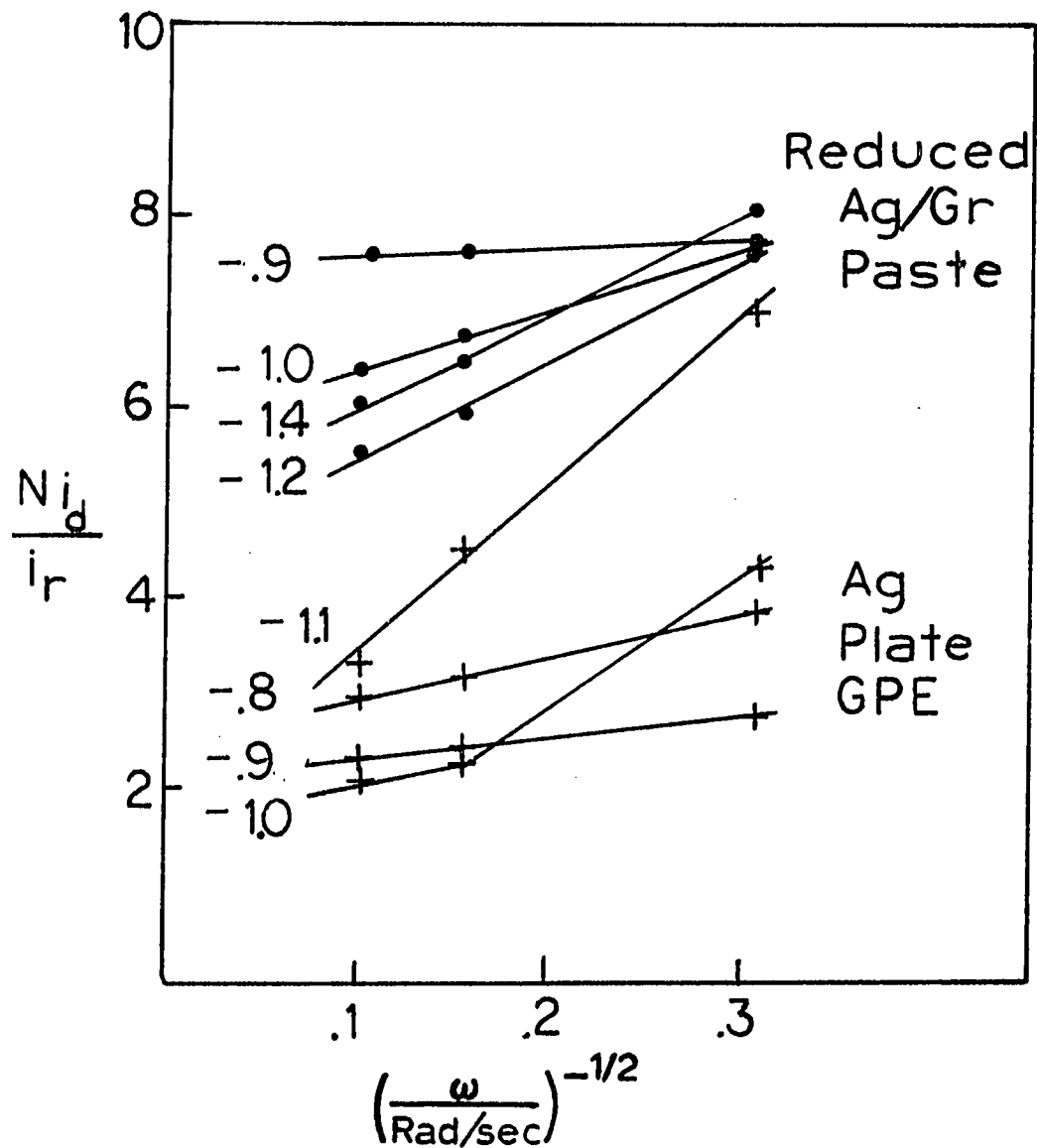
Figure IV-14. Ni_d/i_r versus $\omega^{-1/2}$ for oxygen reduction on silver electrodes at different potentials

electron reduction rate increases as shown by the increase
in the slope/intercept ratio. Even so, the lowest intercept
shows that the k_1/k_2 ratio is greater than one. The ring
current for the solid silver disk RRDE is so low that Ni_d/i_r
for this electrode would be off the scale of the plots shown
in Figure IV-14. Thus, on the solid silver electrode as well
as the reduced silver GPE, oxygen reduction goes primarily by
the four electron process. On the silver plate GPE, the
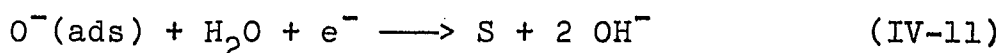major process is the two electron mechanism forming peroxide.

The data from the Tafel plots are shown in Table IV-3.
The slopes are all close to 120 mV/decade f(i) which means

Table IV-3. Tafel slopes for oxygen reduction in 1 $\underline{M}$ NaOH
on silver electrodes

Electrode	Tafel slope mV/decade f(i)
Ag plate Pt RRDE	122
Ag plate GP RRDE	127
Ag/Gr Paste	133

that again the first electron transfer step is rate limiting.
For the silver plated GPE, which reduced oxygen primarily by
the peroxide route, the mechanism is probably similar to that
on gold, that is, reaction IV-3 followed by IV-5 and IV-7.

On the other silver electrodes, a direct four electron mechanism appears to be the major pathway. A possibility for this is the following mechanism:

$$O_2 + S + e^- \longrightarrow O_2^-(ads) \tag{IV-3}$$

$$O_2^-(ads) + S + e^- \longrightarrow 2\ O^-(ads) \tag{IV-10}$$

$$O^-(ads) + H_2O + e^- \longrightarrow S + 2\ OH^- \tag{IV-11}$$
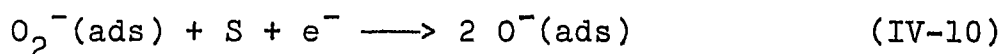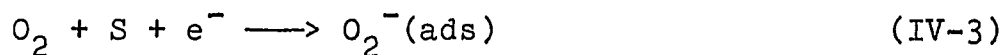
In this mechanism the first step is the initial oxygen adsorption and electron transfer. With the first electron transfer as the rate determining step, it is not surprising that the oxygen reduction wave is similar to that on gold.

Thus, the first step in oxygen reduction on all silver catalysts appears to be the same according to the Tafel slope. The paths after the first step appear to be different for the two catalyzed electrodes. The electro-plated catalyst appears to give more peroxide as product than the reduced silver/graphite paste. The reduced silver GPE reduces oxygen primarily by a four electron process while the silver plated GPE utilizes the two electron mechanism with subsequent decomposition or further reduction of the peroxide.

D. Platinum

A serious difficulty was experienced with the platinum plate GPE. The platinum did not adhere well to the GPE and

would fall off the surface after its initial deposition.
Due to this, all data reported here were taken from the
reduced platinum GPE and the solid platinum electrode.
Figure IV-15 shows the data from all the I/E curves for
oxygen reduction on platinum electrodes. For both electrodes
the amount of peroxide formed is relatively small. Figure
IV-16 shows that the primary route for oxygen reduction is
the direct four electron route. The catalyzed GPE showed a
higher percentage of peroxide than the solid platinum
electrode. On solid platinum, the direct four electron
mechanism is the dominant pathway as shown by the value of
the intercepts:

$$2 \ k_1/k_2 + \tau \geq 8$$

If τ can be no greater than two, the ratio of k_1/k_2 is
greater than three. On the reduced platinum GPE, the ratio
of k_1/k_2 is close to one. The Tafel plots for the reduced
platinum GPE had a steadily increasing slope. This behavior
normally indicates that mass transport limitations have set
in; however, the currents (as shown in Figure IV-15) are
much less than the predicted limiting currents. This may
mean that there were few active platinum sites on the GPE
surface. The result of this would be the onset of mass
transport limitations at currents less than those predicted
by the Levich equation. The oxygen order plots (Figure
IV-17) indicate that the reduction of oxygen on a platinum
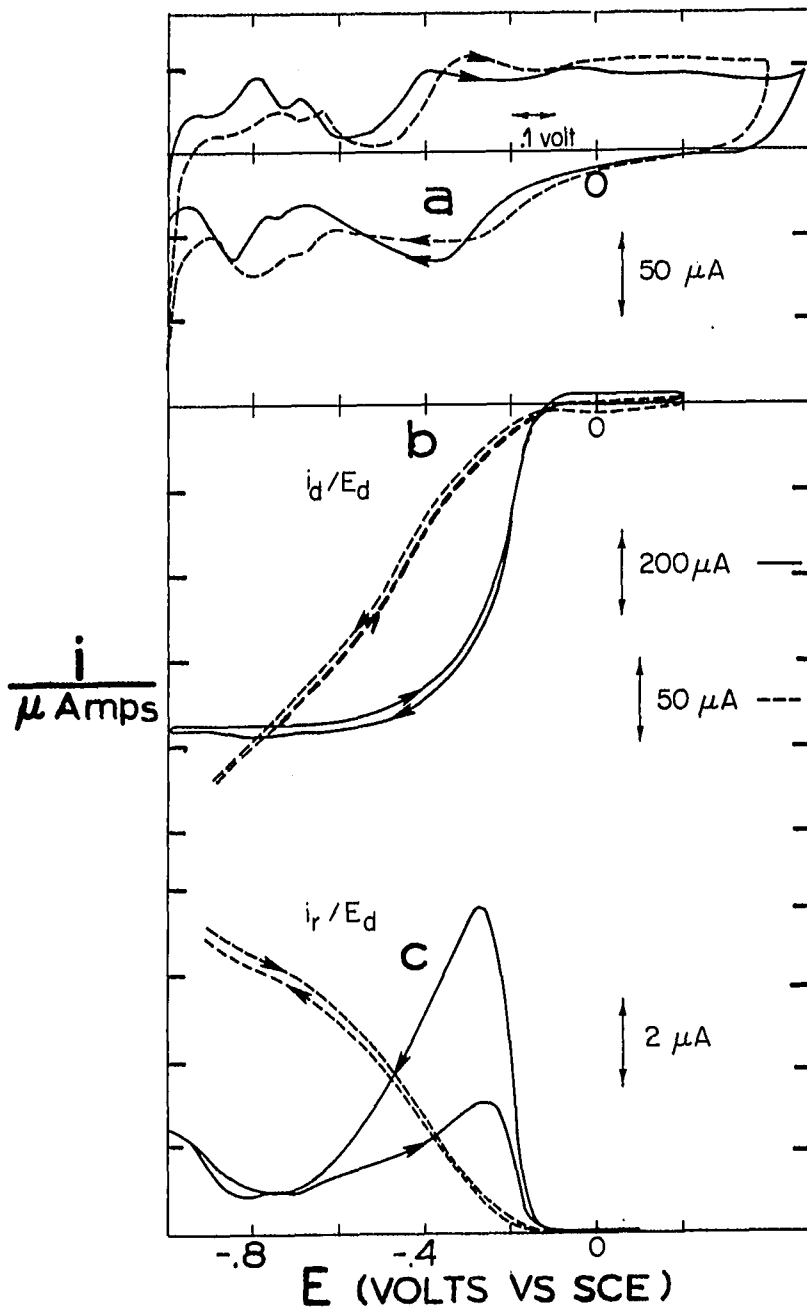
Figure IV-15. I/E waves for oxygen reduction on platinum
electrodes: (a) disk current in N_2 saturated
solution, (b) disk current in oxygen saturated
solution, and (c) ring current in oxygen
saturated solution; (---) reduced platinum
GPE, (——) solid platinum RRDE
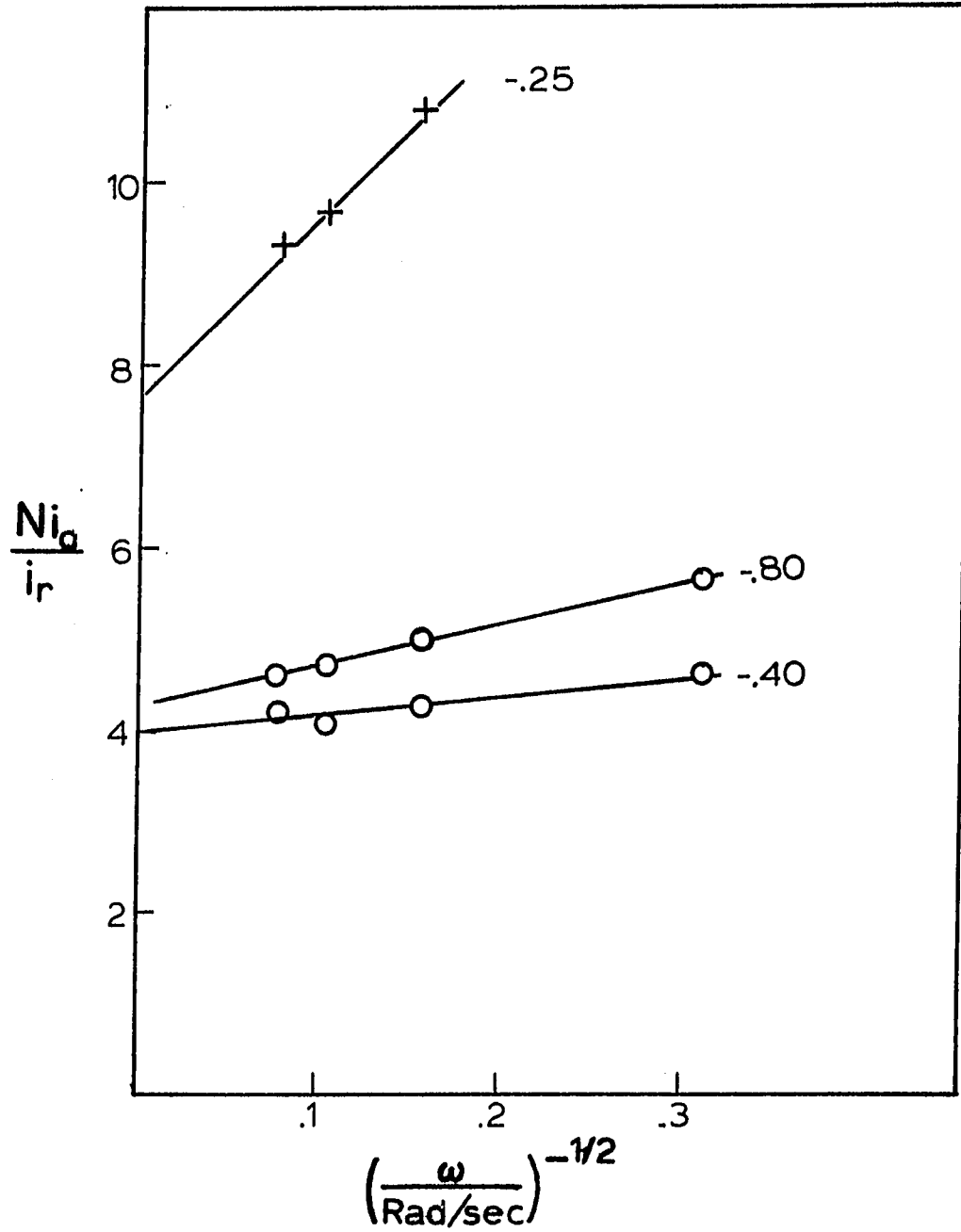
Figure IV-16. Ni_d/i_r versus $\omega^{-1/2}$ for oxygen reduction on platinum electrodes at different potentials: (o) reduced platinum GPE, (+) solid platinum RRDE
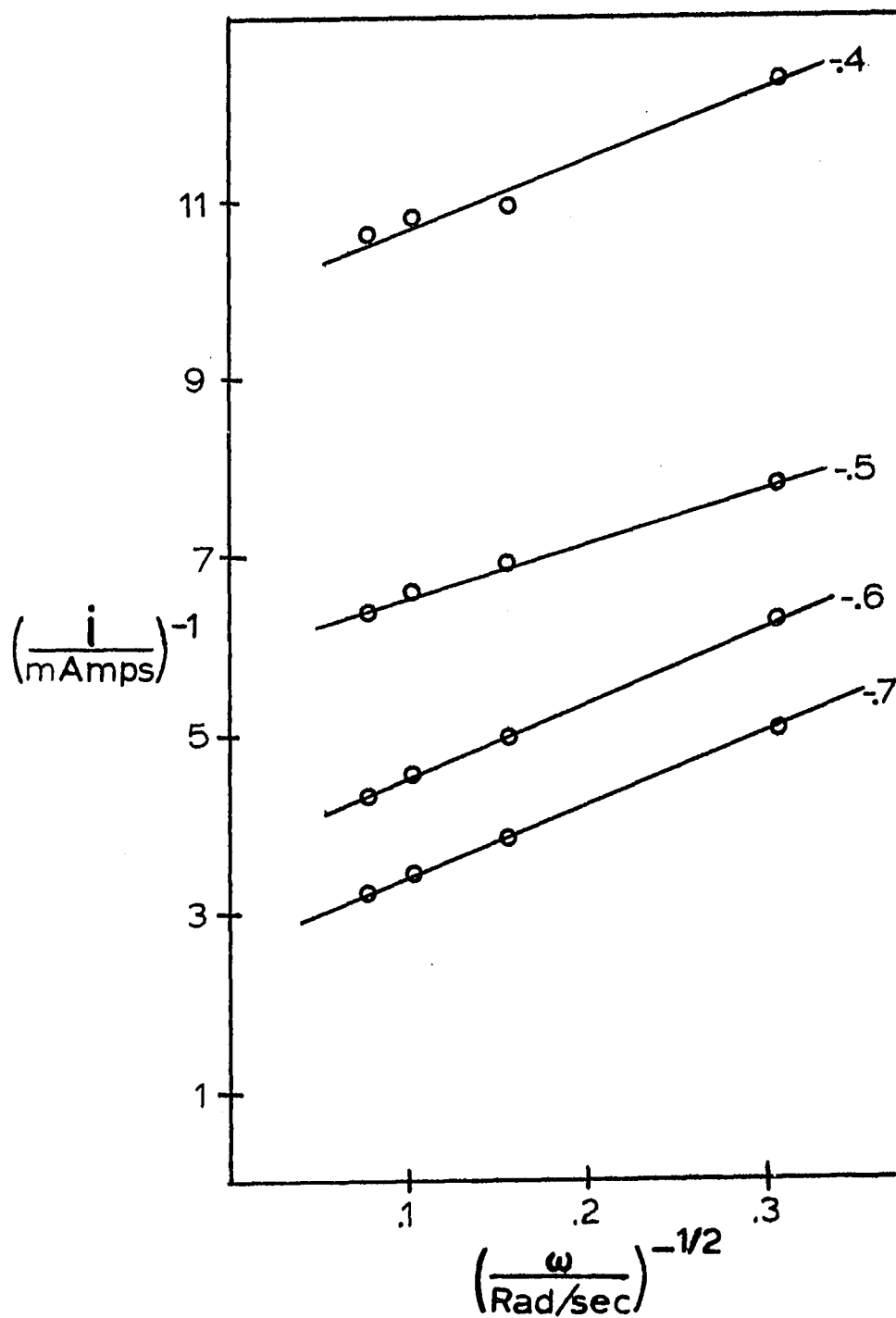
Figure IV-17. $1/i_d$ versus $\omega^{-1/2}$ for oxygen reduction on a reduced platinum GPE

catalyzed GPE is first order. Thus, the reduction of oxygen on platinum appears to be similar to its reduction on silver. At least half of the oxygen reacted goes by the four electron route.

E. Porphyrin

Among the more novel catalysts used for oxygen reduction are compounds which mimic biological oxygen electrocatalysts. Porphyrins, nature's major electron transfer agents, fall into this category. Work thus far shows their catalysis to be less effective than that of noble metals. These catalysts work by the redox method introduced previously. They offer an advantage in that a particular porphyrin can be synthesized which has some particular advantages for oxygen reduction. These possibilities include making a porphyrin with the optimum E_o and/or attaching a porphyrin to an electrode surface.

I/E data are shown for the porphyrins in Figure IV-18. The cobalt porphyrin[1] began reducing oxygen at a more positive potential but the iron porphyrin gave a higher current. The iron porphyrin also appears to give less

---

[1]The cobalt porphyrin was insoluble in 1 $\underline{M}$ NaOH and was essentially a dispersion of porphyrin particles in the solution.
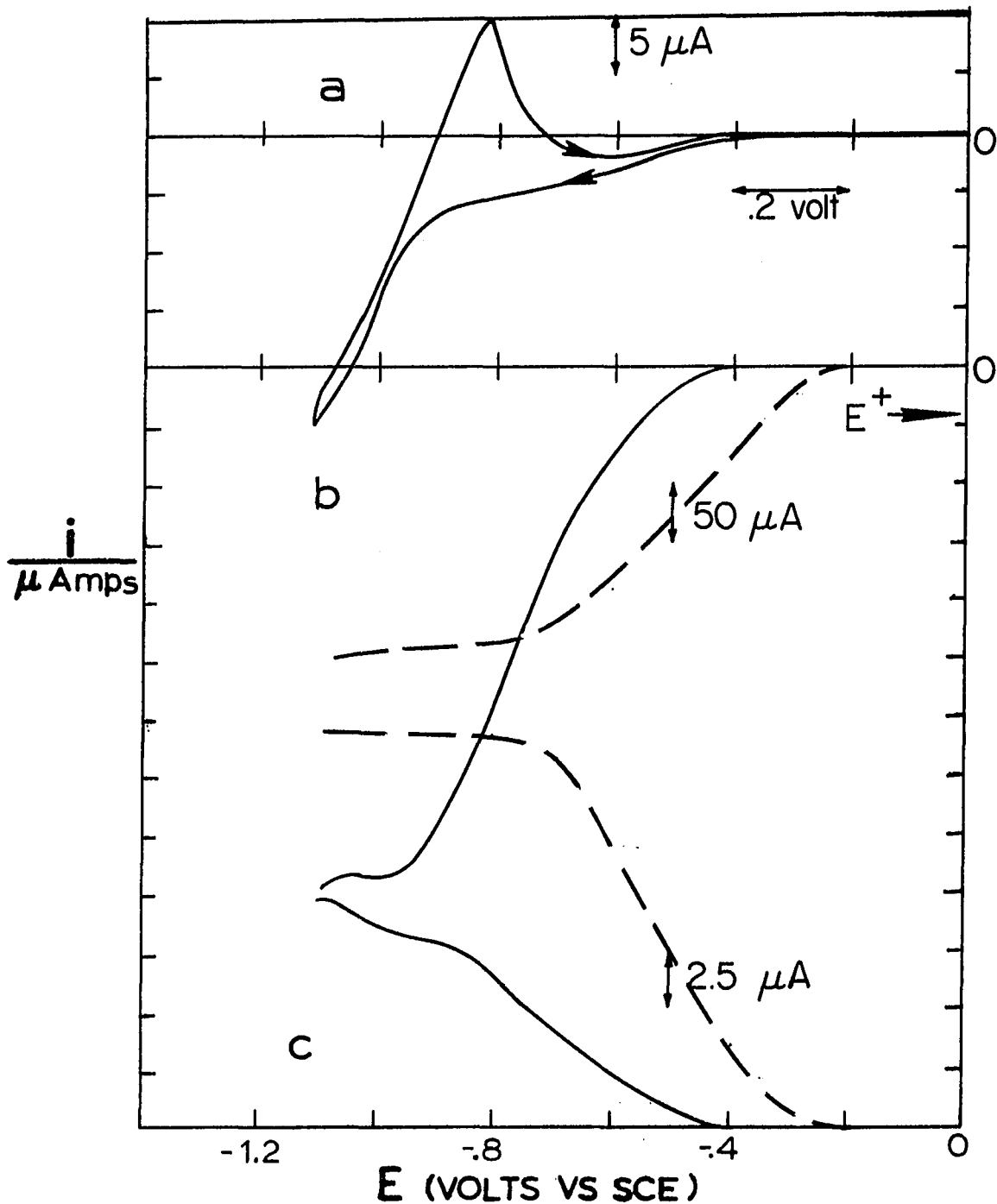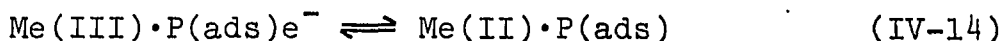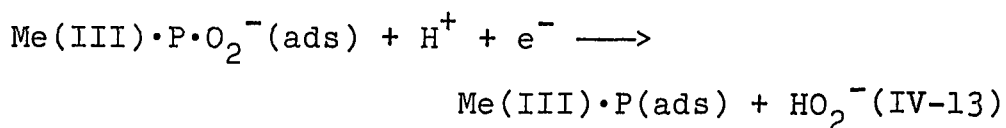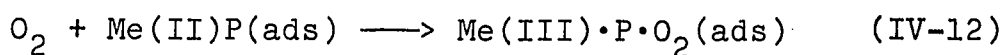
Figure IV-18. I/E waves for oxygen reduction catalyzed by
porphyrins on a GPE: (a) N_2 saturated disk
current, (b) oxygen saturated disk, and
(c) ring currents; (- - -) 1.4×10^{-4} M cobalt
tetra-pyridyl porphyrin, (——) 2.6×10^{-4} M
iron tetra-(4-n-methyl pyridyl)porphyrin

peroxide as product than its cobalt counterpart. This is verified by the data of Figure IV-19. The almost zero slope for the cobalt porphyrin indicates that almost none of the peroxide reacts further. The intercept of just over one indicates that the major product of oxygen reduction on the cobalt porphyrin is peroxide. The iron porphyrin is a more active catalyst for peroxide reduction as shown by the high slope and low intercept. The slopes may be artificially high due to the possibility of peroxide decomposition in the solution between the time it leaves the disk and the time it reaches the ring. Plots of $1/i_d$ versus $\omega^{-1/2}$ are linear confirming that the order with respect to oxygen is one. A mechanism which can explain this involves the interaction of oxygen with a surface bound porphyrin group:

$$O_2 + Me(II)P(ads) \longrightarrow Me(III) \cdot P \cdot O_2(ads) \qquad (IV-12)$$

$$Me(III) \cdot P \cdot O_2^-(ads) + H^+ + e^- \longrightarrow$$
$$Me(III) \cdot P(ads) + HO_2^- (IV-13)$$

$$Me(III) \cdot P(ads)e^- \rightleftharpoons Me(II) \cdot P(ads) \qquad (IV-14)$$

Me(III)·P represents the metal porphyrin in the particular valence state shown. The potential for oxygen reduction using these catalysts is frequently related to the equilibrium potential of the porphyrin. The equilibrium potential shown in Figure IV-18 for the iron porphyrin is about -0.9 volts. In this same figure, the half wave potential for oxygen reduction using the iron porphyrin is
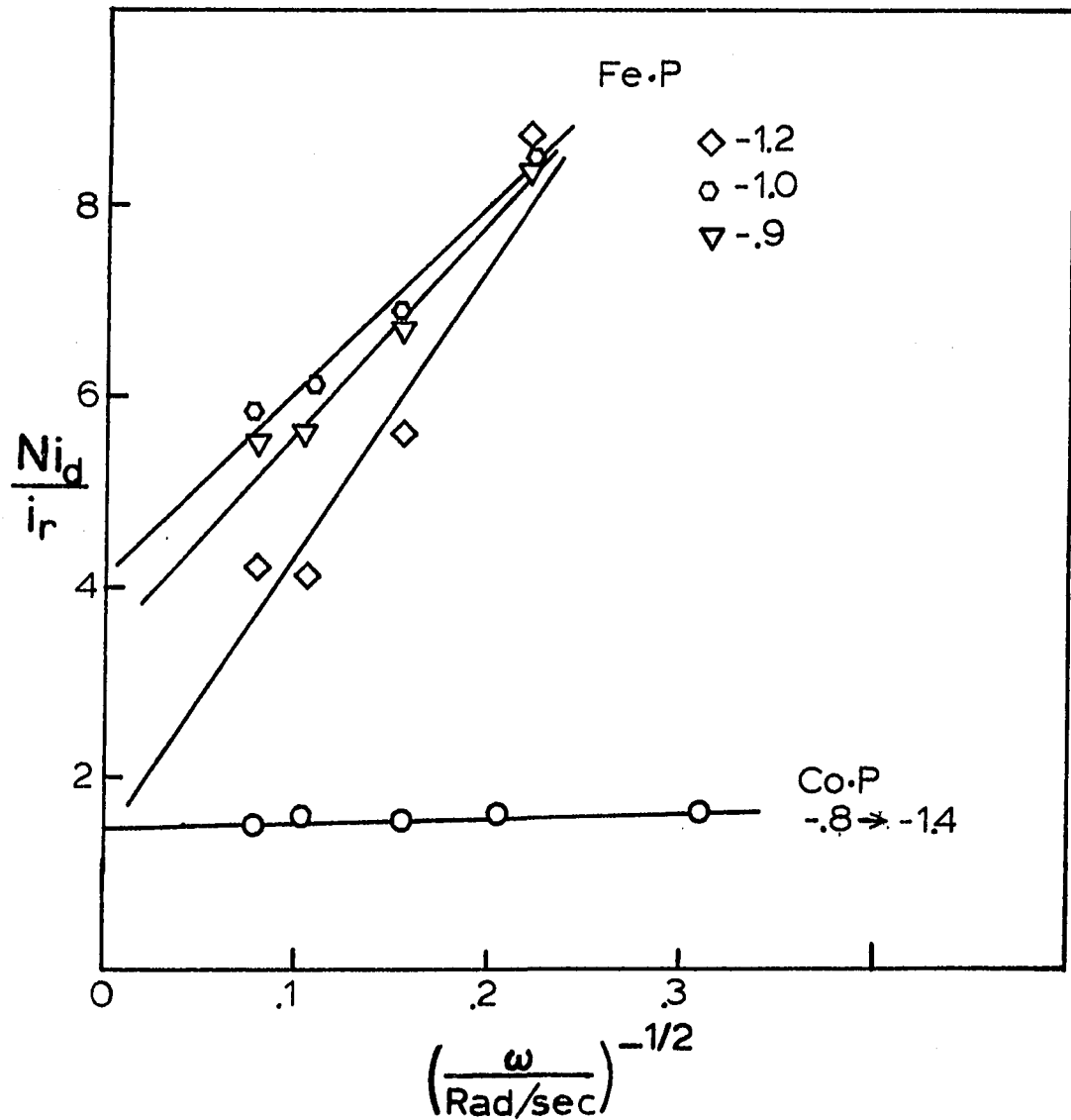
Figure IV-19. Ni_d/i_r versus $\omega^{-1/2}$ plots for oxygen reduction on a GPE catalyzed by metal porphyrins

-0.75 volts. For the porphyrin to catalyze the oxygen reduction at this potential requires a shift in the concentration of porphyrin given by the Nernst equation

$$\log \frac{[Fe(III) \cdot P]}{[Fe(II) \cdot P]} = \frac{0.15}{0.059} = 2.5$$

Thus the concentration of $Fe(III) \cdot P$ at the electrode surface must be 2.5 orders of magnitude greater than the $Fe(II) \cdot P$ concentration. The rate constant of the oxygen porphyrin interaction has been estimated as 1×10^8 under pseudo first order conditions, that is, oxygen concentration much greater than porphyrin concentration (66)

$$Rate = k \cdot [O_2][Fe(II) \cdot P] \tag{IV-15}$$

The rate can be calculated to see if this reaction could support the observed current

$$Rate = (1 \times 10^8) \cdot (8 \times 10^{-4})(2.6 \times 10^{-4}/10^{2.5})$$

$$= 6.58 \times 10^{-2} \text{ moles/sec}$$

The rate calculated from the observed current is given by:

$$Rate = i/nF$$

$$= 2.25 \times 10^{-4}/96500$$

$$= 2.33 \times 10^{-9} \text{ moles/sec}$$

Obviously, the rate of the oxygen-porphyrin reaction does not limit the current at this point. Other possible

limiting factors are (a) mass transport, since the diffusion coefficient of the porphyrin is about 2×10^{-6} cm^2 sec^{-1} (66), and (b) impure porphyrin; the actual concentration of porphyrin may be less than that calculated due to the inclusion of nonmetal porphyrin in the catalyst.

Thus, metal porphyrins are able to mediate oxygen reduction at a GPE. Two porphyrins have been used which show different oxygen reduction characteristics. The currents needed to mediate oxygen reduction are easily achieved by the reaction of oxygen with very low porphyrin concentrations.

V. CONCLUSIONS

Oxygen reduction on a GPE used as the disk for a RRDE electrode has been studied using triangular wave voltammetry. Two reduction waves were observed. Only the current for the second wave was proportional to $\omega^{1/2}$ as described by the Levich equation. The behavior of the first wave was compared to previous results for oxygen reduction on the basal plane of highly oriented graphite crystals. Its lack of dependence on $\omega^{1/2}$ has previously been reported. The formation of a limiting current plateau indicates that a mass transport limited rate has been established but this rate is not dependent on the diffusion layer thickness. This may be due in large part to nonlinear diffusion of oxygen to the active sites. Since the rate of use of oxygen at the first wave is much less than a diffusion limited rate, there is very little concentration gradient in the diffusion layer. With almost no concentration gradient, the oxygen reduction current will show very little dependence on the diffusion layer thickness.

The two waves may have been due to sites of different activity on the graphite surface, the edges of the graphite crystals which appear to be better able to adsorb oxygen, and the graphite basal plane on which oxygen adsorption is inhibited.

The limiting step for oxygen reduction on a GPE may be the initial adsorption step. If this step involves no charge transfer, as in equation IV-6, the Tafel slope

$$O_2 + S \rightleftharpoons O_2(ads) \tag{IV-6}$$

would be expected to be higher than for a single charge transfer reaction (i.e., equation IV-3 for which the Tafel slope would be 120 mV/decade f(i)). It is also possible, however, that the rate is limited by the first electron transfer. Figure A-2 in Appendix A shows the simplified view of electron transfer at an electrode. With symmetrical energy barriers β equals 1/2. This figure also shows how the peak in the energy barrier can be shifted when a potential is applied to the electrode. In the case shown, an anodic potential is applied and β is shown to be greater than 1/2. In a similar fashion a cathodic potential may make β less than 1/2. Since a large cathodic overpotential was common for the conditions of these experiments, a β less than 1/2 would seem likely. This may be the cause of the Tafel slopes of about 180 mV/decade f(i) which would lead to a β of 1/3.

Previous results of oxygen reduction on a GPE were interpreted in a different manner than my results. This study has shown that no decomposition or further reaction of peroxide occurs on a GPE while previous workers (93) felt that the second wave was due to the reduction of

peroxide. This previous study, however, did not have the advantage of a ring electrode which would determine how much peroxide was formed at the GPE disk. Other data in this laboratory indicate that very little reduction of peroxide occurs at potentials more positive than -1.2 volts versus the SCE. For these reasons, it seems most likely that the final product of oxygen reduction on a GPE is peroxide.

Deposition of catalysts on a GPE RRDE for the purpose of studying oxygen reduction catalysis has not previously been described in the literature. In the present study the catalysis afforded the GPE by gold, silver, or platinum was studied with special attention to the amount of peroxide formed as product. The results of oxygen reduction on the catalyzed GPE were compared to similar data from those same metals plated onto a platinum disk RRDE. Since the catalyst plated platinum layers were continuous, these are referred to as solid catalyst electrodes. In these studies some basic trends were established. On all catalyzed GPE electrodes, the fraction of peroxide in the product was greater than that for the solid catalyst electrodes. Similarly, all measured Tafel slopes indicated that the reaction was limited by the first electron transfer step. A simple model can be used to help describe the behavior of these electrodes. The interaction of oxygen with two

adjacent surface sites to facilitate dissociative adsorption was described in section I-A-2 using Figure I-4. A similar model can be used to describe the formation of peroxide (i.e., nondissociative adsorption). Two cases can be considered. In the first case oxygen adsorption involves only a single site, or end on adsorption. The second possibility involves the adsorption of oxygen at an edge site where there is only one adjacent surface hydroxide to facilitate hydrogen donation to the oxygen. In both cases the oxygen receives one H^+ and two electrons and desorbs as peroxide anion. This model can be used to describe oxygen reduction on the plated electrodes by considering the nature of the deposit. The deposition of metal catalysts on the platinum RRDE occurred at much more anodic potentials than deposition on a GPE. The deposits formed appeared smoother and less porous. Thus, large areas of flat surface were available for dual site oxygen adsorption with subsequent O-O bond breaking. The GPE deposited catalysts have much rougher surfaces and a higher ratio of edge-to-flat surfaces. This would lead to more single site and edge adsorption as described above with the concomitant increase in peroxide formation. Moreover, this would be the case even if these edge sites were more active for oxygen adsorption. Thus, it seems that any phenomena that results in roughening the surface would lead to an increase in

the fraction of peroxide as the oxygen reduction product.

Unlike gold and platinum, the behavior of silver electrodes depended significantly on their modes of preparation. The silver plated GPE appeared to have sites active for oxygen adsorption that were not evident in the other silver electrodes. These sites, however, appeared to enhance the two electron reduction of oxygen instead of the four electron mechanism. A Tafel slope for oxygen reduction on silver in alkaline solution at an RRDE has not previously been reported. Tafel slopes of 60 mV/decade f(i) had previously been reported from galvanostatic measurements (9). These data are commonly taken at current densities much lower than those in this study due to the limits of mass transport. Thus, the Tafel slope for oxygen reduction must change between low and high current regimes. This same behavior has been reported for gold (107) and platinum (111) in alkaline solution. The shift in Tafel slope is due to the difference in the E/log i relationship for the different limiting steps.

Oxygen reduction on a reduced platinum GPE appears to follow both pathways equally. As with silver, the solid catalyst electrode produces very little peroxide. However, the reduced platinum GPE produces peroxide

from about half the oxygen that reacts at the electrode. Unlike gold and silver, the oxide reduction on platinum appears more closely related to oxygen reduction. As soon as the reduction of the platinum oxide begins, oxygen reduction begins. This suggests a reduction pathway in which oxygen interacts with the bare platinum to reform platinum oxide. Thus, a surface redox cycle is set up where oxygen oxidizes the bare platinum to platinum oxide which is subsequently reduced. This is not the case for gold or silver whose oxides are reduced at a potential more anodic than the potential for oxygen reduction.

Oxygen reduction by the cobalt and iron porphyrins exhibits the difference in characteristics of two metals in their macrocyclic complexes. The cobalt porphyrin reduced oxygen at more positive potentials with peroxide as the major product. The iron porphyrin was better able to further reduce or decompose the peroxide thus resulting in larger currents. As has been shown in homogeneous oxygen reduction, the interaction of _two_ metal porphyrins with an oxygen molecule can result in complete reduction of the oxygen to water. When only one porphyrin is allowed to interact with oxygen, four electron reduction does not occur. According to this idea, the reduction of oxygen to peroxide should occur at surface bound (or adsorbed) porphyrin groups. This idea is supported by

earlier work (68) in which a carbon electrode is dipped into a solution of the cobalt tetrapyridyl porphyrin, rinsed with distilled water, and then examined for oxygen reduction characteristics. The electrode catalyzed oxygen reduction in a manner similar to that of the same electrode in a cobalt porphyrin solution.

For solid catalysts, all indications are that at the high current regime the first electron transfer (or oxygen adsorption) is rate limiting. Thus, to improve the catalysis of these materials two approaches seem promising:

a) increase the surface area of the electrocatalyst, and

b) disperse the catalyst on a highly divided support which is also capable of adsorbing oxygen thus supplying the product of the slow step to the catalyst and increasing the overall rate. In addition to this, it would be advantageous to have the reduction of oxygen go by the four electron route. In this respect it appears that plated catalysts are less useful than chemically reduced catalysts. This is evident from the comparison of oxygen reduction on a silver plated GPE and a reduced silver GPE. The reduced silver GPE produces a lower fraction of peroxide as product than does the plated GPE as shown in Figure IV-14.

VI. BIBLIOGRAPHY

1. Grove, W. R. Phil. Mag. 1839, 14, 127.

2. Haber, P.; Moser, A. Z. Electrochem. 1905, 11, 593.

3. Nernst, W. German Patent 259 241, 1912; Chem. Abstr. 1913, 7, 2908.

4. Bauer, E.; Ehrenberg, H. Z. Electrochem. 1912, 18, 1002.

5. Davtyan, O. K. Bull. Acad. Sci. USSR, Classe Sci. Tech. Otdel. Tek. Nauk 1946, 107 and 215.

6. Bacon, F. T. Beama J. 1954, 61, 6.

7. Bacon, F. T. In "Fuel Cells"; Young, G. J., Ed.: Reinhold Press: New York, 1960; Vol. I, Chapter 5.

8. Bacon, F. T. J. Electrochem. Soc. 1979, 126, 7C.

9. Hoare, J. P. "Oxygen Electrochemistry"; New York Interscience: New York, 1968.

10. Damjanovic, A. In "Modern Aspects of Electrochemistry"; Bockris, J. O'M.; Conway, B. E., Ed.; Plenum Press: New York, 1969; Vol. 5, Chapter 5.

11. Bockris, J. O'M.; Reddy, A. K. N. "Modern Electrochemistry"; New York Plenum: New York, 1970.

12. Appleby, A. J. In "Modern Aspects of Electrochemistry"; Conway, B. E.; Bockris, J. O'M., Ed.; Plenum Press: New York, 1974; Vol. 9, Chapter 5.

13. Hoare, J. P. In "Encyclopedia of Electrochemistry of the Elements"; Bard, A. J., Ed.; Marcel Dekker Inc.: New York, 1974; Vol. 2, Chapter 5.

14. Sawyer, D. T.; Seo, E. T. Inorg. Chem. 1977, 16, 499.

15. Damjanovic, A.; Genshaw, M. A.; Bockris, J. O'M. J. Electrochem. Soc. 1967, 114, 466.

16. Johnson, D. C.; Bruckenstein, S. Anal. Chem. 1971, 43 1313.

17. Damjanovic, A.; Genshaw, M. A.; Bockris, J. O'M. J. Chem. Phys. 1966, 45, 4057.

18. Myuller, L.; Nekrasov, L. N. _Zh. Fiz. Khim._ 1964, 38, 3028.

19. Tarasevich, M. R. _Sov. Electrochem._ 1967, 4, 182.

20. Bagotskii, V. S.; Filinovskii, V. Y.; Shumilova, N. A. _Sov. Electrochem._ 1968, 4, 1129.

21. Zhutaeva, G. V.; Merkulova, N. D.; Shumilova, N. A.; Bagotskii, V. S. _Sov. Electrochem._ 1968, 4, 1136.

22. Bagotskii, V. S.; Tarasevich, M. R.; Filinovskii, V. Y. _Sov. Electrochem._ 1969, 5, 1158.

23. Tarasevich, M. R.; Burshtein, R. K.; Radyushkina, K. A. _Sov. Electrochem._ 1970, 6, 366.

24. Radyushkina, K. A.; Tarasevich, M. R.; Burshtein, R. K. _Sov. Electrochem._ 1970, 6, 1307.

25. Tarasevich, M. R.; Radyushkina, K. A.; Filinovskii, V. Y.; Burshtein, R. K. _Sov. Electrochem._ 1970, 6, 1468.

26. Tarasevich, M. R. _Sov. Electrochem._ 1973, 9, 578.

27. Goldstein, J. R.; Tseung, A. C. C. _J. Phys. Chem._ 1972, 76, 3646.

28. Maricle, D. L.; Hodgson, W. G. _Anal. Chem._ 1965, 37, 1562.

29. Sawyer, D. T.; Roberts, J. L., Jr. _J. Electroanal. Chem._ 1966, 12, 90.

30. Peover, M. E.; White, B. S. _Electrochim. Acta_ 1966, 11, 1061.

31. Fuginaga, T.; Izutsu, K.; Adachi, T. _Bull. Chem. Soc. Japan_ 1969, 42, 140.

32. Goolsby, A. D.; Sawyer, D. T. _Anal. Chem._ 1968, 40, 83.

33. Dubrovina, N. I.; Nekrasov, L. N. _Sov. Electrochem._ 1972, 8, 1466.

34. Divisek, J.; Kastening, B. _J. Electroanal. Chem._ 1975, 65, 603.

35. Taylor, R. J.; Humffray, A. A. J. Electroanal. Chem. 1975, 64, 63.

36. Kolthoff, I. M.; Miller, C. S. J. Amer. Chem. Soc. 1941, 63, 1013.

37. Zurilla, R. W.; Sen, R. K.; Yeager, E. J. Electrochem. Soc. 1978, 125, 1103.

38. Morcos, I.; Yeager, E. Electrochim. Acta 1970, 15, 953.

39. Yeager, E. National Bureau of Standards Special Publication No. 455; Franklin, A. D., Ed.; U. S. Government Printing Office: Washington, 1976, page 203.

40. Sen, R. K.; Zagal, J.; Yeager, E. Inorg. Chem. 1977, 16, 3379.

41. Behar, D.; Czapski, G.; Rabani, J.; Dorfman, L. M.; Schwarz, H. A. J. Phys. Chem. 1970, 74, 3209.

42. Evans, U. R. Nature 1968, 218, 602.

43. Sepa, D. B.; Damjanovic, A.; Bockris, J. O'M. Electrochim. Acta 1967, 12, 746.

44. Goldstein, J. R.; Tseung, A. C. C. Nature 1969, 222, 869.

45. Tseung, A. C. C.; Hobbs, B. S.; Tantram, A. D. S. Electrochim. Acta 1970, 15, 473.

46. Bertocci, U.; Cohen, M. I.; Mullen, J. L.; Negas, T. National Bureau of Standards Special Publications No. 455; Franklin, A. D., Ed.; U. S. Government Printing Office: Washington, 1976, page 313.

47. Tseung, A. C. C.; Bevan, H. L. J. Electroanal. Chem. 1973, 45, 429.

48. King, W. J.; Tseung, A. C. C. Electrochim. Acta 1974, 19, 485.

49. Hibbert, D. B.; Tseung, A. C. C. J. Electrochem. Soc. 1978, 125, 74.

50. Yeung, K. L. K.; Tseung, A. C. C. J. Electrochem. Soc. 1978, 125, 878.

51. Tseung, A. C. C.; Yeung, K. L. K. _J_. Electrochem. Soc. 1978, 125, 1003.

52. Tseung, A. C. C. _J_. Electrochem. Soc. 1978, 125, 1660.

53. Van Buren, F. R.; Broers, G. H. J.; Boesveld, C.; Bouman, A. J. _J_. Electroanal. Chem. 1978, 87, 381.

54. Matsumoto, Y.; Yoneyama, H.; Tamura, H. _J_. Electroanal. Chem. 1977, 79, 319.

55. Matsumoto, Y.; Yoneyama, H.; Yamura, H. _J_. Electroanal. Chem. 1977, 83, 237.

56. Kudo, T.; Obayashi, H.; Yoshida, M. _J_. Electrochem. Soc. 1977, 124, 321.

57. Matsumoto, Y.; Yoneyama, H.; Tamura, H. _J_. Electroanal. Chem. 1977, 83, 167.

58. Horkans, J.; Shafer, M. W. _J_. Electrochem. Soc. 1977, 124, 1196.

59. Campadelli, F.; Cariati, F.; Carniti, P.; Morazzoni, F.; Ragaini, V. _J_. Catal. 1976, 44, 167.

60. Randin, J. P. Electrochim. Acta 1974, 19, 83.

61. Radyushkina, K. A.; Levina, O. A.; Tarasevich, M. R.; Burshtein, R. K.; Berezin, B. D.; Shormanova, L. P.; Koifman, O. I. Sov. Electrochem. 1975, 11, 916.

62. Behret, H.; Clauberg, W.; Sandstede, G. _J_. Electroanal. Chem. 1976, 74, 393.

63. Brezina, M.; Khalil, W.; Koryta, J.; Musilova, M. _J_. Electroanal. Chem. 1977, 77, 237.

64. Ulstrup, J. _J_. Electroanal. Chem. 1977, 79, 191.

65. Zagal, J.; Sen, R. K.; Yeager, E. _J_. Electroanal. Chem. 1977, 83, 207.

66. Kuwana, T.; Fujihara, M.; Sunakawa, K.; Osa, T. _J_. Electroanal. Chem. 1978, 88, 299.

67. Behret, H.; Binder, J.; Clauberg, W.; Sandstede, G. Electrochim. Acta 1978, 23, 1023.

68. Bettelheim, A.; Chan. R. J. H.; Kuwana, T. J. Electroanal. Chem. 1979, 99, 391.

69. Kazarinov, V. E.; Tarasevich, M. R.; Radyushkina, K. A.; Andreev, V. N. J. Electroanal. Chem. 1979, 100, 225.

70. Collman, J. P.; Marrocco, M.; Denisevich, P.; Koval, C.; Anson, F. C. J. Electroanal. Chem. 1979, 101, 117.

71. Appleby, A. J.; Fleisch, J.; Savy, M. J. Catal. 1976, 44, 281.

72. Shropshire, J. A.; Tarmy, B. L. In "Advances in Chemistry Series"; Gould, R. F., Ed.; A. C. S. Applied Publications: Washington, D.C., 1976; Vol. 47, Chapter 12.

73. Wilson, D. F. University of Pennsylvania School of Medicine, Philadelphia, Pennsylvania, presented at the Workshop on Oxygen Electrochemistry, Painesville, Ohio, May 1979.

74. Adzic, R.; Tripkovic, A.; Atanasoski, R. J. Electroanal. Chem. 1978, 94, 231.

75. Adzic, R. Institute of Electrochemistry, Belgrade, Yugoslavia, presented at the Workshop of Oxygen Electrochemistry, Painesville, Ohio, May 1979.

76. Gland, J. General Motors Research Labs, Warren, Michigan, presented at the Workshop on Oxygen Electrochemistry, Painesville, Ohio, May 1979.

77. Selwood, P. W. J. Catal. 1976, 42, 148.

78. Urbach, F. Case Western Reserve University, Cleveland, Ohio, presented at the Workshop on Oxygen Electrochemistry, Painesville, Ohio, May 1979.

79. Goddard, W. California Institute of Technology, Pasadena, California, presented at the Workshop on Oxygen Electrochemistry, Painesville, Ohio, May 1979.

80. Filinovskii, V. Y.; Pleskov, Y. V. In "Progress in Surface and Membrane Science"; Cadenhead, D. A.; Danielli, J. F., Ed.; Academic Press: New York, 1976; Vol. 10, Chapter 2.

81. Frantisek, O.; Beran, P. J. Electroanal. Chem. 1976, 69, 1.

82. Levich, V. G. "Physiochemical Hydrodynamics"; Prentice-Hall: Englewood Cliffs, NJ, 1962.

83. Albery, W. J.; Bruckenstein, S. Trans. Faraday Soc. 1966, 62, 1920.

84. Adams, R. N. Anal. Chem. 1958, 30, 1576.

85. Olson, C.; Adams, R. N. Anal. Chim. Acta 1960, 22, 582.

86. Galus, Z.; Olson, C.; Lee, H. Y.; Adams, R. N. Anal. Chem. 1962, 34, 165.

87. Olson, C.; Adams, R. N. Anal. Chim. Acta 1963, 29, 358.

88. Soderhjelm, P. J. Electroanal. Chem. 1976, 71, 109.

89. Lundquist, J. J. Electroanal. Chem. 1974, 52, 37.

90. Marcoux, L. S.; Prater, K. B.; Prater, B. G.; Adams, R. N. Anal. Chem. 1965, 37, 1446.

91. Brezina, M.; Hofmanova-Matejkova, A. J. Electroanal. Chem. 1973, 44, 460.

92. Brezina, M. Nature 1966, 212, 283.

93. Brezina, M.; Hofmanova-Matejkova, A. Collect. Czech. Chem. Commun. 1973, 38, 3024.

94. Appel, M.; Appleby, A. J. Electrochim. Acta 1978, 23, 1243.

95. Appleby, A. J. Electric Power Research Institute, Palo Alto, California, presented at the Workshop on Oxygen Electrochemistry, Painesville, Ohio, May 1979.

96. Brezina, M.; Jindra, J.; Mrha, J. Collect. Czech. Chem. Commun. 1968, 33, 2363.

97. Morcos, I. J. Electrochem. Soc. 1975, 122, 1008.

98. Morcos, I. J. Electrochem. Soc. 1977, 124, 13.

99. Landsberg, R.; Thiele, R. Electrochim. Acta 1968, 11, 1243.

100. Wroblowa, H. S.; Pan, Y. C.; Razumney, G. J. Electroanal. Chem. 1976, 69, 195.

101. Appleby, A. J.; Savy, M. J. Electroanal. Chem. 1978, 92, 15.

102. McIntyre, J. D. E. J. Phys. Chem. 1967, 71, 1196.

103. Davis, R. E.; Hovarth, G. L.; Tobias, C. W. Electrochim. Acta 1967, 12, 287.

104. Case, B. Electrochim. Acta 1973, 18, 293.

105. Gubbins, K. E.; Walker, R. D. J. Electrochem. Soc. 1965, 112, 469.

106. Russell, C. D.; Peterson, J. M. J. Electroanal. Chem. 1963, 5, 467.

107. Yeager, E.; Krouse, P.; Rao, K. V. Electrochim. Acta 1964, 9, 1057.

108. Andruseva, S. I.; Tarasevich, M. R.; Radyushkina, K. A. Sov. Electrochem. 1977, 13, 211.

109. Damjanovic, A.; Genshaw, M. A.; Bockris, J. O'M. J. Electroanal. Chem. 1967, 15, 173.

110. Zhutaeva, G. V.; Shumilova, N. A. Sov. Electrochem. 1968, 4, 87.

111. Damjanovic, A.; Genshaw, M. A.; Bockris, J. O'M. J. Electrochem. Soc. 1967, 114, 1107.

112. Smythe, W. R. J. Appl. Phys. 1953, 24, 70.

VII. ACKNOWLEDGEMENTS

VIII. APPENDIX A: RATE OF
ELECTROCHEMICAL REACTIONS

A chemical reaction can be viewed as an activated

process, shown in Figure A-1, where the reactant must pass

over an energy barrier before being converted to the

product. The rate constant of the forward reaction is

related to the size of the barrier $\Delta G_f^{\ddagger}$ by the Arhenius

equation:

$$k_f = (Const.) \exp\left\{- \frac{\Delta G_f^{\ddagger}}{RT}\right\} \qquad (A-1)$$

A similar equation can be written for the reverse reaction.

Electrochemical reactions are related to a barrier in the

same way with the additional feature of an adjustable

barrier height. Changing the potential of the electrode

can cause an electrochemical reaction to speed up, slow down,

or go in reverse. Figure A-2 shows the effect of an elec-

trode potential on an electron transfer reaction. When there

is no potential difference between the electrode and the

solution, the electron feels no electrostatic inducement to

transfer, a situation similar to the pure chemical reaction

(shown in Figure A-2a). If one now applies a potential to

the electrode (shown in Figure A-2b) both the chemical and

electrostatic energies must be summed to obtain the overall

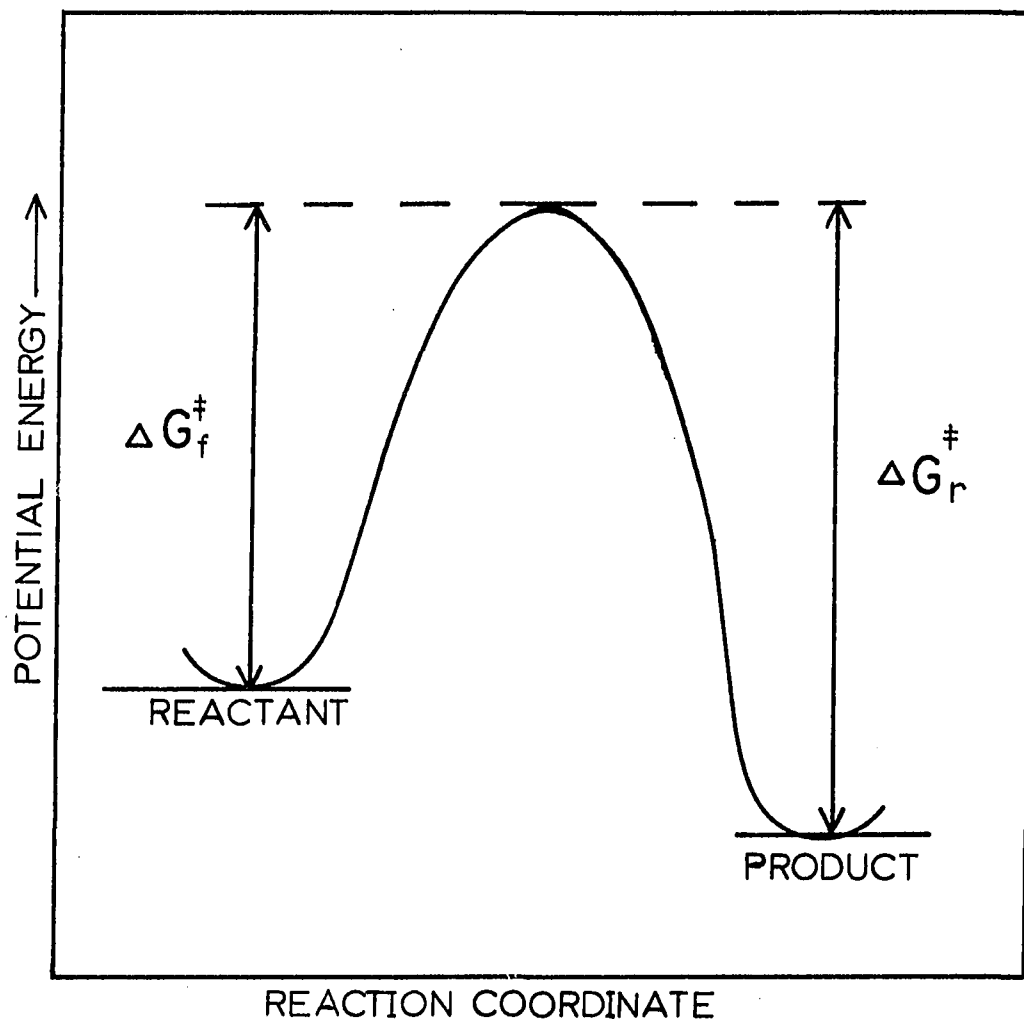barrier (shown in Figure A-2c). Our barriers are no longer

Figure A-1. Diagram of energy versus reaction coordinate. Free energy barriers ($\Delta G^{\ddagger}$) for the forward and reverse processes of a hypothetical chemical reaction are indicated
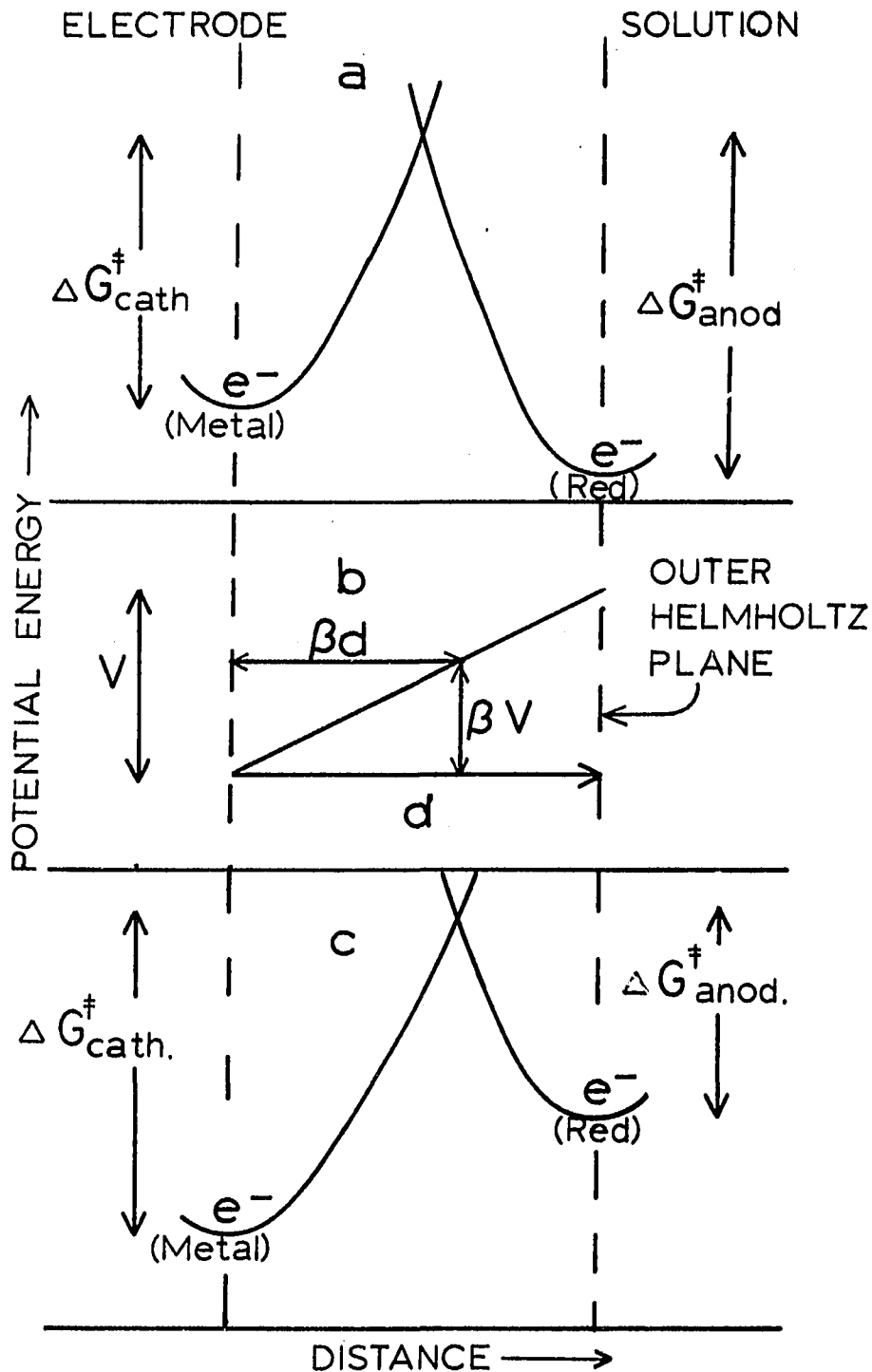
Figure A-2. Effect of electrode potential on electron
transfer: (a) potential energy diagram with no
externally applied potential, (b) potential
profile for an applied potential and (c) energy
diagram with an applied potential

only chemical but electrochemical and k_f is replaced by k_{cath} and k_r by k_{anod} where

$$k_{cath} = (Const.) \exp\left\{-\frac{\Delta G^{\ddagger}_{cath}}{RT}\right\} \qquad (A-2)$$

and

$$k_{anod} - (Const.') \exp\left\{-\frac{\Delta G^{\ddagger}_{anod}}{RT}\right\} \qquad (A-3)$$

As with all barrier processes, the reactant must reach the peak in order to relax into products. Thus, the potential affecting the reduction process is only that potential drop felt by the electron before it reaches the barrier peak, βd from the electrode surface. The potential affecting the reduction process is then βV while that affecting oxidation is $(1-\beta)V$. Armed with this, we can split up the free energy terms into chemical and potential dependent terms

$$k_{cath} = k'_f \exp-\left\{\frac{\beta FE}{RT}\right\} \qquad (A-4)$$

$$k_{anod} = k'_r \exp\left\{\frac{(1-\beta)FE}{RT}\right\} \qquad (A-5)$$

In order to obtain a useful expression, the voltage in the exponential terms must be referenced to some standard voltage, such as E°. E° is the standard reduction potential, the voltage at which the electrochemical reaction is in equilibrium when the concentrations of involves species are one. Under these conditions,

$$k_{cath} = k_{anod}$$

$$k_f' \exp\left\{-\frac{\beta FE^\circ}{RT}\right\} = k_r' \exp\left\{\frac{(1-\beta)FE^\circ}{RT}\right\} \tag{A-6}$$

$$= k_o$$

where k_o is defined as the heterogeneous rate constant. Solving for k_f' and k_r' gives

$$k_f' = k_o \exp\{\beta FE^\circ/RT\} \tag{A-7}$$

$$k_r' = k_o \exp\{-(1-\beta)E^\circ/RT\} \tag{A-8}$$

Combining these with equations A-4 and A-5 results in

$$k_{cath} = k_o \exp\left\{\frac{-\beta F(E-E_o)}{RT}\right\} \tag{A-9}$$

$$k_{anod} = k_o \exp\left\{\frac{(1-\beta)F(E-E_o)}{RT}\right\} \tag{A-10}$$

These two equations give the general form of the rate constants to be used in the development of equations for heterogeneous equations.

IX. APPENDIX B: FLUX TO A ROTATING DISK ELECTRODE

The general description of material balance at a rotating disk electrode is given by

$$\frac{\partial C}{\partial t} = - \text{div } C \cdot V + \text{div}(DVC) \tag{B-1}$$

$$\partial C/\partial t = - [V_x \, \partial C/\partial X + V_r \, \partial C/\partial r + (V_\theta/r)(\partial C/\partial \theta]$$

$$+ D[\partial^2 C/\partial X^2 + \partial^2 C/\partial r^2 + (1/r)\partial C/\partial r$$

$$+ (1/r^2)\partial^2 C/\partial \theta^2] \tag{B-2}$$

If the electrode is rotating at a constant rate some of the terms in equation B-2 can be neglected. At steady state $\partial C/\partial t = 0$; due to symmetry the change in concentration with respect to radius and θ is zero. The resulting equation

$$V_x(\partial C/\partial X) = D \, \partial^2 C/\partial X^2 \tag{B-3}$$

must now be solved using the following boundary conditions:

1. For the case of a limiting current $C_{(X=0)} = 0$

$$C_{(X \to \infty)} = C^{bulk}$$

2. From Faraday's and Fick's laws,

$$(\partial C/\partial X)_{X=0} = i_\ell/nFAD$$

The latter condition depends on the assumption of current limited by diffusion across a boundary layer. Pictorially,

Figure B-1 shows the change in concentration in the solution approaching the electrode. Approximating the gradient with a straight line the value δ for the diffusion layer thickness can be estimated.

The first step in this solution is the single integration of equation B-3 giving equation B-4. At this

$$\frac{dc}{dx} = a_1 \exp \int_0^x \frac{V_x(z)}{D} \, dz \qquad \text{(B-4)}$$

point we can see by our second boundary condition that $a_1 = i_\ell/nFAD$. Remembering this, a second integration gives equation B-5

$$c(x) = a_1 \int_0^x (\exp \frac{1}{D} \int_0^y V_x(z) \, dz) dy + a_2 \qquad \text{(B-5)}$$

Using the first boundary condition $a_2 = 0$. The solution must now be separated into two regions, one of diffusion control and one under convective control. With the advance knowledge that convection will be much faster than diffusion, the contribution to the concentration gradient of the convective region can be neglected. Now with a knowledge of V_x, we can solve the problem. The equations describing V_x and the fluid flow to a rotating disk were solved before being applied to electrochemistry.[1] The

---

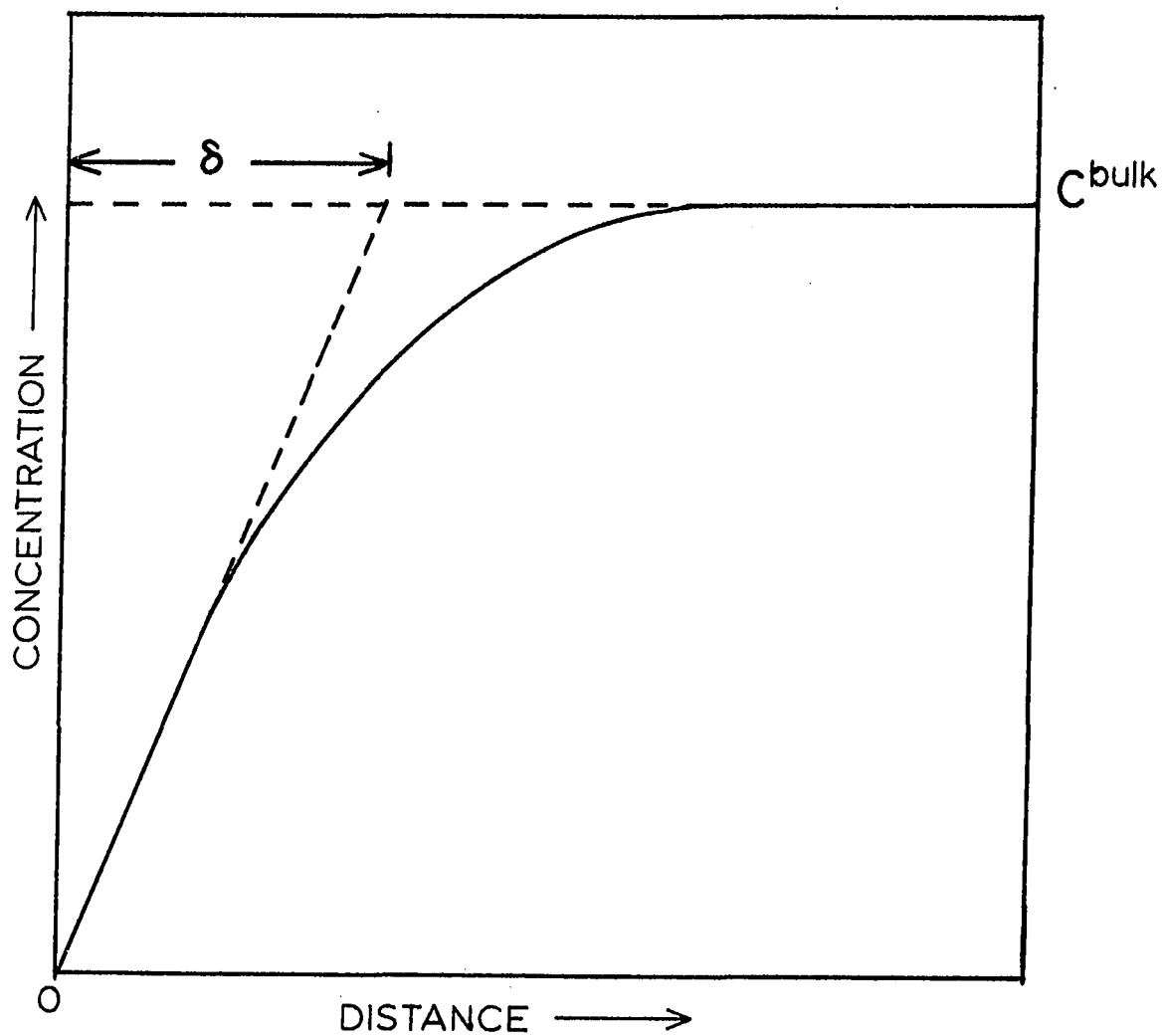[1]For a more thorough development, see reference 82.

Figure B-1. Concentration/distance profile of an electroactive species near the electrode under diffusion limited conditions

radial, tangential and axial flows were given as series functions and in the diffusion layer V_x can be approximated by equation B-6;

$$V_x = - 0.510 \ x^2 \sqrt{\omega 3/\nu} \qquad (B\text{-}6)$$

The appropriate integral is now obtained by combining B-5 with B-6

$$C_x = \frac{I_\ell}{nFAD} \int_0^\infty \exp \frac{1}{D} \int_0^y (- 0.51 \ \sqrt{\omega 3/\nu} \ z^2) \ dz \qquad (B\text{-}7)$$

$$= \frac{I_\ell}{nFAD} \int_0^\infty \exp \left\{ \frac{-0.51 \ \sqrt{\frac{\omega 3}{\nu}} \ z^3}{3D} \right\} dz \qquad (B\text{-}8)$$

$$\text{let } t = \left(\frac{0.51 \ \sqrt{\frac{\omega 3}{\nu}} \ z^3}{3D} \right) \qquad (B\text{-}9)$$

$$\frac{dt}{dz} = \frac{0.51 \ \sqrt{\omega 3/\nu} \ z^2}{D} \qquad (B\text{-}10)$$

$$z = \sqrt[3]{\frac{3 \ Dt}{0.51 \ \sqrt{\omega 3/\nu}}} \qquad (B\text{-}11)$$

Combining equations B-10 and B-11, one obtains

$$\frac{dt}{dz} = \frac{0.51 \ \sqrt{\omega 3/\nu}}{D} \left(\frac{3 \ Dt}{0.51 \ \sqrt{\omega 3/\nu}} \right)^{2/3} \qquad (B\text{-}12)$$

$$\frac{dt}{dz} = \frac{1.66 \ \omega^{1/2} \ t^{2/3}}{D^{1/3} \ \nu^{1/6}} \quad .$$

Substituting t into equation B-7 and substituting for dz from equation B-12 results in equation B-13

$$C_x = \frac{I_\ell}{nFAD} \int_0^\infty \exp\{-t\} \ \frac{D^{1/3} \ \nu^{1/6} \ t^{-2/3}}{1.66 \ \omega^{1/2}} \ dt \qquad \text{(B-13)}$$

$$= \frac{I_\ell \ \nu^{1/6}}{1.66 \ nFAD^{2/3} \ \omega^{1/2}} \int_0^\infty \exp\{-t\} \cdot t^{-2/3} \ dt$$

This integral is a gamma function of argument 1/3 and is tabulated. Note that though the gradient of interest only extends from zero to δ, its value from δ → ∞ is negligible as explained earlier, thus the Γ function tabulated as an integral from zero to infinity is appropriate.

$$C_x = \frac{I_\ell \ \nu^{1/6}}{1.66 \ nFAD^{2/3} \ \omega^{1/2}} \cdot \Gamma(1/3) \qquad \text{(B-14)}$$

$$= \frac{I_\ell \ \nu^{1/6}}{nFAD^{2/3} \ \omega^{1/2}} \ \frac{2.68}{1.66}$$

$$= \frac{1.61 \ I_\ell \ \nu^{1/6}}{nFAD^{2/3} \ \omega^{1/2}}$$

Finally, the proper form is given as

$$I_\ell = \frac{nFAD}{\delta} \ c^b \qquad \text{(B-15)}$$

where $\delta = 1.61 \ \nu^{1/6} \ D^{1/3} \ \omega^{-1/2}$ \qquad (B-16)
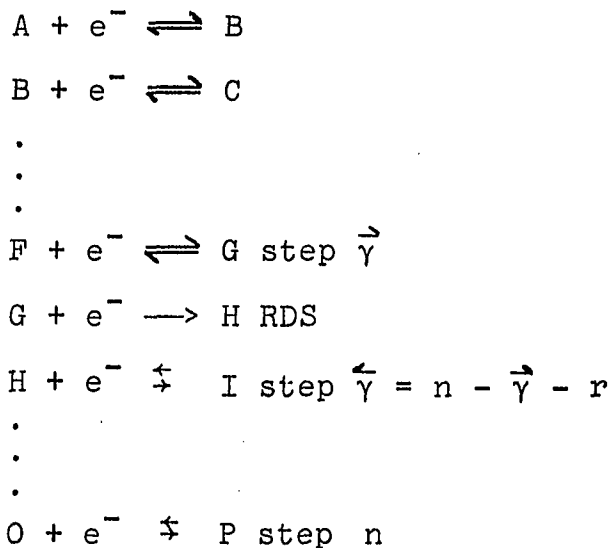
If as mentioned earlier the gradient dc/dx can be approximated as a straight line within the diffusion layer, one can further write

$$I = nFAD \frac{\Delta C}{\Delta X} \qquad (B-17)$$

$$= nFAD \left[\frac{C^b - C^o}{\delta} \right] \, .$$

Equation B-17 is the form commonly used to describe the concentration of electroactive species near the electrode surface.

X. APPENDIX C: MULTISTEP ELECTRON TRANSFER

For a multistep electron transfer reaction such as

$$A + e^- \rightleftharpoons B$$

$$B + e^- \rightleftharpoons C$$

.

.

.

$$F + e^- \rightleftharpoons G \quad \text{step } \overrightarrow{\gamma}$$

$$G + e^- \longrightarrow H \quad \text{RDS}$$

$$H + e^- \rightleftharpoons I \quad \text{step } \overleftarrow{\gamma} = n - \overrightarrow{\gamma} - r$$

.

.

.

$$O + e^- \rightleftharpoons P \quad \text{step } n$$

Where $\overrightarrow{\gamma}$ is the number of electron transfer steps before the RDS and $\overleftarrow{\gamma}$ is the number of electron transfer steps after the RDS, r is the number of electrons transferred in the rate determining step.

If as described, $G + e^- \rightarrow H$ is the rate determining step, that is, its rate is significantly slower than the rates of the other reactions, then we can write for the electrochemical rate (of electronation)

$$\overrightarrow{i}_G = F \, \overrightarrow{k}_G \, C_G \, \exp\{\frac{-\beta\Delta\phi}{RT}\} \tag{C-1}$$

where $\overrightarrow{k}_G$ is the chemical rate constant of the electronation process, C_G the surface concentration of intermediate G and

and $\Delta\phi$ is the potential difference across the double
layer. Since G is the limiting step, the rest of the steps
may be considered in equilibrium. Thus,

$$F \vec{k}_1 C_A \exp\{\frac{-\beta F\Delta\phi}{RT}\} = F \overleftarrow{k}_1 C_B \exp\{\frac{(1-\beta)F\Delta\phi}{RT}\}$$

and

$$C_B = C_A \frac{\vec{k}_1}{\overleftarrow{k}_1} \exp\{\frac{-F\Delta\phi}{RT}\}$$

$$C_B = C_A K_1 \exp\{\frac{-F\Delta\phi}{RT}\} \tag{C-2}$$

Similarly,

$$C_C = C_B K_1 K_2 \exp\{\frac{-2F\Delta\phi}{RT}\} \tag{C-3}$$

$$C_D = C_C K_1 K_2 K_3 \exp\{\frac{-3F\Delta\phi}{RT}\} \tag{C-4}$$

$$C_G = C_A \left(\prod_{i=1}^{\vec{\gamma}} K_i\right) \exp\{\frac{-\vec{\gamma}F\Delta\phi}{RT}\}$$

$$\vec{i} = F \vec{k}_G \left[\prod_{i=1}^{\vec{\gamma}} K_i\right] C_A \exp\{\frac{-(\vec{\gamma}+\beta)F\Delta\phi}{RT}\} \tag{C-5}$$

Analogously for the reverse

$$H \longrightarrow G + e^-$$

where

$$\overleftarrow{i} = F \overleftarrow{k}_G C_H \exp\{\frac{(1-\beta)F\Delta\phi}{RT}\} \tag{C-6}$$

We can devise similarly to the first reaction

$$C_H = C_p \left[\prod_{i=n-\vec{j}-1}^{n} K_i \right] \exp\left\{ \frac{\overleftarrow{\gamma}F\Delta\phi}{RT} \right\}$$

and

$$\overleftarrow{i}_G = F \, \overleftarrow{k}_G \, C_p \left[\prod_{i=n-\vec{\gamma}-1}^{n} K_i \right] \exp\left\{ \frac{(\overleftarrow{\gamma}+r-\beta r)F\Delta\phi}{RT} \right\} \qquad \text{(C-7)}$$

letting

$$\vec{i}_{o,G} = F \, \vec{k}_G \left[\prod_{i=1}^{\vec{\gamma}} K_i \right] C_A \, \exp\left\{ \frac{-(\vec{\gamma}+r\beta)F\Delta\phi_{eq}}{RT} \right\}$$

and

$$\overleftarrow{i}_{o,G} = F \, \overleftarrow{k}_G \left[\prod_{i=n-\vec{\gamma}-1}^{n} K_i \right] C_p \, \exp\left\{ \frac{(\overleftarrow{\gamma}+r-\beta r)F\Delta\phi_{eq}}{RT} \right\}$$

The total current can be represented by

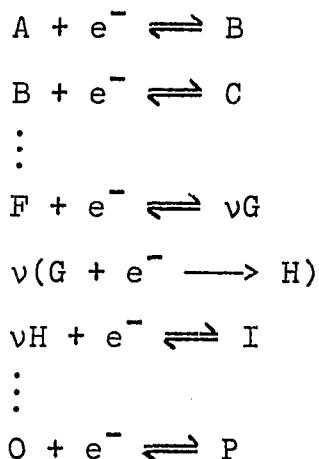$$i = ni_{o,G}\left(\exp\left\{\frac{-(\vec{\gamma}+\beta)F\eta}{RT}\right\} - \exp\left\{\frac{(\overleftarrow{\gamma}+r-\beta r)F\eta}{RT}\right\}\right)$$

$$i = i_o\left[\exp\left\{\frac{-(\vec{\gamma}+\beta)F\eta}{RT}\right\} - \exp\left\{\frac{(n-\vec{\gamma}-\beta r)F\eta}{RT}\right\}\right] \qquad \text{(C-8)}$$

The above equation (C-8) can be rewritten to include the
case where the rate limiting step is not a charge transfer
step as

$$i = i_o\left[\exp\{\frac{-(\overrightarrow{\gamma}+\beta r)F\eta}{RT}\} - \exp\{\frac{(\eta-\overrightarrow{\gamma}-\beta r)F\eta}{RT}\}\right] \qquad (C-9)$$

where r is the number of electrons transferred in the rate
determining step. The stoichiometric number relates the
number of times the RDS occurs for each occurrence of the
overall reaction. If in our initial reaction sequence
step G + e —> H occurred ν times for each execution of
the overall process, then $\eta-\nu r$ electrons would be trans-
ferred in the rest of the steps and, $\overleftarrow{\gamma} = \eta-\overrightarrow{\gamma}-\nu r$. Equation
C-1 still describes the rate of the RDS but for the
reaction steps we now have,

$$A + e^- \rightleftharpoons B$$

$$B + e^- \rightleftharpoons C$$

$$\vdots$$

$$F + e^- \rightleftharpoons \nu G$$

$$\nu(G + e^- \longrightarrow H)$$

$$\nu H + e^- \rightleftharpoons I$$

$$\vdots$$

$$O + e^- \rightleftharpoons P$$
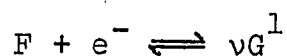
and similar to equations C-2 → C-4, we can derive

$$C_B = K_1 C_A \exp\{\frac{-F\Delta\phi}{RT}\}$$

$$C_C = K_1 K_2 C_A \exp\left\{\frac{-2F\Delta\phi}{RT}\right\}$$

$$C_D = K_1 K_2 K_3 C_A \exp\left\{\frac{-3F\Delta\phi}{RT}\right\}$$

But when we get to step

$$F + e^- \rightleftharpoons \nu G^1$$

we have

$$C_G^\nu = \left[\prod_{i=1}^{\vec{\gamma}} K_i\right] C_A \exp\left\{\frac{-\vec{\gamma}F\Delta\phi}{RT}\right\}$$

and

$$C_G = \left[\prod_{i=1}^{\vec{\gamma}} (K_i C_A)^{1/\nu}\right] \exp\left\{\frac{(-\vec{\gamma}/\nu)F\Delta\phi}{RT}\right\}$$

thus

$$\vec{i}_G = F \vec{k}_G \left[\prod_{i=1}^{\vec{\gamma}} (K_i C_A)^{1/\nu}\right] \exp\left\{\frac{-(\beta r+\vec{\gamma}/\nu)F\Delta\phi}{RT}\right\} \qquad \text{(C-10)}$$
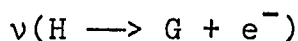
or

$$\vec{i}_G = i_{o,G} \exp\left\{\frac{-(r\beta+\vec{\gamma}/\nu)F\eta}{RT}\right\}$$

---

[1]This step can be combinations of other steps, _i.e._,
$E + e^- \rightleftharpoons 2F$ and $2(F + e^- \rightleftharpoons \nu/2\ G)$ etc.

Thus, for the total electronation current

$$i = i_{o,G} \exp\{-(r\beta + \frac{\overrightarrow{\gamma}}{\nu})\ \frac{Fn}{RT}\} \qquad\qquad (C\text{-}11)$$

Similarly, for the reverse reaction we have

$$\nu(H \longrightarrow G + e^-)$$

$$C_H = \left[\prod_{n-\overleftarrow{\gamma}-\nu r}^{n} (K_i C_p)^{1/\nu}\right] \exp\{\frac{\overleftarrow{\gamma}/\nu\ F\Delta\phi}{RT}\}$$

and

$$\overleftarrow{i}_G = Fk_G \left[\prod_{n-\overleftarrow{\gamma}-r\nu}^{n} (K_i C_p)^{1/\nu}\right] \exp\{(\frac{\overleftarrow{\gamma}}{\nu} + r(1-\beta))\ \frac{F\Delta\phi}{RT}\}$$

$$= i_{o,G} \exp\{\frac{\overleftarrow{\gamma}}{\nu} + r - r\beta)\ \frac{Fn}{RT}\}$$

The total current is then,

$$i = i_o [\exp -(\frac{\overrightarrow{\gamma}}{\nu} + r\beta)\ \frac{Fn}{RT}\} - \exp(\frac{n-\overrightarrow{\gamma}}{\nu} - r\beta)\ \frac{Fn}{RT}\}]$$

where $i_o = \eta\ i_{o,G}$, and $\overleftarrow{\gamma} = \eta - \overrightarrow{\gamma} - \nu r$

We now have the generalized form of the Butler-Volmer equation

$$i = i_o [\exp\{\frac{-\alpha_c Fn}{RT}\} - \exp\{\frac{\alpha_a Fn}{RT}\}] \qquad\qquad (C\text{-}12)$$

where

$$\alpha_c = \frac{\overrightarrow{\gamma}}{\nu} + r\beta; \quad \alpha_a = (\frac{n - \overrightarrow{\gamma}}{\nu} - r\beta)$$

and

$$\alpha_c + \alpha_a = \frac{n}{\nu}$$

These are the coefficients that determine the slope of the E vs ln i plots -- the Tafel slope -- of an electrochemical reaction.

XI. APPENDIX D: NONLINEAR DIFFUSION

The problem of partially deactivated electrodes is especially acute for solid electrodes. One particular theory developed by Landsberg et al. used the solution by Smythe to the analogous electrical diffusion problem. According to Smythe (112), a conducting cylinder, Figure D-1, of length δ with electrodes of radius a and b, has a resistance to current flow given by:

$$R = \frac{\rho}{\pi b^2} (\delta - \psi(\delta,a,b)). \qquad (D-1)$$

$$\rho = \text{resistivity}$$
$$\psi(\delta,a,b) = \text{calculated constant}$$

In this figure voltage increases from left to right and the area outside the a electrode is nonconductive; thus, current flows from right to left between electrode b and electrode a. The current in such a system is then described by

$$i = \frac{\Delta V}{R} = \frac{\Delta V(\pi b^2)}{\tau(\delta - \psi(\delta,a,b))} \qquad (D-2)$$

This solution was applied by Landsberg to a model rotating disk electrode (RDE). Figure II-1 shows the representation of the model disk surface with many small active areas, a, surrounded by nonconductive inactive areas b. For the case of N parallel cylinders the total resistance is:
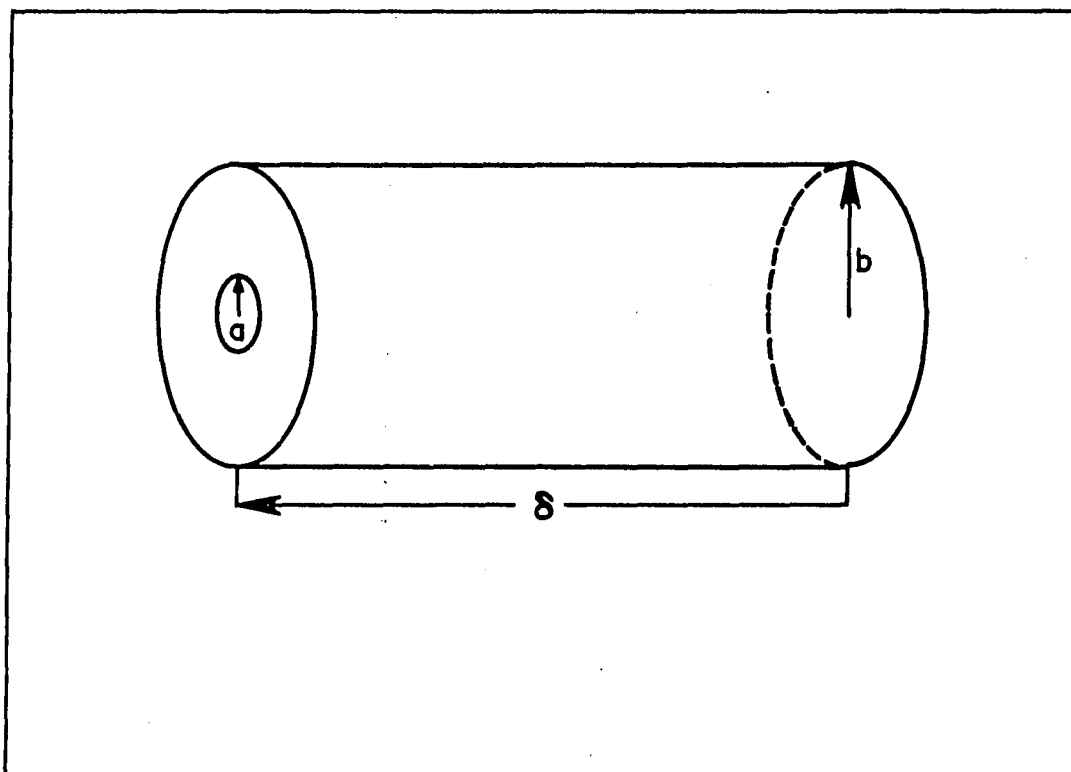
Figure D-1. Model for nonlinear diffusion of charge from a conductive surface of radius b to the conductive surface of radius a. δ is the diffusion width

$$R = \frac{\rho(\delta-\psi(\delta,a,b))}{\pi b^2 \cdot N} \tag{D-3}$$

If N is the number of cylinders per unit area and if the cylinders overlap slightly, $N(\pi b^2)$ is approximately equal to one. The total resistance is thus

$$R = \rho(\delta-\psi(\delta,a,b)) . \tag{D-4}$$

accordingly, the electrical current is given by

$$I = \frac{\Delta V}{R} = \frac{(1/\rho)\Delta V}{\delta-\psi(\delta,a,b)} . \tag{D-5}$$

Similarly, one can write for the ionic diffusion analog

$$i_d = \frac{(nFAD)\Delta C}{\delta-\psi(\delta,a,b)} . \tag{D-6}$$

$$i_d = \text{disk current}$$

When $b \ll \delta$, $\psi(\delta,a,b)$ is given by the tabulated constant $- \left| \sum_n A_n \right|$. Substituting this and

$$\delta = 1.61 \, D^{1/3} \nu^{1/6} \omega^{-1/2} \tag{D-7}$$

into equation 6 gives

$$i_d = \frac{nFDA\Delta C}{1.61 \, D^{1/3}\nu^{1/6}\omega^{-1/2} + \left| \sum_n A_n \right|} , \tag{D-8}$$

and in final form

$$1/i_d = \frac{1.61\nu^{1/6}}{nFAD^{2/3}\omega^{1/2}\Delta C} + \frac{\left| \sum_n A_n \right|}{nFAD\Delta C} \tag{D-9}$$

Accordingly, a plot of $1/i_d$ versus $\omega^{-1/2}$ should give a
straight line (for $b \ll \delta$) with a slope of
$1.61 \, \nu^{1/6}/nFAD^{2/3}\Delta C$ and an intercept containing the term
$\sum_n A_n$.